EFFECT OF DISPERSION ON SPECTRUM-SLICED WDM SYSTEMS

By

Virach Wongpaibool

Thesis submitted to the Faculty of the
Virginia Polytechnic Institute and State University
in partial fulfillment of the requirements for the degree of
MASTER OF SCIENCE
in
Electrical Engineering

Approved:

_____
Dr. Ira Jacobs
(Chairman)

_____ _____
Dr. Brian D. Woerner Dr. Ioannis M. Besieris

September 1998
Blacksburg, Virginia

EFFECT OF DISPERSION ON SPECTRUM-SLICED WDM SYSTEMS

By

Virach Wongpaibool

Committee Chairman: Dr. Ira Jacobs

Electrical Engineering

ABSTRACT

The purpose of this thesis is to investigate the effect of dispersion on a spectrum-sliced WDM (SS-WDM) system, specifically a system employing a single-mode optical fiber. The system performance is expressed in term of the receiver sensitivity defined as the average number of photon per bit N_p required for a given probability of bit error P_e. The receiver sensitivity is expressed in terms of two normalized parameters: the ratio of the optical bandwidth per channel and the bit rate $m = B_0 / R_b = B_0 T$, and the transmission distance normalized by the dispersion distance z / L_D. The former represents the effect of the excess beat noise caused by the signal fluctuation. The latter represents the effect of dispersion. The excess beat noise can be reduced by increasing the value of m (increasing the optical bandwidth B_0 for a given bit rate R_b). However, a large m implies that the degradation due to the dispersion is severe in a system employing a single-mode fiber. Therefore, there should be an optimum m resulting from the two effects. The theoretical results obtained from our analysis have confirmed this prediction. It is also shown that the optimum m (m_{opt}) decreases with an increase in the normalized distance. This suggests that the dispersion strongly affects the system performance. The increase in the excess beat noise is traded for the decrease in the dispersion effect. Additionally, the maximum transmission distance is relatively short, compared to that in a laser-based system. This suggests that the SS-WDM systems with single-mode fibers are suitable for short-haul systems, such as high-speed local-access network where the operating bit rate is high but the transmission distance is relatively short.

Acknowledgments

Firstly, this thesis is dedicated to my parents, Sinthu and Suda who encourage and support me throughout my life. Their encouragement and concern, especially when I was here, are invaluable. Without their support, my dream to study abroad would have never been fulfilled.

I am grateful to Prof. Ira Jacobs for his kindness and help. He also provided me the opportunity to conduct the research in this field. I sincerely appreciate it. His ability to simplify difficult problems always amazes me. There is still a lot for me to learn from him. Indeed, he is my idol.

I also thank Drs. Besieris and Woerner for being my committee. Through his course, Dr. Besieris taught me stochastic processes, which I used extensively in this thesis. Dr. Woerner is among the best teachers in my mind. His talent in teaching is excellent.

To my younger brother, Atthasit, I do not know how to repay your kindness and support. I wish you success in the graduate study at our department.

To my true friends, too many to be named here, I deeply appreciate your encouragement. They make my life full of joy and happiness. I thank you all for urging me to finish this thesis. See you soon.

Finally, I would like to thank Virginia Tech for giving me the opportunity to study in this great department.

Table of Contents

List of Figures

Chapter 3

Chapter 4

Chapter 1

INTRODUCTION

In the past dating back to the beginning of our civilization, people ingeniously used fire and smoke signals to transfer information. Such ideas were still used in the 18th century with signaling lamps, flags, and other semaphore apparatus being used instead. These kinds of communications were relatively slow, compared to the modern-day communications. The method of communications was advanced further with the advent of telegraphy, which used electricity instead of light as a signal. The invention of telegraphy brought the world into the electrical-communication era. However, a single major event that considerably affected our world was the invention of the telephone in 1876 [1]. This event has drastically transformed the development of communication technology.

The use of the telephone has increasingly grown from a pair of telephones to telephone networks. Therefore, technology in transmission has had to be continuously developed in order to sufficiently increase the capacity of telephone networks. At first, wire pairs were replaced by coaxial cables to improve the capacity; however, the capacity of the coaxial cables is also not sufficient. This led to the development and deployment of microwave communication systems. The capacity is usually measured in term of the bit rate-distance product BL where B is the bit rate and L is the repeater spacing. The most advanced microwave system was able to operate at BL product of around 100 Mbps-km. Technological advances in various communication systems have been investigated in order to increase the BL. Such increase is shown in the Fig 1.1. It is clearly seen that the operating frequency has been continuously shifted to higher frequency to increase the BL product. This is because the bit rate-distance product BL fundamentally depends on the

magnitude of the carrier frequency. Thus, the microwave systems had reached their inherent limitation.

However, the demand in the bit rate-distance product BL continues to increase. Thus, the microwave and coaxial systems could no longer support such demand cost-effectively and efficiently. Consequently, it was necessary that the carrier frequency had to be higher in order to overcome the fundamental limitation. The next higher frequency band is in the region of light; thus, the term "optical (fiber) communication systems" has emerged.

1.1 EVOLUTION IN OPTICAL FIBER COMMUNICATION SYSTEMS

As their name implies, these kinds of communication systems use optical waves as carriers; hence, the bit rate-distance product BL can be improved several orders of magnitude compared to the microwave and coaxial systems as seen in Fig. 1.1. The most appropriate media that are used as channels in these systems are the optical fibers, which was proposed in 1966 [2]. However, the first-encountered problem was that available fibers during that time had extremely high loss which exceeded 1000 dB/km. This problem challenged the researchers and engineers to find processes by which low-loss optical fibers could be fabricated. Finally, this problem was solved in 1970 [3], when optical fibers having acceptable attenuation was first obtained.

The combination of low-loss optical fibers and the advance in semiconductor technology made the optical fiber communication system practically possible. In 1978, the first systems were commercially deployed. Their operating wavelength was at 0.8 μm, and they were capable of carrying bit rates of 50 –100 Mbps with a repeater spacing of approximately 10 km [1]. As the technology in optical-fiber fabrication progressed, lower-loss optical fibers became feasible, which led to higher bit rate-distance product BL. The progress in the bit rate-distance product BL of the optical fiber communication systems is shown in Fig. 1.2. It is usually divided into five generations and they are briefly described as follows.

1.1.1. First Generation

The first generation of optical fiber communication systems utilized multimode optical fibers and operated in the 0.8-μm wavelength region. The advantage of the multimode fibers is that their core is large; thus, coupling of the light from the source into the fiber is not difficult. However, large core diameter also leads to an unavoidable drawback. The major drawback is that the optical waves travel in the fiber with different paths; therefore, the optical waves arrive at the receiver with slightly different time delays, which causes pulse spreading. This phenomenon is termed multimode dispersion, also called intermodal dispersion.

In addition, there is another type of dispersion called intramodal dispersion or chromatic dispersion, which is due to nonlinear phase response of the optical fiber. The nonlinear phase response results in the optical waves at distinct frequencies arriving the receiver at different time delays. Both types of dispersion generate intersymbol interference (ISI), which limits the system performance. The bit rate-distance product BL of the first generation is therefore limited by both types of dispersion and fiber loss.

1.1.2. Second Generation

One way to eliminate intermodal dispersion is to utilize a single-mode optical fiber. In this type of fiber, there is only one path (mode) in which the optical wave is allowed to travel; therefore, only intramodal dispersion exists. Another advantage of using the single-mode optical fiber is that this type of fiber has less internal (Rayleigh) scattering [3]; thus, the attenuation is also less than that of the multimode fiber.

It was found that in the 1.3-μm wavelength region, the attenuation is less than in the 0.8-μm wavelength region as shown in Fig. 1.3. In addition, as seen in Fig. 1.4 the optical fiber exhibits the lowest dispersion effect in this new region. Both advantages could lead to higher BL product. With the advance in semiconductor technology, operating the systems at 1.3-μm window was finally realized. As a result, larger bit rate-distance product BL of the order of 200 Gbps-km was achieved and it was solely limited by fiber attenuation. At this figure of BL product, the undersea fiber optic system became feasible. The first transatlantic system called TAT-8 was implemented, and started operating in 1988 [4]. It consists of three pairs of single-mode optical fibers (one pair for backup purpose), and each pair operated at 296 Mbps (one for each direction).

1.1.3. Third Generation

As seen in Fig. 1.3, the attenuation in the single-mode fiber is lowest in the 1.55-μm wavelength region (0.2 dB/km). However, the intramodal dispersion in this wavelength region is so severe that its effect is intolerable for very high BL systems. In order to take the advantage of lowest attenuation at this wavelength window, it was realized that the optical fibers need to be modified to have low dispersion in this window, and narrow-linewidth lasers were needed. This obstacle was overcome by the development of dispersion-shifted fibers and single longitudinal mode lasers. Dispersion-shifted fibers are fibers that are tailored to provide minimum dispersion near 1.55 μm; thus, allowing the use of conventional lasers exhibiting relatively large spectral width (several nm). On the other hand, the narrow-linewidth lasers have to be employed in the systems that use conventional optical fibers in order to take advantage of lowest attenuation. With both approaches, the bit rate-distance product BL of 500 Gbps-km was achievable.

1.1.4. Fourth Generation

It is clearly seen that the increase in the BL product for single channel seemed to reach its saturation point. The systems were designed to operate at lowest attenuation region to overcome the attenuation problem and the narrow-linewidth lasers were utilized to minimize the dispersion effect. However, the modulation technique was still primitive -- intensity modulated/direct detection (IM/DD) which offers simple system configuration. Since the narrow-linewidth lasers were available, it is possible to employ other techniques that provide lower (better) receiver sensitivity, which would result in larger repeater spacing. Such systems are referred to as coherent optical communication systems. Nevertheless, the system configurations were too complex to implement in practice. Consequently, the coherent systems are not commercially attractive.

1.1.5. Fifth Generation

With the development of optical amplifiers, the extreme improvement in the BL product became practically possible. The huge amount of bandwidth offered by the

optical fiber could be utilized by using the wavelength division multiplexing (WDM) technique. In addition, with the help of optical amplifiers all channels could be simultaneously amplified without optical-electrical-optical conversion; thus, the spacing between regenerative repeaters could be extended considerably. As a result, the bit rate-distance product BL was increased and can be larger than 100,000 Gbps-km. Because the WDM systems with optical amplifiers are our interest, the next section is dedicated to this topic.

There is another approach that can combat the dispersion effect; hence, increasing the repeater spacing. Such approach is to make use of fiber nonlinearity, which results in the shape of the optical pulses being preserved while traveling in the fiber. The systems that utilize this technique are called soliton-based systems. However, this technique is still in the experimental stage.

1.2 IN-LINE ERBIUM-DOPED FIBER AMPLIFIERS (EDFAs)

The general rule in system implementation and design is that the systems can be upgraded to support future demands. There are several factors that have to be considered. The initial costs have to be kept at a minimum, and the initial systems should be flexible enough to be expanded in the future. Therefore, the fiber optic systems are usually implemented with a limited number of fibers in order to reduce the initial costs. However, the number of installed fibers has to be sufficient in order to support the future demands. The number of installed fibers is commonly referred to as fiber count, which can be as low as four and generally is less than thirty-two [5]. Moreover, it is uncommon to install additional fibers to increase the system capacity at a later time due to technical difficulties in installation. Consequently, the system upgrade has to be accomplished with the initially-installed fibers. However, it should be noted that in almost all systems, not all of the installed fibers are utilized at the initial operation -- some are reserved for future use.

Before the 1990s, the technology in fiber optic communication generally permitted only the use of a single wavelength in an optical fiber. The block diagram of such a system is shown in Fig. 1.5 (a). There are two ways of expanding capacity in this system. The first is to utilize the reserved fibers, and the second is to increase the bit rate

transmitted in each fiber, which is commonly referred to as time division multiplexing (TDM) upgrade. The first option does not create any difficulties as long as there are reserved fibers left. However, there are several factors that complicate the TDM upgrade. The increase in bit rate results in higher required power at the receiver and larger chromatic dispersion. Therefore, there are limitations in the extent to which the bit rate can be increased. In addition, for each TDM upgrade all in-line repeaters have to be modified to support the new bit rate, which may not be cost-effective. Although the systems installed before the 1990s were not flexible due to technologies and knowledge at that time, their high capacities compared to other media still made them economically attractive for high capacity applications.

The effect of severe dispersion around the 1.55 μm-window in standard single-mode fiber can be reduced by employing distributed-feedback (DFB) lasers that provide narrow spectral linewidth. Consequently, the distance between the transmitter and the receiver could be enhanced as long as the total dispersion is tolerable. In addition, the dispersion can also be made negligible, if the systems employ dispersion-shifted fibers as the transmission media. This implies that the limitation would be reduced to only the unavoidable attenuation. Since the dispersion, which distorts the shape of the optical pulse, is no longer the critical factor compared to the attenuation, the optical pulse shaping performed by the regenerative repeaters placed along the fiber links are dispensable. That is, electronic regenerative repeaters are not necessary as long as the pulse distortion due to dispersion is tolerable. Thus, the remaining and necessary function of these repeaters is to boost the signal power, which can be accomplished optically. Two apparent advantages in optically boosting the signal are that the intermediate equipment between the transmitter and the receiver is bit-rate transparent (changes in bit rate do not require any change in the intermediate equipment), and that optical amplification of signals is independent of the signal format. In addition, with such intermediate equipment, it is unnecessary to install the new in-line equipment to support the new bit rate for TDM upgrade. The system configuration of fiber optic systems employing in-line optical amplifiers is shown in Fig. 1.5 (b).

Systems without intermediate electrical repeaters were realized when the optical amplifier technology, especially erbium-doped fiber amplifiers (EDFAs), was developed

in the early 1990s. Details of the amplification mechanism of the EDFAs are provided in the next chapter. With EDFAs, the bit rate-distance product BL can be improved dramatically. Additionally, deployment of EDFAs also provides higher reliability than the electronic repeaters since the optical amplifiers require fewer active components.

In the systems installed before the 1990s, the single-mode fibers were usually deployed. At the time of installation, the optical amplifiers were not available; therefore, the deployment of EDFAs were the replacement of electronic repeaters in order to provide TDM upgrade flexibility. In the case of systems with single-mode fibers and EDFAs, the chromatic dispersion is the dominant limitation in the long-haul systems. Therefore, at some distance, the electronic repeaters are periodically required to shape the signal pulses. Replacement of installed single-mode fibers with dispersion-shifted fibers seems to be the solution to overcome the dispersion but two problems have to be considered in doing so. Firstly, replacement of installed fibers is not economically cost-effective. In addition, nonlinear effects are more likely to occur in the dispersion-shifted fibers than in the single-mode fibers.

As the pulses travel along the fiber, they are distorted by chromatic dispersion. If the pulses traveling in the second half of the transmission link are the complex conjugate of the distorted pulses propagating in the first half of the link, then the pulses exiting the fibers are undistorted, which can be explained graphically as shown in Fig. 1.6. This technique is called phase-conjugation technique [6]-[8]. The equipment placed at the midway point is called the phase conjugator, which can be realized by using the four-wave mixing process in a nonlinear medium, such as a dispersion-shifted fiber or a semiconductor optical amplifier. The interaction between the input signal and the pump signal within the nonlinear medium results in the newly-generated signal that is the complex conjugate of the input signal. Simulation of this technique has shown that the bit rate-distance product BL could be as large as 180,000 Gbps-km [6]. Unfortunately, this technique is currently in the experimental stage and there are several limiting factors that cause imperfect compensation. They are variation in dispersion property along the transmission link, and the in-line amplifiers that causes periodic power fluctuation [7]. The former is usually unavoidable in practice and the latter produces a nonlinear phase shift that disturbs the compensation.

In the case of the systems employing dispersion-shifted fibers, the bit rate-distance product BL is increased dramatically with the deployment of EDFAs. Although the loss limitation is overcome by EDFAs and the dispersion is negligible, the nonlinear effect becomes the major limitation. For the nonlinear effect to be strong the phase-matching condition must be satisfied, and that is easily obtained in the absence of dispersion. This nonlinear process results in four-wave mixing of the ASE noise, which increases nonlinearly with the distance. Despite this nonlinear effect, the bit rate distance product BL is enhanced considerably compared to that of systems without EDFAs.

Therefore, it is desirable that the transmission link exhibits non-zero dispersion along the link to minimize the effect of nonlinearity while having zero dispersion from end to end. One ingenious solution, known as dispersion management scheme or dispersion map [9], is to deploy different types of optical fibers that have opposing chromatic dispersion. At any point in the link, the chromatic dispersion is nonzero; therefore, the nonlinear effect is avoided. However, the end-to-end chromatic dispersion can be managed to zero, which results in no pulse spreading due to chromatic dispersion. It is clearly seen that this system configuration is extremely beneficial; both chromatic dispersion and nonlinear phenomenon are avoided. When it is combined with the EDFAs, the bit rate-distance product BL can exceed 40,000 Gbps-km. This type of system is widely deployed in long-haul fiber optic systems, such as, TAT (Transatlantic Telephone)-12/13 [10], TPC (Transpacific Crossings)-5 [11], FLAG (Fiberoptic Around the Globe) [12] linking TAT-12/13 and TPC-5, and APCN (Asia Pacific Cable Network) [13] which services Asia-Pacific countries. In all of these systems, there are no electronic repeaters installed, and the distance between end terminals can be of the order of 8,000 km with the bit rate of 5 Gbps.

1.3 WAVELENGTH DIVISION MULTIPLEXING (WDM)

Although the bit rate provided by single-channel fiber optic systems is extremely high compared to the systems using other media, the traffic demand is also large and increasing more rapidly than previously predicted during the past few years. Such unexpectedly increasing demand has been driven by many factors, such as globalization in business, liberalization in worldwide telecommunication markets, and Internet and

broadband access. Therefore, there is continuing need for increasing system capacity. Increasing the operating bit rate is one solution to this problem. However, the maximum bit rate that can be practically achieved is often under 10 Gbps due to speed limitations of electronic devices, chromatic dispersion, and polarization mode dispersion. The polarization mode dispersion is caused by deviation in the fiber core from perfect circularity, which leads to different indices of refraction for two orthogonal waves. This effect is difficult to control because of its dependence on wavelength and ambient temperature [14], [15].

It is also apparent in the previous section that the vast bandwidth provided by the optical fibers is ineffectively utilized in single-channel systems. Thus, the unused part of the bandwidth can be used to expand the system capacity. This method is called wavelength division multiplexing (WDM), which utilizes a multichannel scheme to increase the system capacity. Multiple channels located at different wavelengths are transmitted over the same fiber simultaneously; thus, the bandwidth efficiency and the aggregated bit rate in the single fiber are increased dramatically. In addition, the WDM technique can be employed not only in new systems but also in the currently-operating systems to expand their capacity. A schematic diagram of a WDM system is shown in Fig. 1.5 (c). All signals at different wavelengths are multiplexed together into the same fiber by the WDM multiplexer, and are periodically amplified by the EDFAs to compensate for the loss in the fiber. At the receiver, all channels are demultiplexed and are passed to corresponding receivers to convert them back to electrical signals. With the use of WDM, larger than 200,000 Gbps-km bit rate-distance product BL was recently reported [16]. In that experiment, 32 channels, each at 10 Gbps, were transmitted over 640 km with less than 3-dB difference in receiver sensitivity.

The WDM technique provides not only the enhancement in system capacity but also the flexibility in network management – the group of distinct wavelengths acts as an additional dimension of the system. For example, any wavelength can be added or dropped at an intermediate node between the transmitter and the receiver without affecting the other wavelengths when an add-drop multiplexer is employed. Additionally, the intermediate node can route any wavelength to the specified destination with the help of an optical router. Most importantly, such add-drop multiplexer and router can be

realized from the WDM (de)multiplexer. The first actual system that implements such flexibility is Africa ONE (Africa Optical Network) [17]. It will encompass the Africa continent with a single optical ring network, which will link all countries on the continent. It is expected to be ready for service around 1999.

Details of the equipment needed to achieve such flexibility are presented in Chapter 2. However, it should be noted at this point that the characteristic of the WDM (de)multiplexer evidently differs from that of the conventional power splitter, i. e, $1\times N$ coupler. The WDM (de)multiplexer is wavelength selective whereas the power splitter is not. That is, only the corresponding wavelength would appear at each output port of the $1\times N$ WDM demultiplexer for any given input port. Consequently, it is not necessary to place the optical filters at the transmitter, and the receiver as shown in Fig. 1.5(c) since the multiplexer and the demultiplexer already act as the filters.

1.4 SPECTRUM-SLICED WDM SYSTEMS

It is clearly seen from the previous section that the conventional WDM systems require multiple laser diodes, tuned to operate at different wavelengths that match the corresponding ports of the (de)multiplexers. Therefore, the WDM systems are not cost-effective in terms of the number of lasers used, and need some mechanism to precisely control the operating wavelengths of the laser diodes. This implies that the WDM technique is justified to implement in long-haul communication systems where the benefits from the WDM technique overcome its cost and complexity.

However, the benefits mentioned in the previous section may also apply for passive optical networks (PONs). The PON is the network that connects the central offices (CO) and the optical network units (ONUs) located at or near subscriber premises depending on the network purpose. The PONs are the necessary foundation for fiber-to-the-home (FTTH) and fiber-to-the-curb (FTTC) applications. The main purpose of the PONs is to deliver broadband access to the subscribers, such as, video on demand (VOD), and high-speed data [18]. As its name implies, the components employed in such a network all are passive in order to reduce the maintenance cost and complexity. All active components are, thus, located at both ends, i. e., at the CO and at the ONUs. The conventional PON utilizes the TDM or subcarrier multiplexing (SCM) format in

conjunction with a passive coupler at the remote node (RN) to simplify the network configuration and devices [19]. The single-wavelength downstream signal from the CO is power-split at the RN to divide the signal to all ONUs. This configuration provides sharing the single optical fiber among the ONUs in order to minimize the amount of equipment, and thus, cost of the network. However, the simplicity of the network configuration has to be traded for difficulty in TDM upgrade, and inefficient usage of signal power because of single-carrier sharing among ONUs. If the number of ONUs sharing the same optical fiber is N, then the signal power would suffer N^2 power penalty compared to a point-to-point link [19]. This power penalty results from the 1/*N* power splitting at the remote node and the 1/*N* time sharing in the TDM signal format. In addition, the processing capability at each receiver is wastefully utilized, since each receiver has to operate at the aggregate bit rate ($N \times$ individual bit rate).

While the WDM technique can solve these limitations and even enhance the network performance, its cost and complexity are still the major obstacle. With WDM, a distinct wavelength is assigned to each ONU; hence, power splitting can be avoided. Each ONU also operates at its own bit rate, not the aggregate bit rate; thus, the required processing power at the ONU is reduced. Moreover, the security and privacy are strengthened due to the wavelength-selective property of the WDM (de)multiplexer [20]. The signal leakage into neighboring channels is exclusively attributed to the crosstalk characteristic of the WDM (de)multiplexer. Therefore, the leakage signal in the neighboring channels is hard to detect by neighboring ONUs.

1.4.1 Broadband Light Emitting Diodes as Light Sources in SS-WDM Systems

One apparent contribution to the cost and complexity of the WDM PON is the number of lasers required. Moreover, such lasers have to be tunable to the specific wavelengths. If these constraints are eliminated, the cost and complexity of the WDM PON should be reduced dramatically which would facilitate its deployment. This leads to the introduction of spectrum-sliced WDM (SS-WDM) technique in the PON in the late 1980s [21]. At that time, the SS-WDM avoided the using of expensive tunable lasers by utilizing broadband light emitting diodes (LEDs), which were less expensive and more reliable than lasers. The schematic diagram of SS-WDM systems is the same as that of

conventional WDM systems shown in Fig. 1.5 (c). However, the only difference between them is that each transmitter contains the broadband LED instead of the tunable laser. One additional benefit from utilizing the LEDs is that all sources are identical; hence, maintenance is easier.

The WDM multiplexer acts as a wavelength-selective component by providing each ONU a distinct wavelength channel, sliced from the identical LEDs. That is, the output port of the WDM multiplexer contains a number of slices at different wavelengths; each slice is taken from the LED assigned to the individual ONU. Since only a fraction of the LED power spectrum is used, the signals experience an additional power penalty accounted for the slicing operation. This power penalty is usually termed as "slicing loss." Consequently, the SS-WDM systems are limited to small bit rate-distance product BL due to their stringent power budget which is traded for cost reduction and system simplicity. Therefore, the first generation of SS-WDM systems is suitable for PONs.

1.4.2 Broadband ASE Noise from EDFA as Light Sources in SS-WDM Systems

It is clearly seen that there are N LEDs required for the SS-WDM configuration as shown in Fig. 1.5 (c). The number of light sources could also be reduced to only one by using the configuration as shown in Fig. 1.7. However, the light source used in this configuration should have high output power and be broadband since there are additional insertion losses from the demultiplexer and external modulators. Although the LED has a broad power spectrum, typically of the order of 50nm to 100 nm [22], its output power is not sufficient to take the advantage of such configuration.

Fortunately, the ASE noise at the output from an EDFA exhibits broad power spectrum with high output power. Therefore, it is suitable for such a configuration. However, there is an additional power penalty accounted for signal fluctuation since the signal is stochastic in nature, i. e., the signal is noise-like. Moreover, SS-WDM could also be potentially applied to long-haul lightwave systems due to the high power of the output ASE noise obtained from the EDFA. Researchers around the world have been intensively investigating the potential applications of the SS-WDM and its limitations. Since the source is noise-like, some assumptions and formulations used in conventional laser-based systems may not be applicable to SS-WDM systems. Numerous papers and articles

concerning this kind of system have been published and proposed. These are discussed in Chapter 3. However, many interesting subjects relating to SS-WDM are still waiting to be researched.

1.5 MOTIVATION FOR THIS THESIS

This thesis is mainly concerned with the theoretical analysis of SS-WDM employing the EDFA as the broadband noisy source for transmission over conventional single-mode fiber. Arya and Jacobs [23] have analyzed the performance of SS-WDM under the condition that the dispersion caused by the optical fiber is negligible. This condition is satisfied in many applications, such as systems with dispersion-shifted fibers. It is shown in their analysis that the receiver sensitivity, in term of the number of photons per bit for a given probability of bit error, strongly depends on the bandwidth of the source. The narrower the source, the poorer (higher) the receiver sensitivity required for a given probability of bit error. Therefore, in order to reduce power penalty, the channel bandwidth should be large, compared to the operating bit rate. However, the number of channels is reduced when the bandwidth per channel is increased. Moreover, in the systems employing conventional single-mode fibers, the noise-like signal would suffer severe dispersion due to its large bandwidth. Hence, there should be an optimum source bandwidth due to the competing effects of dispersion and inherent signal fluctuation, both of which strongly depend on the channel bandwidth. Pendock and Sampson [24] have observed such optimum bandwidth in their simulation. However, their results are confined to a limited range of parameters.

The ultimate objective of this thesis is to analyze SS-WDM systems employing single-mode fibers. To facilitate application over a broad range of conditions, the analytical results are expressed in term of normalized parameters. The receiver sensitivity is expressed as functions of the channel bandwidth and the normalized distance. The former represents the effect of inherent signal fluctuation. The latter accounts for the effect of chromatic dispersion in the single-mode fiber. The fiber dispersion causes the signal to spread in time; hence, this phenomenon can be modeled as a multipath effect where distinct frequency components of the signal arrive at different time delays. There are two approaches that can be used to find the receiver sensitivity. The first approach is

to assume that the decision statistics for bit ‘1’ and bit ‘0’ are Gaussian. This approach is simple to analyze. However, it is not accurate since the actual distributions for both bit ‘1’ and bit ‘0’ are not Gaussian. The second approach, which is much more difficult than the first one, is the modification of the Gaussian approach. The decision statistic for bit ‘0’ is assumed to be Gaussian due to thermal noise being dominant. On the other hand, the decision statistic for bit ‘1’ is approximated to be chi-square because the signal fluctuation dominates.

The results show that there exists an optimum source bandwidth that minimizes the receiver sensitivity. In addition, our results, when compared with [24], suggest that the source used in SS-WDM systems should be unpolarized. The unpolarized source results in a narrower required channel bandwidth and better receiver sensitivity. This results in a larger number of channels for a given usable bandwidth provided by the sources and a longer transmission distance. As SS-WDM systems are still in their infancy, we hope that our work will be helpful in understanding the nature of these systems, and useful in their practical design and implementation.

1.6 OUTLINE OF THIS WORK

This thesis is divided into five chapters. The second chapter relates to the important equipment employed in the WDM systems. More specifically, they are EDFAs and WDM (de)multiplexers. The fundamental concepts and their applications are discussed. Moreover, the methods of making them practically suitable for actual deployment are explained. Chapter 3 is dedicated to the SS-WDM systems. Their development and progress are discussed in this chapter. Included in this chapter are the details in some prior publications, which are significant to the problem we consider. Chapter 3 helps understanding the fundamental characteristic and concepts of SS-WDM systems, in which the signal is sliced from a broadband noise source.

Chapter 4 is the main part of this thesis. The approach that is used to simplify dispersion to a multipath effect is described in this chapter. The mathematical model and simplification developed to find the receiver sensitivity are also presented. The resultant mathematical formulations are analytically solved by using both a Gaussian assumption and a modification of this assumption. The latter is more accurate than the primitive

Gaussian approach; however, the more accurate approximation poses some difficulties in evaluating the results. When the results from both approaches are compared, it is apparent that the Gaussian approach is inadequate to characterize the SS-WDM systems; it is overly conservative. The Gaussian approach underestimates the performance of SS-WDM systems. Nevertheless, both the Gaussian approach and its modification show an optimum channel bandwidth resulting from the two competing effects: signal fluctuation and chromatic dispersion. The final chapter, Chapter 5, is the conclusion of this thesis.

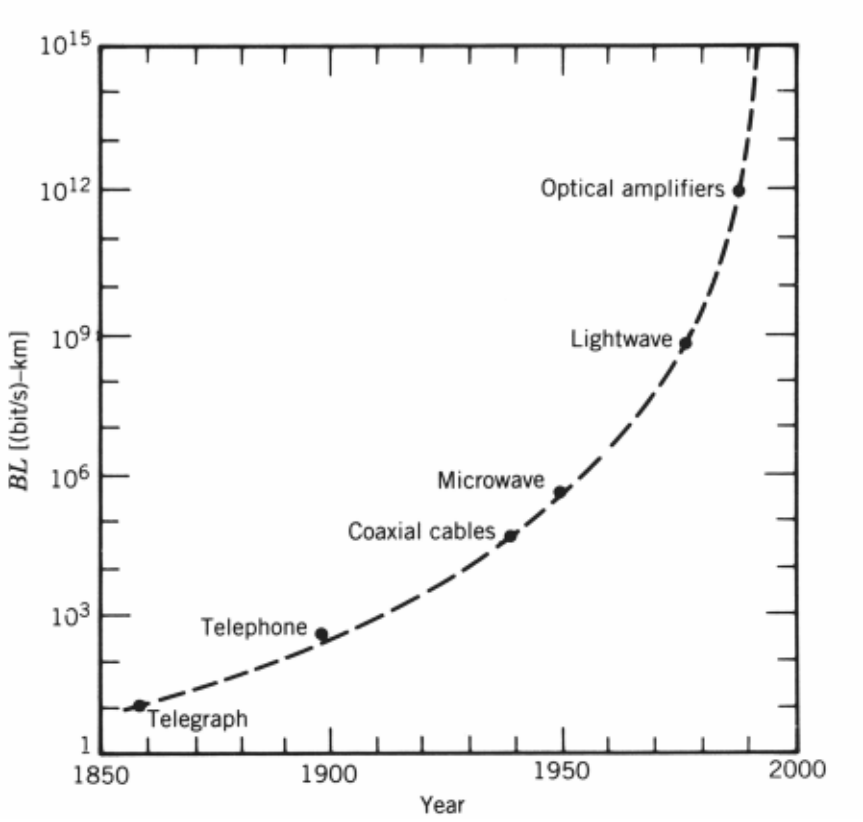

Fig. 1.1: Increase in bit rate-distance product during 1850-2000 [1].

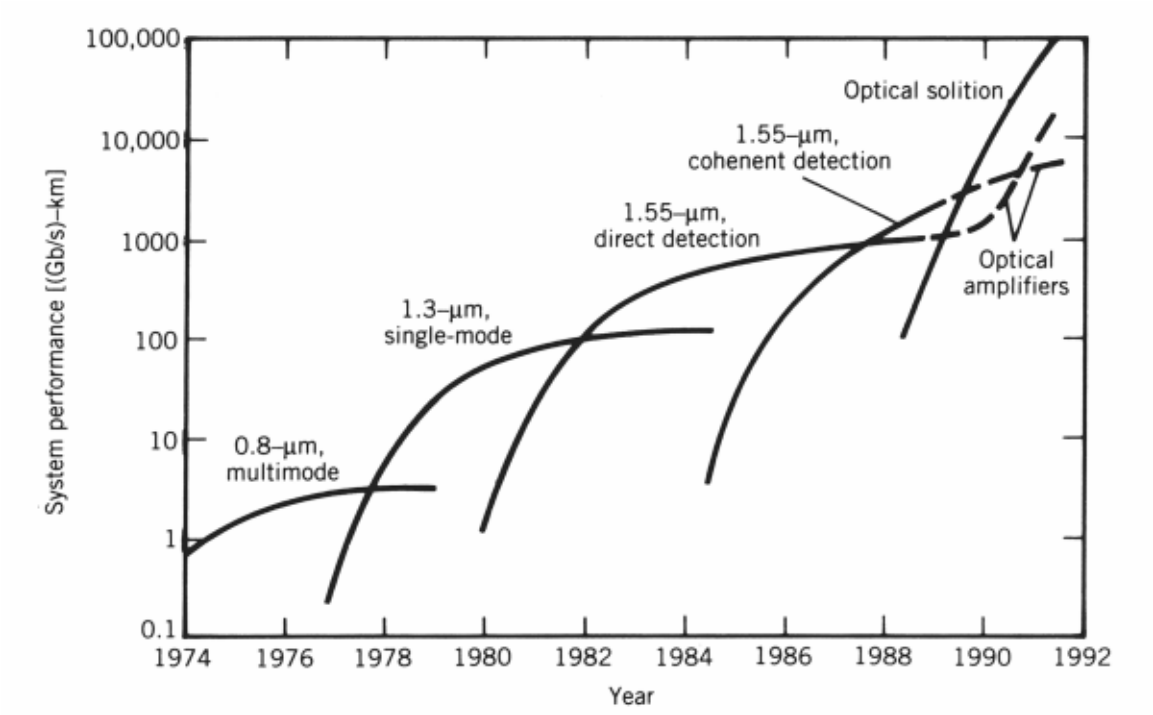

Fig. 1.2: Progress in lightwave communication technology over the period of 1974-1992. Different curves show the increase in the bit rate-distance product for five generations of fiber-optic communication systems [1].

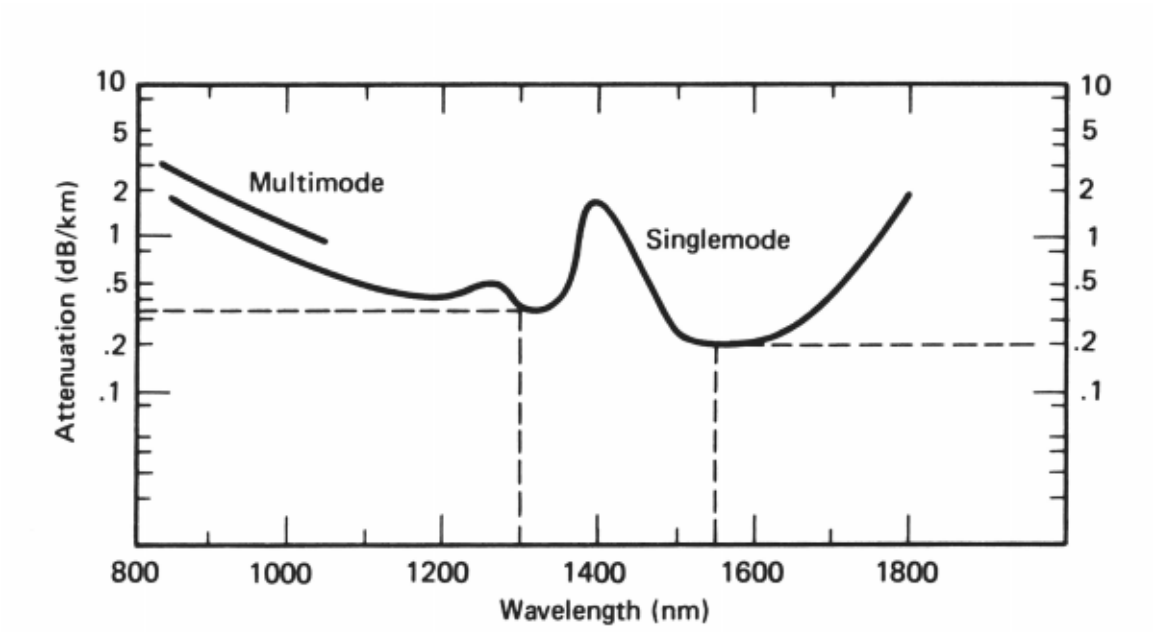

Fig. 1.3: Fiber attenuation (dB/km) versus wavelength (nm) [3].

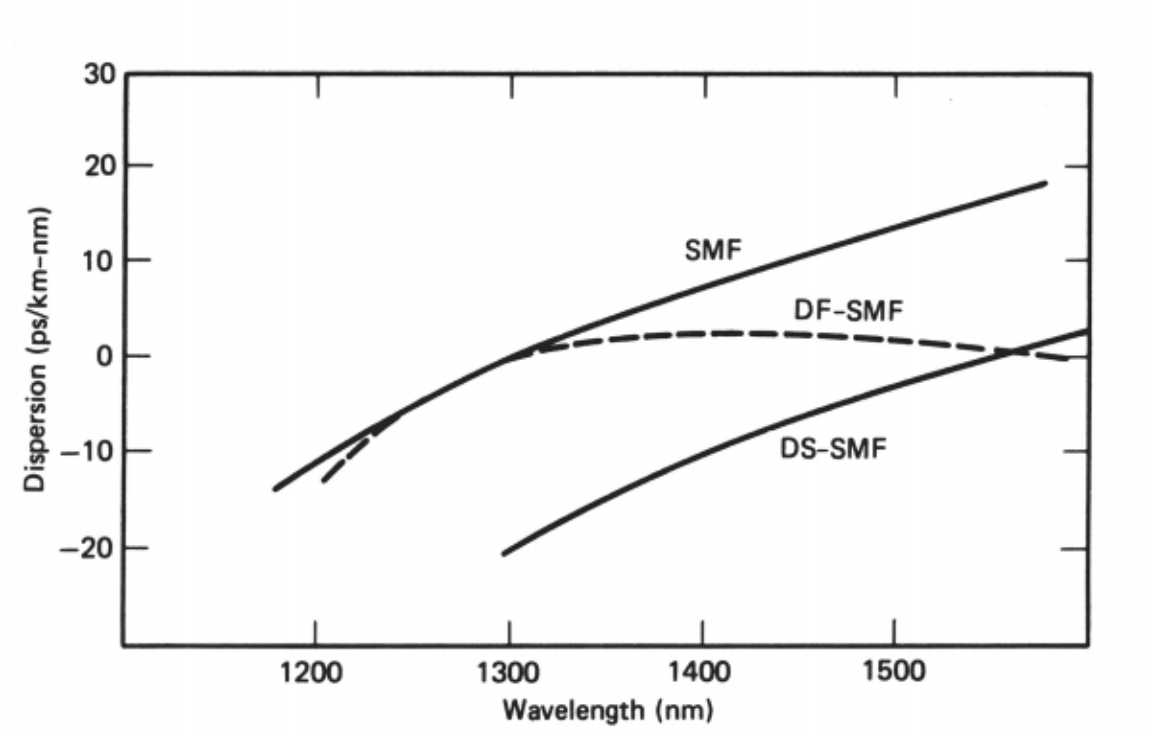

Fig. 1.4: Dispersion of single-mode fiber and dispersion-shifted single-mode fiber [3].

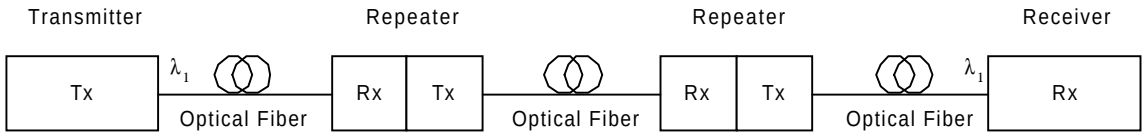

(a)

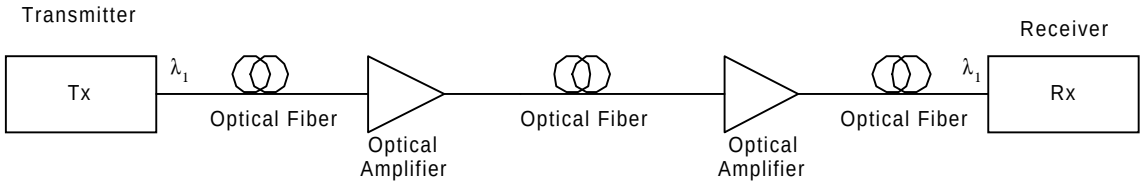

(b)

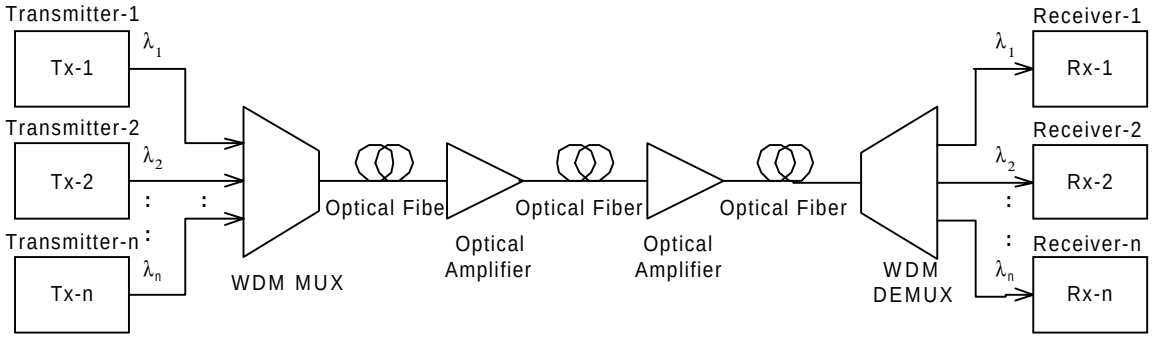

(c)

Fig. 1.5: Block diagrams of optical fiber communication systems: (a) conventional single-channel systems; (b) single-channel systems with optical amplifiers; (c) WDM systems with optical amplifiers.

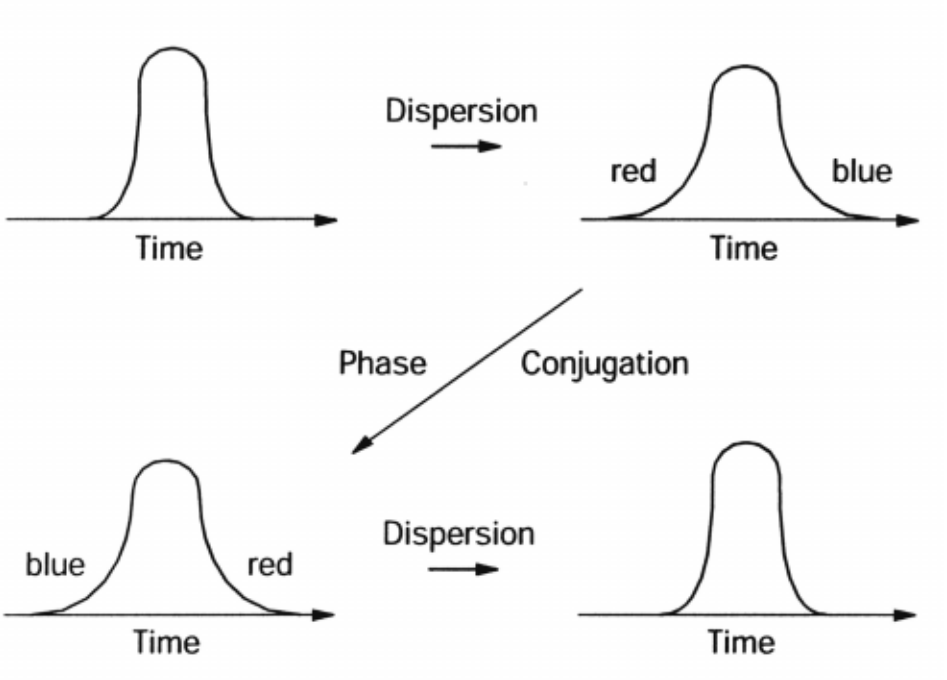

Fig. 1.6: Graphical explanation of phase-conjugation technique used to compensate for dispersion.

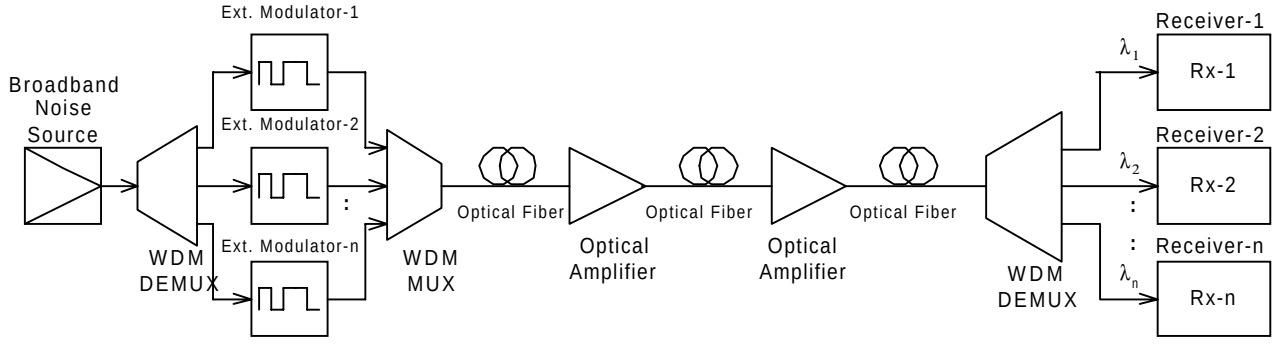

Fig. 1.7: Block diagrams of optical fiber communication systems employing spectrum-sliced WDM (SS-WDM) technique.

Chapter 2

OPTIMIZATION TECHNIQUES IN WDM SYSTEMS

This chapter is devoted to discussing the breakthroughs in lightwave technology that have resulted in the realization of wavelength division multiplexing (WDM) systems. One attractive aspect of the optical fibers is their enormous bandwidth compared to other media, such as radio waves and twisted-pair wires. The full bandwidth capability of fibers cannot be realized by time division multiplexing (TDM) techniques alone, and some channelization of the spectral band is required. However, there were technological obstacles to the implementation of WDM systems. In order to effectively implement WDM systems, broad-bandwidth optical amplifiers and WDM (de)multiplexers are required. The former is necessary to amplify all signals at different wavelengths simultaneously to compensate for unavoidable loss in all channels. The latter is used to combine or separate the signals at different frequencies to their corresponding destinations.

All limiting factors in single-channel systems, such as chromatic dispersion and fiber nonlinearity, still exist in the WDM systems Moreover, some factors exhibit more deleterious effects in the WDM systems. Hence, it is worth discussing the fundamental concepts and technologies of the WDM components and the techniques employed in practical systems to overcome the limiting factors. This chapter is organized as follows. Details of erbium-doped fiber amplifiers (EDFAs) are discussed and explained in Section 2.1, and the techniques to optimize and to enhance the EDFA capability and performance are discussed in Section 2.2. WDM (de)multiplexers, especially arrayed waveguide grating (de) multiplexers, are discussed in Section 2.3. In Section 2.4, the effect of fiber nonlinearity, and methods to minimize their impacts are explained. The last section, Section 2.5, is a summary of this chapter.

2.1 ERBIUM-DOPED FIBER AMPLIFIER

In the past, electronic regenerators were employed to periodically compensate for the loss in the optical fibers. This posed some limitations in system flexibility and capability. To increase the operating bit rate, the electronic equipment in the regenerator had to be modified to support the new bit rate. The basic function of electronic regenerators is to convert the optical signal to an electrical signal for signal processing, and then convert back to an optical signal. Therefore, electronic regenerators are not appropriate to be employed in WDM systems because each channel requires its own regenerator.

In order to compensate for the attenuation in all channels simultaneously and efficiently, it is essential that all channels are amplified optically. This is the main task of the optical amplifier. One additional benefit from optical amplification is that the process of amplification is independent of signal format. Thus, the amplifiers can operate at any bit rate, which results in ease of TDM upgrade. Most current optical communication systems operate in the 1.55 μm window which provide lowest attenuation. In this region, the most useful optical amplifiers are the EDFAs. Consequently, this section describes the fundamental concept of light amplification in the EDFAs [25], [26]. Their applications are discussed in the next section.

2.1.1 Principle of Operation

When an electromagnetic field is incident on an atom the electrons in the ground states may be excited to higher states. Since higher states are not stable, the excited electrons tend to fall down to the ground state again. This may result in the emission of electromagnetic radiation (non-radiative transitions are also possible). There are two distinct emission processes: stimulated emission and spontaneous emission. Stimulated emission is the physical mechanism of optical amplification whereas the other is the origin of undesirable noise, called amplified spontaneous emission (ASE) noise. Amplification occurs when the amount of stimulated emission is larger than the amount of absorption. That is, the amplification requires that the number of excited electrons needs to be larger than that in the ground state. This condition is called population

inversion. When this condition is satisfied, the optical signal, having the same wavelength as the energy gap between two states, will be amplified via stimulated emission. The population inversion can be achieved by injection of some energy into the medium, and the amount of injected energy must be sufficient to produce population inversion.

Not all of the excited electrons amplify the desired signal. Some may decay without interaction with the amplified signal. The electromagnetic field radiated from such emission would have random phase, polarization, and direction. It is referred to as spontaneous emission noise, which may then be amplified by stimulated emission. Therefore, the output noise is called amplified spontaneous emission (ASE) noise. The ASE noise is undesirable, but can be kept low by proper design of the amplifier.

2.1.2 Amplification Mechanism in Erbium-Doped Fiber

In the case of an EDFA, the medium of amplification, the so-called gain medium, is a silica-based optical fiber doped with erbium ions Er^{3+}. The energy-level diagram of the erbium ions in the silica fiber is shown in Fig. 2.1. Generally, the energy levels of an erbium ion are discrete and denoted by E_1, E_2, and E_3. However, each energy level is split into multiple sublevels when the erbium ion is surrounded by the silica glass. The interaction between individual erbium ions and the surrounding silica glass is different. Consequently, each energy level is spread into a continuous energy band when all of the interactions are considered. The optical signal, whose wavelength coincides with the energy difference between the E_2 band and E_1 band, would be amplified by stimulated emission. This suggests that the amplification occurs in a wavelength band rather than at a discrete wavelength. This characteristic of the EDFA makes it extremely attractive since multiple signals having distinct wavelengths could be amplified at once. In addition, the energy difference covers the wavelength range from 1525 nm to 1570 nm, which fortunately is the same as the low loss 1550 nm window in fibers.

As previously explained, the amplification process occurs when the population inversion is achieved. Therefore, there should be some scheme to inject the energy into the doped fiber to generate population inversion. Such energy injection is known as pumping, which can be performed by using a high-power laser whose operating

wavelength corresponds to an appropriate energy-level difference in the doped fiber. When an optical signal at the wavelength of 980 nm is injected into the doped fiber the electrons in the ground level E_1 are excited to the E_3 band, and then fall down to the E_2 band due to spontaneous emission with a lifetime of 1 μs. The excited electrons in the E_2 band will then fall down to the ground level, however, with the spontaneous-emission lifetime as large as 10 ms. Therefore, if the pump power is sufficiently high, the electrons in the ground state will be excited rapidly to the E_3 band. Shortly, they will drop down to the E_2 band. Since the lifetime between the E_3 and E_2 bands is considerably shorter than that between E_2 and E_1 bands, the excited electrons accumulate in the E_2 band. Thus, the population inversion is created, and the signals whose wavelengths correspond to the energy difference between E_2 and E_1 bands will be amplified.

Despite high population inversion when the EDFA is pumped at 980 nm, it is inefficient because the pump photon energy is so much larger than the signal photon energy. Higher pump efficiency can be achieved by pumping at 1480 nm, which corresponds to the energy difference between the top of E_2 band and the bottom of E_1 band. However, the amount of population inversion is less in this case; therefore, the ASE noise is higher for 1480-nm pumping. Both 980-nm and 1480-nm pumping schemes have their own advantage; thus, which pumping scheme should be employed depends on the specific application.

Although the combination of discrete energy sublevels of all erbium ions is continuous, the population of the sublevels is not uniform over the entire energy band. Thus, the gain profile of the EDFA is not uniform over its usable bandwidth, but rather it peaks around 1532 nm. The gain profile of the EDFA as a function of wavelength is shown in Fig. 2.2. The non-uniform gain profile poses a problem in WDM systems because the channels located at different wavelengths will experience different gains. This results in different signal to noise ratio (SNR), and consequently different performance of the individual wavelength channels. Consequently, gain equalization is required to eliminate the wavelength-dependent gain profile of the EDFA.

2.1.3 EDFA Configurations

The main components of an EDFA should at least consist of the erbium-doped optical fiber, the pump laser, and the wavelength-selective coupler. The last is used to couple the pump signal into the doped fiber. Additionally, an isolator is generally placed at the output of an amplifier to prevent back reflection, which can degrade amplifier performance or cripple the amplifier due to laser oscillation in the amplifier. Typically, the EDFA configuration can be categorized by pumping schemes into three particular arrangements, all of which have their own advantage. These schemes are forward-pumped (co-pumped), backward-pumped (counter-pumped), and dual-pumped. These are shown graphically in Fig. 2.3. The forward-pumped scheme as shown in Fig. 2.3 (a) provides high gain, and low ASE noise. This is because high population inversion at the input to the EDFA results in less spontaneous emission to be amplified in the doped-fiber; thus, less ASE noise appears at the output. On the contrary, the backward-pumped scheme will provide high output power with inferior noise figure. The dual-pumped or two-stage scheme is the optimized version combining the two schemes. With proper design, it can yield low noise and high output power. In practice, the dual-pumped scheme is often deployed with additional optical components placed between the two stages. Such optical components are designed to improve the performance of the EDFA. An example is to flatten the EDFA gain profile.

In addition to the pumping scheme, the pump wavelength is the other factor that affects the EDFA performance. Since the 980-nm pump wavelength provides high population inversion, it will result in high gain and low noise. Therefore, pumping the EDFA at 980 nm is suitable for realizing a low-noise amplifier, which can be employed as a preamplifier at the receiver. On the contrary, higher-power pump lasers whose wavelength is 1480 nm are commonly available. Therefore, an EDFA pumped at 1480 nm is desirable in applications that require high output power, such as a power amplifier at the transmitter to boost the signal power.

2.2 SNR EQUALIZATION AND EDFA OPTIMIZATION

As seen from Fig. 2.2, the gain profile of an EDFA is wavelength dependent. Although it is relatively flat, a cascade of EDFAs would result in increasing the non-uniformity of the gain profile. Additionally, a chain of EDFAs causes reduction in the

usable gain bandwidth due to self-filtering effect [27]. In multichannel systems, the wavelength dependence of gain profile would lead to different SNR among channels. Such SNR differential might results in unacceptable performance in some channels. The narrow usable bandwidth means that fewer channels can be employed. Therefore, uniform gain profile and wide usable bandwidth is preferable. Various techniques to minimize the SNR differential and to enhance the gain bandwidth have been proposed. Some of them are discussed in the following subsections.

2.2.1 Fluoride-Based Erbium-Doped Fiber Amplifiers [26], [28], [29]

The non-uniform gain profile of an EDFA is mainly due to interaction between the erbium ions and the surrounding silica host. Therefore, one way to reduce the wavelength dependence is to substitute the silica host with fluoride, which provides flatter gain profile. This type of amplifier is known as erbium-doped fluoride fiber amplifiers (EDFFAs) to distinguish it from erbium-doped silica fiber amplifiers (EDSFAs). Gain flatness of 2 dB extended beyond 28 nm can be achieved with this type of amplifier as shown in Fig. 2.4.

However, the major drawbacks of the EDFFAs are that they provide poorer noise performance than the EDSFA, and that they must be pumped at 1480 nm due to excited state absorption (ESA). As seen from fig. 2.1, the fluoride glass has additional E_4 energy level above the E_3 level. The energy difference between these two levels unfortunately corresponds to 980 nm. Therefore, some of 980-nm pump power will be absorbed and thus does not contribute to any useful gain. Despite these limitations, the EDFFAs have been successfully demonstrated in many experiments. One recent result showed that seven in-line EDFFAs provided sufficient gain and usable bandwidth to transmit 16 channels occupying 24 nm with bit rate of 10 Gb/s in each channel over 531 km of conventional fiber.

2.2.2 Pre-Emphasis Technique [27], [30], [31]

This technique makes use of the fact that the SNR differential is due to channel-power discrepancy at the receiver, which can be compensated by adjusting the transmitted powers. A schematic explanation of the pre-emphasis is shown in Fig. 2.5.

The algorithm is to increase the transmitted power of channels that suffer small gain, and to reduce the transmitted power of channels that experience high gain. Equalization of the powers or SNRs of all channels can be achieved; however, equalized SNRs is preferable because the performance depends on the SNR. Fig. 2.6 shows the results in one experiment. Eight channels, each at 1.7 Gbps, with 2-nm channel spacing are successfully transmitted over 840 km of a conventional single-mode fiber. The SNR differential among channels can be completely eliminated, which results in identical performance among channels

The main advantage of the technique is that it requires no modification of in-line EDFAs, and also does not depend on system parameters, such as, amplifier gain, and link losses. It requires only the values of unequalized SNRs in all channels at the receiver to compute the optimum transmitted power in each channel. That data can be sent back to the transmitter end via telemetry. In addition, the adjustment can be made in real time. However, the major drawback of this scheme is that the transmitted powers should be sufficiently large in order to cover the entire range of the required powers calculated from the algorithm.

2.2.3 EDFA Gain Profile Optimization by Passive Filters

This method is to place a passive filter in the middle of the EDFA [32]-[34], after the EDFA [35], [36], or periodically after multiple EDFAs [37]. The filter is intended to minimize the wavelength dependence of the gain profile, and maximize the usable gain bandwidth. The transmission characteristic of the filter compensates for the wavelength dependence of transmission characteristic of the EDFAs; hence, the overall transmission characteristic is flatter and broader than that without the filter. Many types of filters have been proposed in the literature; they are a Mach-Zehnder optical filter [35], Bragg-grating filter [36], and long-period grating filter [33], [34], [37].

The benefit of employing passive optical filters is their reliability – passive components are more reliable than active ones. However, they lack flexibility and ability to dynamically track changes in gain profile. Among the various types of optical filters the long period grating filters are most promising due to their ease of fabrication, low cost, low back reflection, and low temperature sensitivity [34], [38]. In addition, the filter

is all-fiber, which results in low insertion loss. The basic concept of the long-period grating is to scatter the light at specific wavelengths to the lossy cladding of the optical fiber. Such scattering can be accomplished by mean of periodic perturbation of the index of refraction in the fiber core. Additionally, the transmission characteristic of the long-period filter can be tailored by employing multiple gratings.

For example, the dual-pumped EDFA as shown in Fig. 2.7 (a) employs the long-period grating filter [34]. The transmission characteristic of the grating filter is computed by using measured parameters of the EDFA. The filter consists of three long-period gratings. The combined transmission characteristics nearly follow the computed one as shown in Fig. 2.7 (b). From Fig. 2.7 (c), it is clearly seen that the resultant gain spectrum provides approximately 22 dB of gain over a 40-nm bandwidth. This extremely wide bandwidth could considerably magnify the throughput of the system compared to that employing EDFAs without gain equalization.

2.2.4 EDFA Gain Profile Optimization by Active Filters

It should be noted that the gain profile of each EDFA is different depending on amplifier condition, such as pump condition. Moreover, the gain profile changes with time due to aging, input signal power, etc. Therefore, it is desirable to dynamically flatten the EDFA gain profile. The adaptive gain flattening could be achieved by making use of an active filter whose transmission characteristic can be tailored to flatten the resultant gain profile. The active filter could be a tunable Mach-Zehnder (MZ) filter [39]-[41], or an acousto-optic tunable filter (AOTF) [42], [43].

The configuration of the MZ filter is shown in Fig. 2.8. Two tunable symmetric MZ interferometers are joined together by two waveguides having different lengths. The tunable characteristic is obtained from three phase shifters made of chromium (Cr) heaters to change the refractive index of the corresponding waveguides. The tunable MZ filter has a sinusoidal transmission characteristic whose period is determined by the length difference between the two main waveguide paths. Two tunable symmetric MZ filters act as tunable couplers, which can be used to adjust the extinction ratio of the filter. The phase shifter in the middle is used to adjust the center wavelength of the filter. As a result, the wavelength dependence of the EDFA gain profile is compensated by the

adjustable slope and center wavelength of the filter. The tunable MZ filter can be placed after each EDFA or after several EDFAs; however, the latter is desired. With the MZ filter placed at the middle of the link, transmission of 128 channels, each at 622 Mbps, was demonstrated over 480 km of dispersion-shifted fibers with power penalty among channels less than one dB [41].

Another type of active filter that can be employed to flatten the EDFA gain profile is the AOTF. This device makes use of the interaction of a sound wave and a light wave. The acoustic wave launched in the fiber causes periodic change in the density of the medium. This periodic perturbation gives rise to acoustooptic mode conversion of the optical wave from the fundamental mode to distinct cladding modes. The transmission characteristic of the AOTF is determined by the frequency and amplitude of the launched acoustic wave. The acoustic wave is generated by an acoustic transducer, which converts the electrical signal to an acoustic signal; therefore, the device can be controlled externally and electrically. Moreover, launching multiple acoustic signals having different amplitudes and frequencies enables us to adjust the resultant spectral characteristic of the filter to best fit to the EDFA gain profile. Since this device can be made all-fiber, its insertion loss can be less than 0.9 dB. When it is employed as a mid-stage device in the double-stage EDFA, a gain flatness of less than 0.7 dB over the usable bandwidth of 35 nm was achieved [43]. The AOTF can also be placed after several EDFAs to equalize the SNR among channels. Simulation in [42] showed that the SNR discrepancy among nine channels reduced from 18.2 dB to 2.4 dB by placing the AOTF after every 10 EDFAs in a total transmission distance of 10,000 km.

2.3 WDM (DE)MULTIPLEXER

Prior to the development of WDM (de)multiplexers, the only (de)multiplexers available were power splitters or combiners. These devices are not wavelength-selective; therefore, the (de)multiplexing function is not power efficient. As the number of channels increases, the splitting loss also increases. Therefore, it is desirable that a WDM (de)multiplexer be wavelength-selective. The function of a WDM multiplexer is to combine the signals at different wavelengths or frequencies. On the other hand, a WDM demultiplexer separates the signals at different wavelengths to the corresponding output

ports. These two functions are graphically displayed in Fig. 2.9 (a) and (b). As seen from this figure, both functions have a reciprocal relationship with each other; therefore, they are generally built from the same device. Among proposed multiplexers, arrayed waveguide grating WDM multiplexers are most attractive due to their superior performance, which will be discussed later in this section.

2.3.1 Arrayed Waveguide Grating (AWG) Multiplexer

The design concept of the WDM (de)multiplexer based on arrayed waveguide grating (AWG) was firstly proposed by Dragone [44], [45]. It consists of two $N \times M$ slab waveguides connected together by M arrayed waveguides having constantly increasing length as shown in Fig 2.10 [46]. The slab waveguide at the input acts as a $N \times M$ coupler – it combines N input signals and evenly splits them to M output. The input signal from any of the N input waveguides is split into M parts, which are fed to the corresponding arrayed waveguides. At the output $M \times N$ coupler, all M signals are combined, and distributed among the N output ports. The difference in distances that the individual M signals propagate causes relative phase shifts between them. The waveplate placed in the midway point of the arrayed waveguides as shown in Fig. 2.10 is used to minimize polarization dependence of the device [46]. Since the relative phase shifts are a function of the wavelength, the interference at the output slab waveguide results in specific wavelengths emerging from the output ports for a given input port. That is, the interference gives rise to input-output port mapping for a given wavelength.

Since the AWG multiplexer can be fabricated by using silica-based waveguide technology, its size can be as small as 3 cm×4 cm [46], and it can be produced at low cost [47]. Additionally, it exhibits low insertion loss due to its compatibility with a single-mode fiber [47]. The insertion loss, including fiber-waveguide connection loss waveguide propagation loss, and grating loss, of 3 dB has been reported [46]. With proper design, the AWG multiplexer will also exhibit loss uniformity among different wavelengths [48]. This results in the reduction of the SNR discrepancy among channels, which is important in WDM systems.

One additional benefit of the AWG multiplexer is that it can be constructed to exhibit negligible temperature dependence [49]. This is important in field application

because equipment for temperature control is not necessary when the device is temperature-insensitive. All of these benefits have made AWG multiplexers attractive in many applications. In addition, an AWG multiplexer can be employed as an add-drop multiplexer in an intermediate node.

2.3.2 Add- Drop Multiplexer [52]

The main function of an add-drop multiplexer is to add and drop any wavelength channel at an intermediate node without affecting the other channels in a WDM system. The add-drop functionality enhances network flexibility as well as capacity since the dropped wavelength can be reusable. Several devices, such as Mach-Zehnder-based fiber gratings [50], and Bragg gratings with circulators [51], can also perform the add-drop function. However, they are not widely-used in practice; thus, only an add-drop multiplexer using an AWG multiplexer is discussed here.

An AWG multiplexer can be employed as an add-drop multiplexer as shown in Fig 2.11. An $N \times N$ AWG multiplexer as shown in this figure is capable of performing an add-drop function up to $N-1$ channels. All N optical signals at different wavelengths are fed to the common input port. Due to input-output mapping property of the AWG multiplexer, each signal will appear at its corresponding output port. Then, all $N-1$ output signals are looped back to their corresponding ports as shown in Fig. 2.11. This results in all N signals being multiplexed again, and the multiplexed signals will appear at the common output port as shown in Fig. 2.11. By opening the loop-back path, the corresponding signal can be dropped and added. The dropped signal will appear at the output of the opened path while the signal having the same wavelength can be added at the input port of the same opened path.

As in the case of a normal WDM multiplexer, all N signals fed to an add-drop multiplexer will experience loss imbalance due to the N signals having different paths. The further away the signal is from the center wavelength of the multiplexer, the higher loss it experiences. Fortunately, the loss imbalance can be minimized by properly selecting the common input port, the common output port, and the loop back connections [53]. Moreover, by employing two $N \times N$ AWG multiplexers in conjunction with N crossbar switches, a reconfigurable add-drop multiplexer can be created [54]. It is capable

of arbitrarily adding and dropping multiple channels up to $N-1$ channels. This capability provides unprecedented flexibility in network management. The number of added/dropped channels can be configured based on the traffic that varies with time; thus, systems are utilized efficiently.

2.4 Fiber-Nonlinearity Alleviation

One factor that degrades the system performance is the optical fiber nonlinearity, which depends on the amount of total signal power injected into the optical fiber. The nonlinear effects give rise to signal distortion, interference, and SNR degradation. In general, high injected power is desired in order to enhance the system throughput, such as, transmission distance, operating bit rate, and system performance. However, the detrimental nonlinear effects will be manifolded when the injected power is increased. In WDM system, these nonlinear effects will be enhanced since the total optical power injected into the fiber is the sum of individual channel powers. The major nonlinear effects causing degradation in WDM lightwave systems are [55]:

Stimulated Raman Scattering (SRS): It is the result of interaction between the incident light and molecular vibrations. When two optical waves having different wavelengths travel along the fiber, the longer-wavelength will be amplified via the energy transfer from the shorter-wavelength wave. This nonlinear effect will cause excess signal loss in the shorter wavelength channel.

Cross Phase Modulation (XPM): Refractive index is power dependent. A certain channel can cause nonlinear phase shift in the other channels since index of refraction depends on the total optical power of all channels. This leads to interchannel interference called crosstalk.

Stimulated Brillouin Scattering (SBS): This nonlinear effect is due to the interaction between the optical signal and acoustic vibration in the fiber. Its resultant effect will exhaust energy of the incident optical signal and generate another counter-propagating signal scattered back to the transmitter.

Four-Wave Mixing (FWM): Power dependence of refractive index also causes intermodulation products among optical signals traveling along the fiber. If there are three optical waves propagating along the fiber with frequencies denoted

by f_1, f_2, and f_3, the FWM process will generate an additional nine optical signals at frequencies $f_{ijk} = f_i + f_j - f_k$ where i, j, and k can be 1, 2, or 3 as seen in Fig. 2.12. These new generated signals can interfere with the desire signals.

Among all of these nonlinearities, the FWM is the most deleterious effect [27]. In WDM systems, if all channels are equally spaced, the new generated signals will coincide with the intended signals. This results in crosstalk and depletion of intended signals.

The FWM efficiency depends on several factors [56]. One factor is that the FWM process requires phase matching among channels, which can be readily obtained when all signals are located near the zero-dispersion wavelength. However, FWM efficiency is reduced if there is dispersion fluctuation along the fiber, which is common in practice. The other factor is channel spacing. The larger the channel spacing, the poorer the FWM efficiency. This is because larger channel spacing leads to higher dispersion discrepancy, which reduces the possibility of phase matching.

Unequally spaced channel allocation (USCA), and dispersion mapping are the techniques that can be employed to combat the FWM effect. Both techniques apply different approaches to minimize the FWM effect, and can be employed together to effectively decrease the deleterious effect of the FWM process. They are discussed in following subsections.

2.4.1 Unequally Spaced Channel Allocation (USCA) [27]

The new generated signals resulting from the FWM process will be located at the same frequencies as the intended signals if the signals are equally spaced. The simplest way to avoid such collocation is to assign unequal frequency spacing among channels as shown in Fig. 2.12. In this method, the FWM efficiency is not completely eliminated; however, its effect, which can cause crosstalk, is avoided. As a result, the FWM process only leads to loss of signal power when the USCA is employed.

The advantage of USCA is that it requires no modification of the transmission media – only the frequency selective components along the transmission link need to be matched with the channel allocation. In order to take advantage of this technique in WDM systems, AWG multiplexers need to have unequal channel spacing. Fortunately,

unequal channel spacing AWG multiplexers with low insertion loss are available [57]. Those AWG multiplexers can also be modified to serve as add-drop multiplexers [58]. One experiment has confirmed the possibility of employing unequal channel spacing AWG multiplexers. The transmission of 10 channels $\times$ 10 Gb/s over 240 km of dispersion-shifted fiber, including an add-drop multiplexer, has been successfully demonstrated [58]. In that experiment, three channels were added and dropped at the intermediate node with a power penalty of less than 2 dB.

2.4.2 Dispersion Mapping [9], [59], [60]

As stated earlier, the efficiency of the FWM process depends on channel spacing, and phase matching among channels. This phase matching is easily met in systems employing dispersion-shifted fibers when channels are located near the zero-dispersion wavelength. Although locating all channels far apart from one another can reduce the FWM efficiency, this results in fewer channels for a given usable bandwidth of a transmission link. Moreover, the usable bandwidth of the transmission link employing EDFAs is reduced as the transmission distance increases due to the self-filtering effect of cascaded EDFAs [27]. Therefore, it is desirable that all channels be located as close as possible while the total dispersion that channels experience should be kept at a minimum to avoid intersymbol interference.

Since dispersion prevents phase matching among channels, at any point along the transmission link, the local dispersion should be nonzero to minimize FWM effect. On the other hand, the end-to-end dispersion should also be small to avoid pulse distortion. These two requirements cannot be achieved simultaneously in conventional lightwave systems. The answer to this problem, known as dispersion mapping, is to alternately employ two types of optical fibers having opposite dispersion values, which is shown in Fig. 2.13. In this example, negative dispersion fibers and conventional single-mode fibers are employed along the transmission link carrying eight channels, each at 5 Gb/s. A negative dispersion fiber of length 900 km is alternated with a conventional single-mode fiber along the transmission link. These fibers provide nonzero dispersion along the transmission link while their total dispersions are zero at the receiver end. It should be noted that only one channel in a WDM system can be managed to achieve zero dispersion

from end to end. Therefore, appropriate fibers are attached to the other channels at the receiver to return the total dispersion to zero value. This technique is superior to the USCA in the sense that the FWM process is suppressed. However, it cannot be deployed in installed systems.

2.5 SUMMARY

In this chapter, two important devices in WDM systems were discussed. They are the erbium-doped fiber amplifier (EDFA), and the arrayed waveguide grating (AWG) multiplexer. Both enable the realization of high throughput WDM systems. Various techniques employed to optimize and to maximize the system performance were also discussed. The next chapter will deal with a specific type of WDM system known as spectrum-sliced WDM (SS-WDM) systems. The sources used in these systems are noise-like instead of deterministic, which make them substantially different from the laser-based systems. However, these systems still utilize the amplifier and filter technology discussed in this chapter.

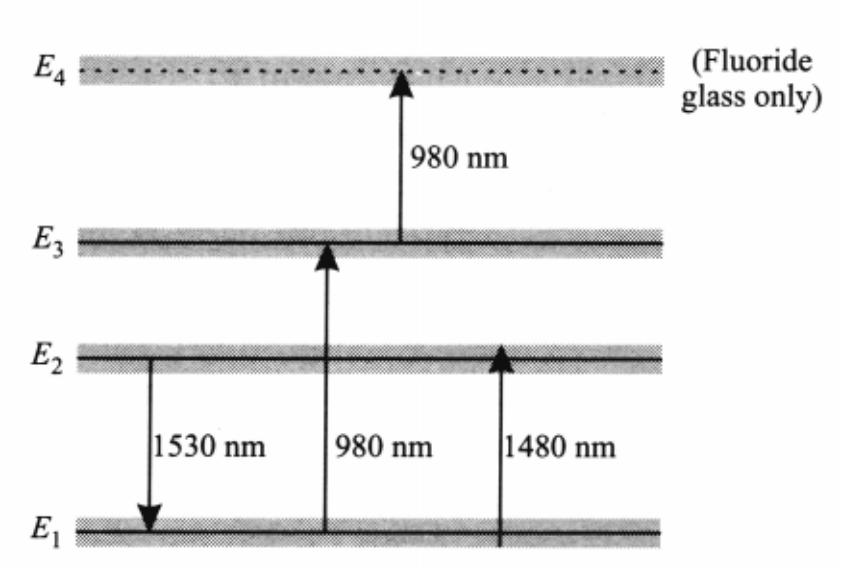

Fig. 2.1: Energy-level diagram of Erbium ions in silica-based fiber and fluoride-based fiber. The wavelength in nm corresponds to the difference of photon energy between two levels [26].

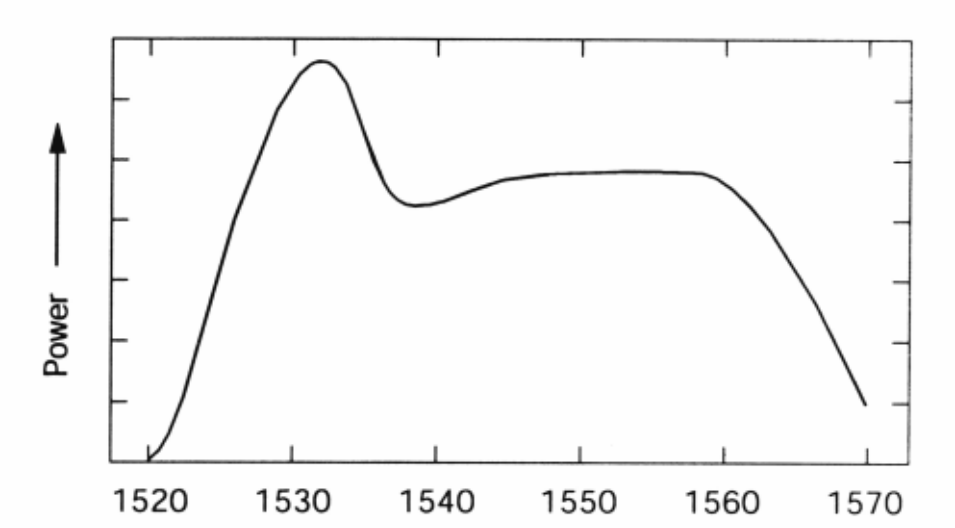

Fig. 2.2: Gain profile of the typical EDFA as a function of wavelength [6].

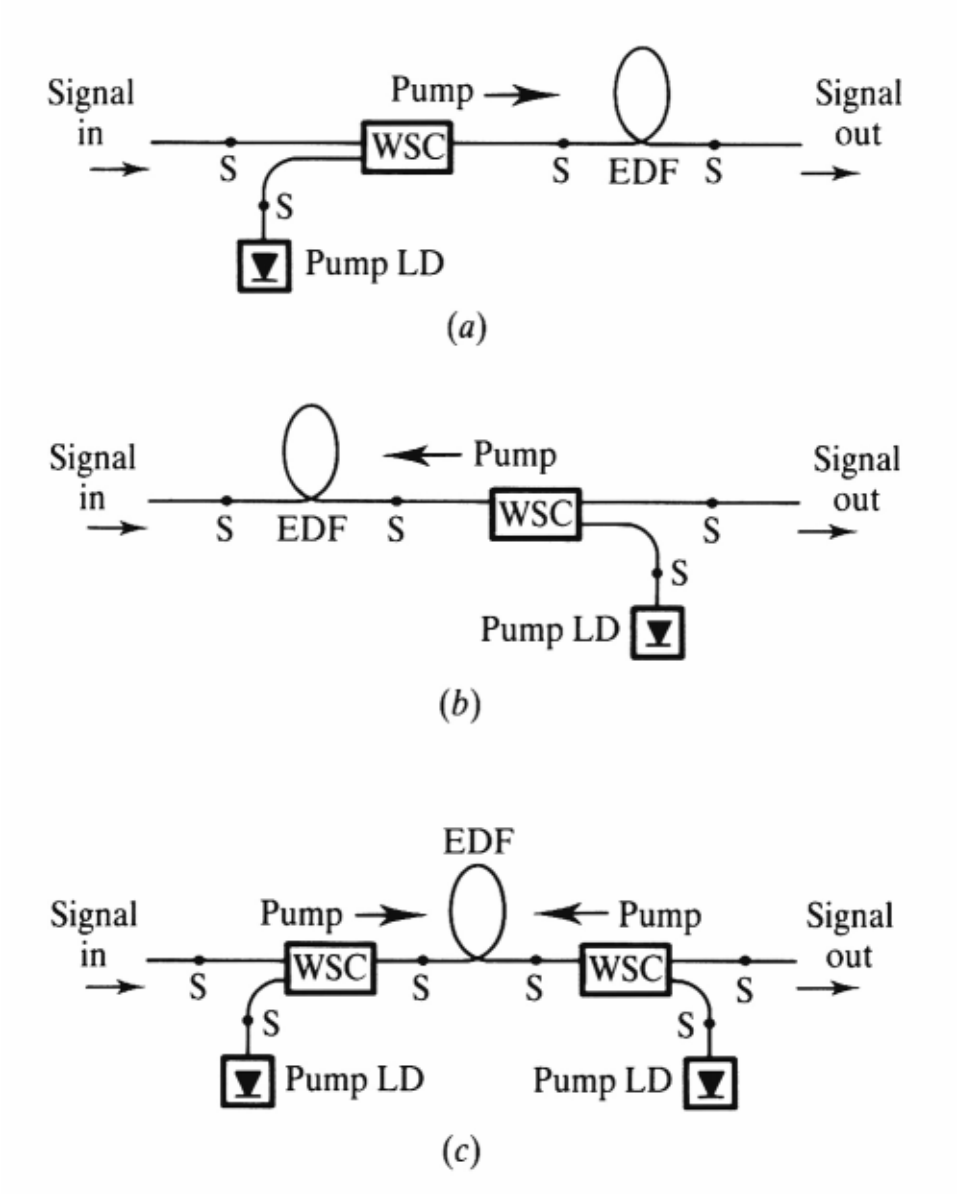

Fig. 2.3: Basic EDFA device architectures: (a) with unidirectional forward pumping, (b) with unidirectional backward pumping, and (c) with bidirectional pumping. **S**: fiber splice, **WSC**: wavelength selective coupler, **EDF**: Erbium-doped fiber [25].

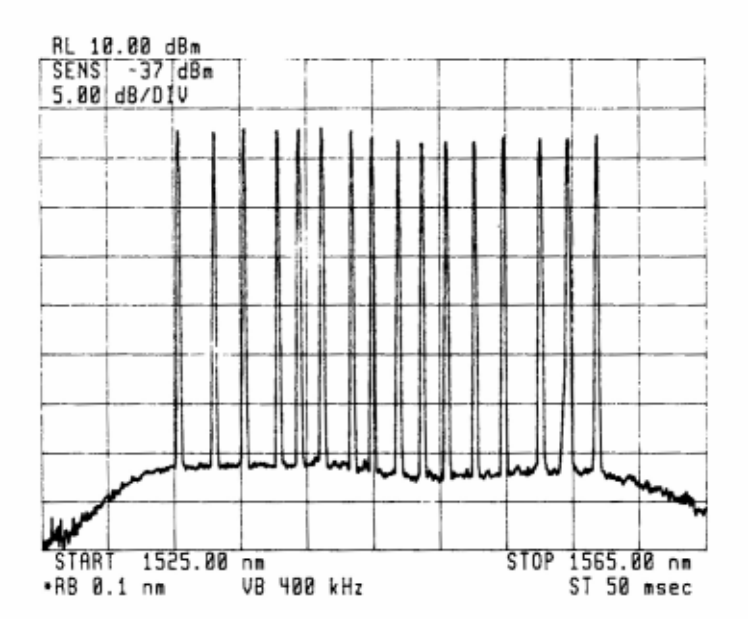

Fig. 2.4: Typical output spectrum of an EDFFA, showing a 16-channel multiplex spanning 25.2 nm [29].

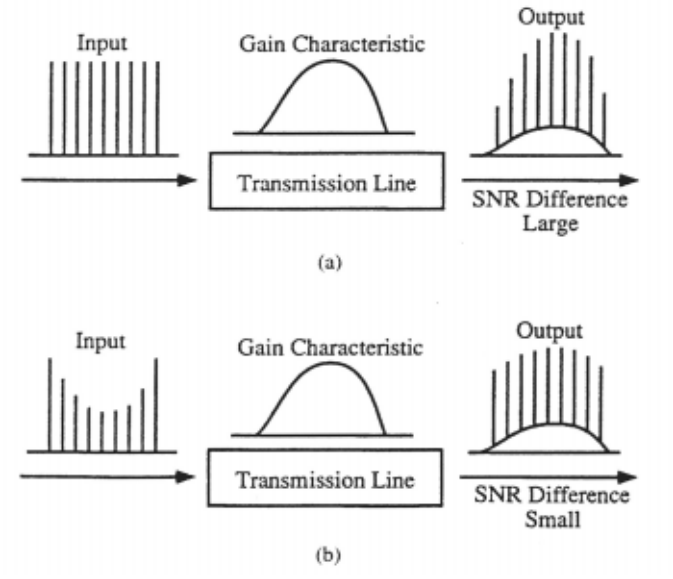

Fig. 2.5: A schematic explanation of the pre-emphasis technique. (a) Conventional WDM system. (b) Pre-emphasis WDM system [27].

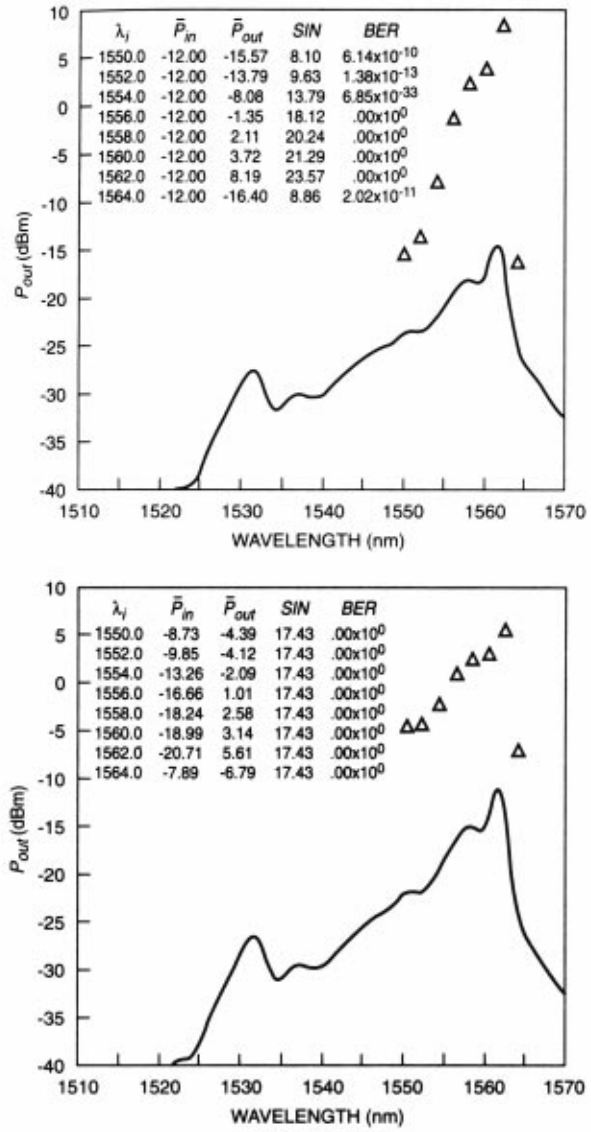

Fig. 2.6: Upper figure shows output powers after 840-km transmission without SNR equalization while the lower figure shows the output powers using SNR equalization. Solid curve denotes ASE noise in 0.2 nm optical bandwidth. Triangles denote signal powers. Inset lists signal wavelengths, input/output powers, SNR (ratio of signal power to noise power in a 0.2 nm optical bandwidth), and calculated bit-error rate (BER) [30].

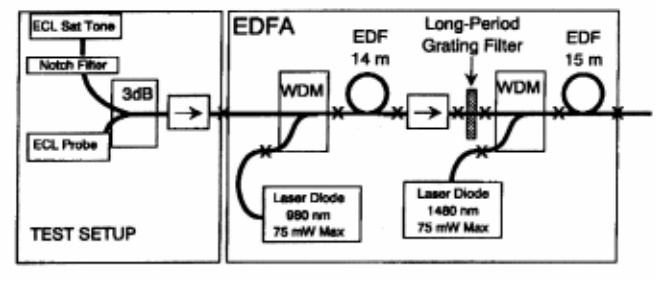

(a)

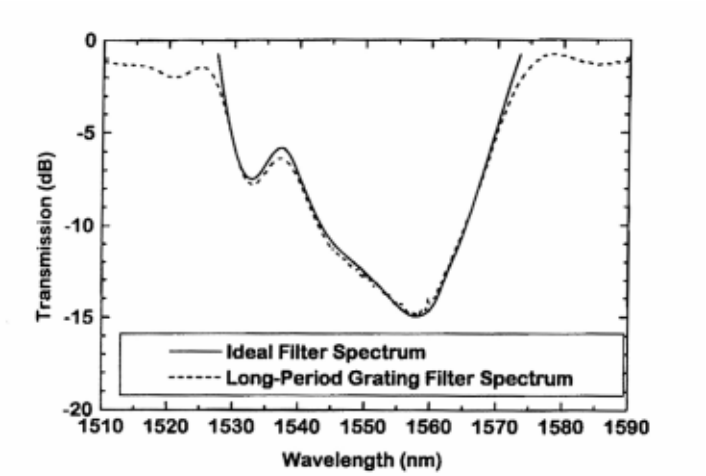

(b)

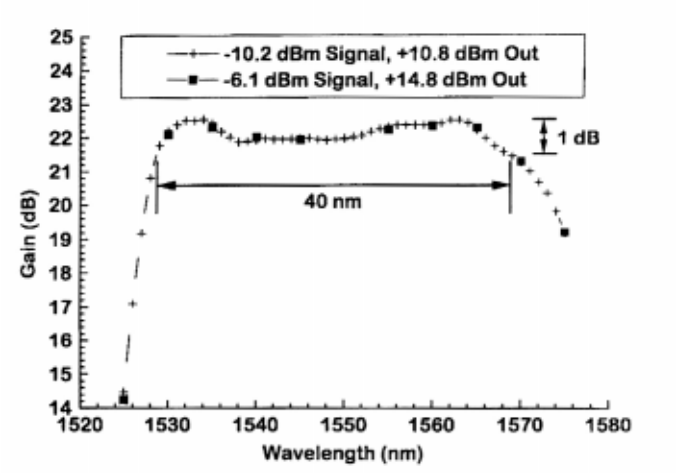

(c)

Fig. 2.7: (a) Schematic of flat EDFA using long-period grating filter. (b) Spectrum of long-period grating filter used in flat EDFA and the ideal spectrum for the design computed using modeling parameters. (c) Detailed composite gain spectrum for flat EDFA for two signal levels. Stage 1was pumped by 76 mW at 980 nm. Stage 2 was pumped by 34.5 mW and 74.5 mW at 1480-nm pump for the two cases [34].

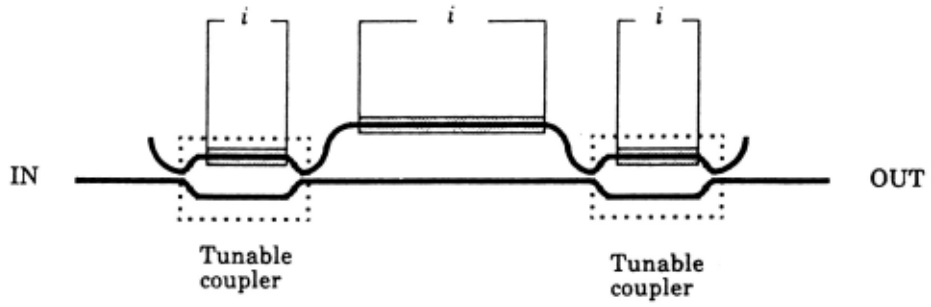

Fig. 2.8: Configuration of MZ filter used as tunable equalizer.

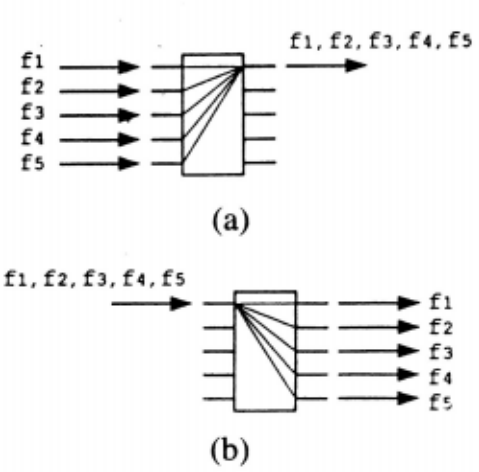

Fig. 2.9: Basic functions of $N \times N$ WDM multiplexer. (a) Multiplexing. (b) Demultiplexing [46].

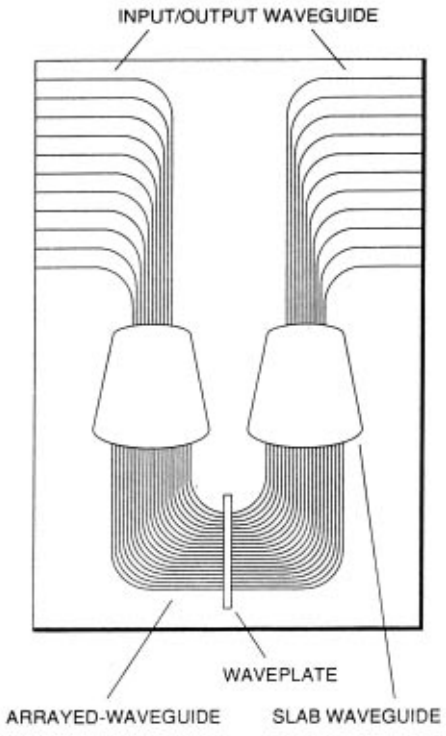

Fig. 2.10: Schematic waveguide layout of arrayed-waveguide $N \times N$ multiplexer [46].

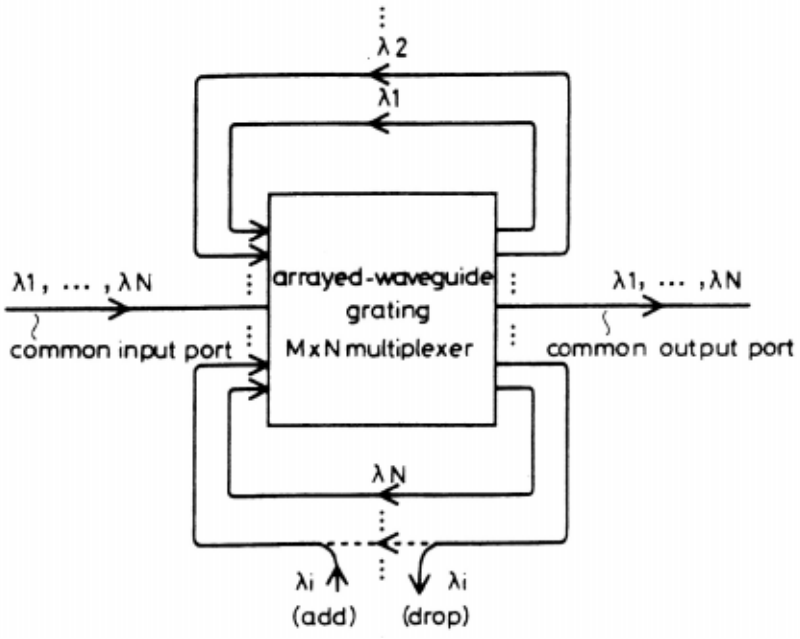

Fig. 2.11: Configuration of an add-drop multiplexer [52].

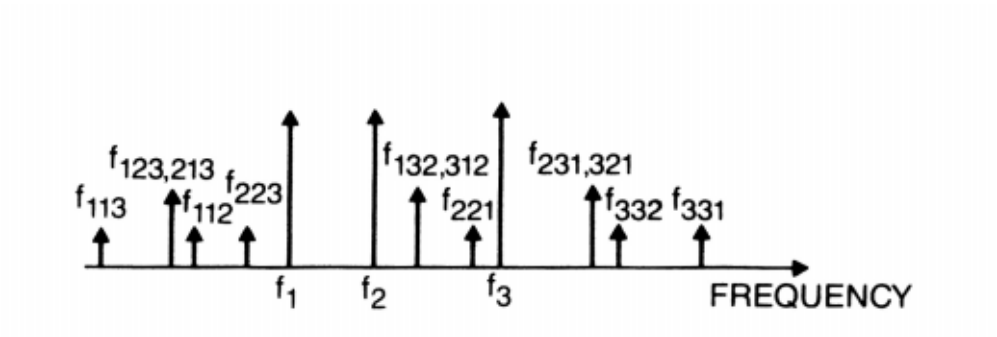

Fig. 2.12: Four-wave mixing with three injected waves at frequencies f_1, f_2, and f_3. The generated frequencies $f_{ijk} = f_i + f_j - f_k$ [55].

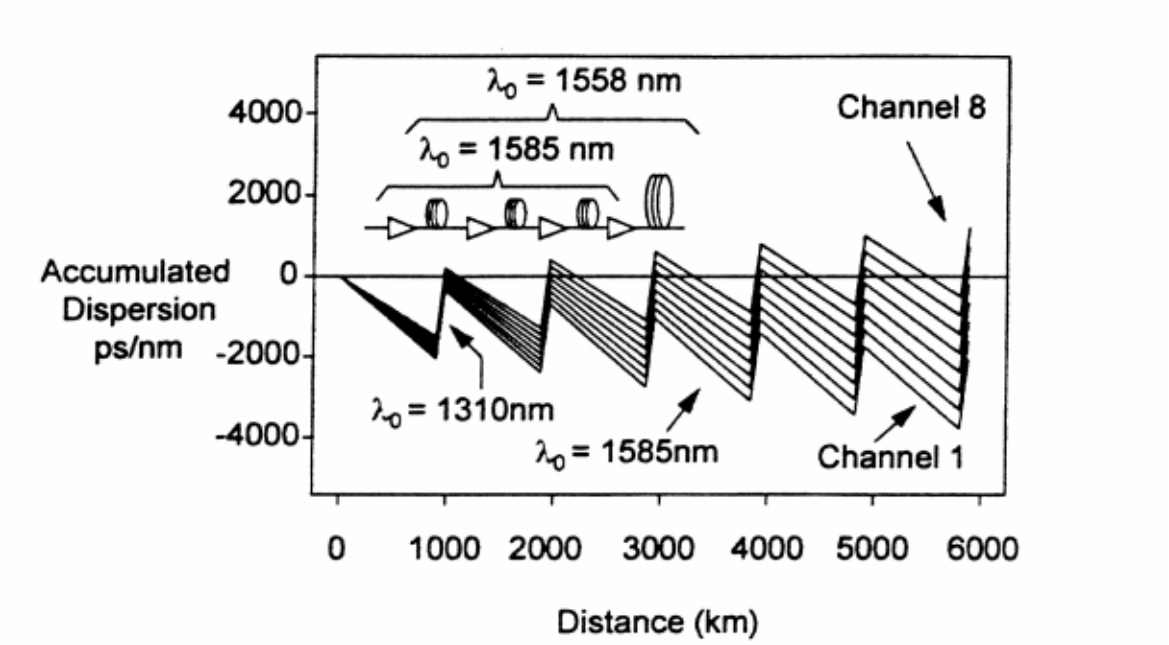

Fig. 2.13: Accumulated chromatic dispersion versus transmission distance for eight channels of a WDM transmission experiment. The majority of the amplifier spans use negative dispersion fiber $\lambda_0 \approx 1585$ nm and $D \approx -2$ ps/km-nm. The dispersion is compensated every 1000 km using conventional single-mode (i.e., $\lambda_0 = 1310$ nm) [9].

Chapter 3

SPECTRUM-SLICED WDM SYSTEMS

In this chapter the development and advances in spectrum-sliced WDM (SS-WDM) systems are discussed. The sources employed in SS-WDM systems are completely different from those used in conventional WDM systems. In SS-WDM systems, the transmitters are broadband noise sources; therefore, design criteria and strategy used in both types of systems are quite different. Thus, it is interesting to discuss some aspects of SS-WDM systems in this chapter. Details of the discussion in this chapter provides background knowledge, important in the next chapter, which contains the primary results of our research.

3.1 SS-WDM EVOLUTION

Today's world is the world of broadband communications. In the past, high-speed communications were restricted to the backbone telephone networks due to the cost of the necessary equipment. It has been long realized that broadband access is also beneficial to end-users. Many applications, such as video on demand and teleconferencing, require high-speed connection to subscribers. However, cost and complexity of systems have prevented installation of broadband systems dedicated for those services. There are the attempts to utilize the existing cable-TV networks and local-loop telephone networks to provide broadband access to customers. Since those networks were not designed to provide broadband access, limitations and complexities are unavoidable in providing broadband access in such networks.

The installation of fiber optic systems seems to be the primary solution to fulfill demands for broadband access. The incomparably huge bandwidth provided by the optical fibers is ideally suitable for broadband access. Although the technology in conventional lightwave systems is capable of providing broadband access to customers,

the cost of such systems is of great concern. The cost of fiber-based broadband systems is often too high for them to be economically viable for such applications. A solution, which will result in cost reduction, is to share components among as many users as possible, and to avoid the deployment of expensive equipment. These two concepts led to the development of passive optical networks (PONs).

3.1.1 WDM PON

Cost sharing in PONs is achieved by sharing a single fiber among customers. In addition, all deployed components between the transmitter and receivers are passive in order to reduce maintenance cost and network complexity. There are several transmission schemes deployed in PONs to increase the degree of cost sharing among users; they are TDM, subcarrier multiplexing, and WDM. However, the WDM scheme is the most technically beneficial since it provides point-to-point connections between the central office (CO) and particular optical network units (ONUs), and higher security and privacy due to the wavelength-selective property of WDM (de)multiplexers [20]. In addition, the active components are operated at individual channel bit rates, compared to the TDM scheme which operates at an aggregate bit rate. Thus, the processing requirements in the components are less.

However, a WDM PON requires transmitters that can be tuned to particular wavelengths. These transmitters are usually tunable lasers. Therefore, they require wavelength-stabilizing devices to control their wavelengths to match those of the wavelength-selective components in the networks. These tunable lasers and their necessary components have obstructed widespread installation of WDM PON due to their high cost although the advantages provided by WDM PONs are extremely attractive. This led to the introduction of SS-WDM PONs.

3.1.2 SS-WDM PON [61]

Instead of employing expensive tunable lasers, SS-WDM PONs are equipped with less expensive LEDs. However, cost reduction is achieved with lower output power and slower speed LEDs. The name “SS-WDM” is gained from the fact that these systems utilize LEDs whose output power spectra are considerably broader than conventional

lasers, and the distinct operating wavelengths are obtained from wavelength-selective characteristic of components in networks. The schematic explanation of SS-WDM system is shown in Fig. 3.1. The output power spectra of all LEDs are sliced by the WDM multiplexer located at the transmitter end. Since passbands of corresponding input ports of a WDM multiplexer have different center wavelengths, a different slice is assigned to each ONU.

SS-WDM systems offer several technical advantages over laser-based WDM systems. Identical LEDs are used in all transmitters; therefore, the systems are easy to maintain. They are more reliable because LEDs have longer lifetime than lasers. Additionally, components in the networks that have to be wavelength-controlled are only WDM multiplexers and demultiplexers located at each end of the PONs. Since these devices are usually AWG multiplexers, which can be fabricated to have temperature-insensitive property [49], the wavelength-control function might not be necessary.

3.1.3 Limitations of SS-WDM PONs Employing LEDs

From an economical point of view, SS-WDM PONs employing LEDs are better than those using lasers. However, LEDs are slower and produce less output power than lasers. Furthermore, there is an additional loss inherent in SS-WDM systems, called slicing loss. This loss results from the fact that only a portion of the output power spectrum of each LED will pass the multiplexer at the transmitter end. This slicing loss can be as large as 18-dB [62]. This loss poses stringent power budget limitations in SS-WDM systems employing LEDs, compared to laser-based WDM systems. Therefore, the first generation of SS-WDM systems is usually limited to local loop applications where the bit rate and distance are not large.

Moreover, the output power spectrum of an LED is not flat over the operating-wavelength range. When this is combined with loss imbalance among channels caused by WDM (de)multiplexers in the system, the performance discrepancy among channels is unavoidable [61]. This may result in some channels being inoperable for a given bit rate and transmission distance. Thus, the number of channels that can be utilized is limited.

It is appropriate to briefly mention at this point that the output signal from an LED is due to spontaneous emission. Its mechanism is similar to that of thermal noise in

electronic devices; therefore, the output signal will fluctuate with time like well-known thermal noise. Since the photodetector at a receiver obeys a square law, there is an additional noise term due to beating among signal components located at different frequencies. This was first pointed out by Liu [63]. This signal-signal beat noise, usually called excess beat noise, will limit achievable SNR at a receiver. Therefore, the excess beat noise can cause BER floor due to insufficient SNR when it is the dominant noise at a receiver.

The excess beat noise is inversely proportional to the optical bandwidth per channel, and increases with the electrical bandwidth of the lowpass filter at the receiver. The explanation of this phenomenon is described in detail elsewhere in this chapter. The bandwidth of the lowpass filter is usually determined by the operating bit rate. It is generally kept sufficiently narrow to minimize the thermal noise generated from electrical components in the receiver while it should be large enough to avoid unacceptable signal distortion. Since the excess beat noise depends on optical bandwidth per channel and bit rate, the performance of SS-WDM systems is usually expressed in term of the normalized parameter $m = B_0 T$ where B_0 is the 3-dB optical bandwidth per channel, and T is the bit period. Finally, the strength of excess beat noise can be expressed in term of this single parameter m, and its strength increases monotonically as m decreases.

3.1.4 Experimental Results and Demonstrations of LED-based SS-WDM

The SS-WDM in PONs employing 1.3-μm LEDs was first demonstrated by Reeve *et al.* [21]. In their demonstration, four 2-Mb/s channels were successfully transmitted over 2 km of standard single-mode fiber. Due to low output power from LEDs, the achieved transmission distance, and the bit rate is quite small. In order to increase the transmission distance and the bit rate, higher power LEDs are necessary. With superluminescent diodes (SLDs) which provide higher output power, the transmission of 50 Mb/s on each of 16 channels over 7 km of a standard single-mode fiber was demonstrated [61]. The transmission can be further extended by employing an EDFA as a power amplifier at the transmitter. When the EDFA power amplifier and

SLDs were used, three 140 Mb/s WDM channels over 110 km of a single-mode fiber were successfully demonstrated [62].

The optical bandwidths of signals in all of these experiments were of the order of a few nm, corresponding to of the order of hundreds of GHz. Since the demonstrated bit rates were well below 1 Gb/s, the corresponding values of $m = B_0 T$ far exceeded thousands. Hence, the excess beat noise was negligible compared to the thermal noise at the receiver, and a BER floor due to the excess beat noise was not observed. However, it should be noted that system capacity per channel could be increased by increasing the operating bit rate $R_b = 1/T$. For a given usable bandwidth, the number of channels can be increased by reducing the optical bandwidth B_0. These will result in a reduction of m. Therefore, it is desirable to operate at a small value of m with acceptable power penalty caused from the excess beat noise. The power penalty caused by reduction of m will be clearly seen in the following sections when the bit rate is high and the optical bandwidth per channel is narrow in order to efficiently utilize the limited bandwidth provided by the source.

3.2 BROADBAND SOURCE USING OUTPUT ASE FROM EDFA

As seen in the previous section, insufficient output power from LEDs and SLDs allows SS-WDM systems to operate only at relatively low bit rate and short distance. In order to achieve higher bit rate and longer distance, higher power sources is necessary. With advanced technology in photonic devices, WDM multiplexers whose passbands are fractions of a nm are available. Therefore, considerable increase in system capacity could be achieved if such multiplexers are employed with a broadband high power source in SS-WDM systems.

In 1993, Lee and his colleagues proposed an alternative source that can be employed in SS-WDM systems [64]. Their proposed source is an EDFA configured to produce high power ASE noise at the amplifier output. Their EDFA can produce 21 mW of ASE noise over the bandwidth of 40 nm. The advantages of the proposed EDFA over an LED are that the EDFA provides considerably higher output power than an LED, and that it is easier and more efficient to connect the EDFA to other devices because it is

made of a single-mode fiber. High ASE power from an EDFA implies that achievable bit rate and transmission distance are larger than those obtained from LEDs. With this high power source, SS-WDM systems are not restricted to only low capacity networks, as PONs are due to stringent power budget. Instead, the SS-WDM systems can potentially be employed in larger-scale networks where the operating bit rate is high and the transmission distance is large.

The schematic diagram of the proposed light source is shown in Fig. 3.2. The EDFA is backward pumped at 1.48 μm to produce high ASE noise at the output. The output ASE noise is fed to the WDM demultiplexer in order to share a single source among channels located at different wavelengths. The transmitted data in each channel is embedded into the noise-like signal by the corresponding modulator. All channels are combined together by a WDM multiplexer. At the receiver, all channels are separated by a WDM demultiplexer, and each channel is connected to its corresponding photodetector to extract the embedded data.

In their experimental results, the performance degradation due to excess beat noise was apparently observed. Their results are shown in Fig. 3.3. Both increase in bit rate and decrease in optical bandwidth per channel result in performance degradation as expected. Additionally, a BER floor was also observed when the operating bit rate is 1.7 Gb/s and the optical bandwidth per channel is 0.6 nm. These values correspond to m equal to 44, which is relatively low compared to those in previously-discussed LED-based SS-WDM experiments.

Considerable progress and experiments related to EDFA-based SS-WDM systems have been reported since then. These are discussed in section 3.4. In order to clearly understand performance degradation due to the excess beat noise, it is useful to mathematically describe the effect of the excess beat noise on receiver sensitivity. In lightwave systems, the receiver sensitivity is usually expressed in term of the average number of photons per bit N_p required for the system to operate at a probability of bit error P_e equal to 10^{-9}. A model for determining receiver sensitivity is presented in the next section.

3.3 EFFECT OF EXCESS BEAT NOISE ON RECEIVER SENSITIVITY [23], [65]

The ASE noise at the output from an EDFA is due to spontaneous emission, which is similar to well-known thermal noise generated in electronic devices. Therefore, it can be modeled as Gaussian noise whose power spectral density is flat over the frequency range of interest. The ASE noise power in one polarization can be written as [25]

$$P_N = n_{sp} h f_c B_o (G-1) \tag{3.1}$$

where n_{sp} is the spontaneous emission factor, h is Planck's constant, f_c is the operating frequency, B_o is the optical bandwidth, and G is the amplifier gain. The electric field of ASE noise in one polarization can be written as [66]

$$E(t) = x(t)\cos(\omega_c t) - y(t)\sin(\omega_c t) \tag{3.2}$$

where $x(t)$ and $y(t)$ are in-phase and quadrature components of the ASE noise. Both $x(t)$ and $y(t)$ can be modeled as independent identically distributed baseband Gaussian processes with zero-mean and bandwidth $B_0/2$. The variance of each process is equal to $\sigma^2 = P_N$.

3.3.1 Receiver Structure and Mathematical Model

The receiver structure is shown in Fig. 3.4. It consists of an optical bandpass filter followed by a square law detector and integrator, which are used to represent the photodetector and the low-pass filter, respectively. The output current from the integrator is then compared with a threshold current. The optimum threshold depends on the probability distribution of the output current in the on-state and in the off-state, and is given by

$$p_1(I_{th}) = p_0(I_{th}) \tag{3.3}$$

where p_1 and p_0 are the probability density functions (pdf) of the output current in the on-state and in the off-state, respectively. The receiver decides that bit "1" was transmitted when the output current exceeds I_{th}, and that bit "0" was transmitted when the output current is less than I_{th}. If maximum likelihood is assumed, then the probability of bit error is found from

$$P_e = \frac{1}{2}\int_{-\infty}^{I_{th}} p_1(x)dx + \frac{1}{2}\int_{I_{th}}^{\infty} p_0(x)dx \tag{3.4}$$

The problem in solving the equation (3.4) is reduced significantly when both p_1 and p_0 are Gaussian distributed and using the assumption that both integrals in (3.4) are equal. In that case, the probability of bit error P_e is given by

$$P_e = \frac{1}{2\pi}\int_{Q}^{\infty} \exp\left(-\frac{x^2}{2}\right)dx \tag{3.5}$$

where

$$Q = \frac{\mu_1 - \mu_0}{\sigma_1 + \sigma_0} \tag{3.6}$$

and μ_1 and σ_1 are the average photocurrent and variance in the on-state, respectively, and μ_0 and σ_0 are the average photocurrent and variance in the off-state, respectively. When both p_1 and p_0 are Gaussian, the only parameters that are required are the means (μ_1 and μ_0) and variances (σ_1 and σ_0) of the currents in the on-state and in the off-state. The value of Q indirectly represents the probability of bit error; for example, $Q = 6$ for $P_e = 10^{-9}$. It is clearly seen that the Gaussian approximation is fairly simple.

However, in some cases, it is not adequate to represent the pdf of the signal with a Gaussian distribution, as we will see later.

The square-law detector converts the optical signal to an electrical signal. The output current from the detector is proportional to the square of the input electric field. Therefore, by using (3.2), the output current from the integrator can be expressed as

$$I = \frac{1}{2T}\int_0^T [x^2(t) + y^2(t) + \tilde{x}^2(t) + \tilde{y}^2(t)]dt + I_n \tag{3.7}$$

where T is the bit period, $x(t)$, $y(t)$, $\tilde{x}(t)$, and $\tilde{y}(t)$ are independent identically distributed baseband Gaussian processes with zero-mean and bandwidth $B_0/2$. The variance of each process is equal to σ^2. $\tilde{x}(t)$ and $\tilde{y}(t)$ correspond to the electric field in the polarization orthogonal to that of $x(t)$ and $y(t)$. In addition, the power spectrum of these processes is rectangular in shape since the optical bandpass filter is modeled to have a rectangular transfer function. The thermal noise current due to the electrical components of the receiver is represented by I_n, and is assumed to be a Gaussian random process having zero-mean. It should be noted that the shot noise, generated from the photodetector, is negligible compared to the signal fluctuation, and to the thermal noise since a p-i-n photodetector is employed.

Another assumption is that the received signal has perfect extinction ratio and the effect of dispersion is neglected. Therefore, in the on-state, $x(t)$, $y(t)$, $\tilde{x}(t)$, and $\tilde{y}(t)$ represent the noise-like signal whereas these terms are equal to zero in the off-state. The integral in (3.7) can be approximated by a summation, which results in [23], [65]

$$I = \frac{1}{2m}\sum_{i=1}^{m}[x_i^2 + y_i^2 + \tilde{x}_i^2 + \tilde{y}_i^2] + I_n \tag{3.8}$$

where x_i, y_i, $\tilde{x}_i$, and $\tilde{y}_i$ are independent Gaussian random variables with zero-mean and variance σ^2. The first term, corresponding to the noise-like signal, consists of the sum of the squares of independent Gaussian random variables scaled down by $1/2m$. Therefore,

the first term is a modified chi-square random variable with $4m$ degrees of freedom. Its pdf is given by [23], [65]

$$p_X(x) = \frac{\left(\frac{m}{\sigma^2}\right)^{2m}}{(2m-1)!} x^{2m-1} \exp\left(-\frac{mx}{\sigma^2}\right) \tag{3.9}$$

where X represents the first term in (3.8). It is clearly seen from (3.8) that the pdf of the current in the on-state at the decision circuit is not Gaussian. Instead, it is the result of the convolution between $p_X(x)$ in (3.9) and the pdf of the thermal noise, which is assumed to be Gaussian. However, the Gaussian approximation is usually used to find the receiver sensitivity in laser-based lightwave systems. Thus, it is interesting to compare the result obtained from the Gaussian approximation with that obtained from the actual distribution.

3.3.2 Gaussian Approximation [23], [65]

As seen from (3.6), this approximation readily gives us the closed-form solution from the means and variances of the currents in the on-state and in the off-state. From (3.8), the mean and variance of the photocurrent at the input to the decision circuit are given by

$$\begin{aligned} \mu_1 &= 2\sigma^2 \\ \mu_0 &= 0 \end{aligned} \tag{3.10}$$

$$\begin{aligned} \sigma_1^2 &= \left(\frac{2}{m}\right)\sigma^4 + \sigma_g^2 \\ \sigma_0^2 &= \sigma_g^2 \end{aligned} \tag{3.11}$$

where σ_g^2 is the variance of the thermal noise, and σ^2 is the variance of the noise-like signal in one polarization. By substituting (3.10) and (3.11) into (3.6), the parameter Q is given by

$$Q = \frac{2\sigma^2}{\sqrt{\left(\frac{2}{m}\right)\sigma^4 + \sigma_g^2} + \sigma_g} \tag{3.12}$$

From the above equation, if the excess beat noise dominates over the thermal noise (m is small), then

$$Q \approx \sqrt{SNR_{excess}} = \sqrt{2m} \tag{3.13}$$

where SNR_{excess} is the electrical signal to noise ratio of the continuous ASE light. (3.13) implies that the BER performance is solely determined by m when m is small. However, the pdf of the excess beat noise is not Gaussian whereas (3.13) is analyzed based on the Gaussian assumption. Both contradict each other; therefore, the Gaussian assumption is questionable at small value of m. From the SNR point of view, it is clearly seen that at small value of m, SNR is limited by m, which is the effect of excess beat noise. The variance σ^2 is related to N_p by

$$\sigma^2 = N_p \eta q R_b \tag{3.14}$$

where η is the quantum efficiency of the photodetector, q is the electron charge. The thermal noise can be related to the receiver parameters by

$$\sigma_g^2 = 2\pi V_T C_T q R_b^2 \tag{3.15}$$

where V_T is the thermal potential (product of Boltzman's constant and the temperature (300K) divided by the electron charge), C_T is the effective noise capacitance of the receiver. By substituting (3.14) and (3.15) into (3.12), the receiver sensitivity N_p can be expressed as

$$N_p = \frac{\frac{Q}{2\eta}\sqrt{\frac{8\pi V_T C_T}{q}}}{1-\frac{Q^2}{2m}} \tag{3.16}$$

This result is plotted as a function of m in Fig. 3 for $Q = 6$ ($P_e = 10^{-9}$), $\eta = 0.7$, and C_T =0.1 pF. As we expect, the receiver sensitivity becomes poorer (higher) as m becomes smaller. Additionally, a bit-error-rate (BER) floor is observed at small value of m due to high signal fluctuation causing large excess beat noise. On the other hand, the receiver sensitivity approaches that of the deterministic signal at large value of m because the excess beat noise is negligible. It should be noted that the BER floor is observed at m equal to 18 when the Gaussian approximation is used. The SS-WDM system can actually be operated at m smaller than 18 [24]. Therefore, the Gaussian approximation is not adequate to describe the distribution of noise-like signal when the value of m is small.

3.3.3 Modified Chi-Square Analysis [23], [65]

The following is a more accurate analysis of receiver sensitivity. As stated earlier, in the on-state the distribution of the photocurrent at the integrator output due to signal alone can be approximated to be modified chi-square with $4m$ degrees of freedom. When the thermal noise is also taken into account, the pdf of the photocurrent due to the signal and thermal noise is the resultant convolution of the pdf of the signal current and the pdf of the thermal noise. Such convolution yields the following distribution:

$$p_1(x) = \frac{K(m\alpha)^{2m}}{(2m-1)!}\frac{a^{-(1+2m)/2}}{2\exp(c)}\left[\sqrt{a}\Gamma(m)Hyg\left(m,1/2,b^2/4a\right)\right.$$
$$\left. - b\Gamma(m+1/2)Hyg\left(m+1/2,3/2,b^2/4a\right)\right] \tag{3.17}$$

where

$$K = \frac{1}{\sqrt{2\pi\sigma_g^2}} \tag{3.18}$$

$$\alpha = \frac{1}{\sigma^2} \tag{3.19}$$

$$a = \frac{1}{2\sigma_g^2} \tag{3.20}$$

$$b = m\alpha - 2ax \tag{3.21}$$

$$c = ax^2 \tag{3.22}$$

where "Hyg", which appears in (3.17), refers to the Kummer confluent hypergeometric function and Γ is the gamma function.

In the off-state, there is no signal; the fluctuation in the photocurrent is solely due to the thermal noise, which is Gaussian with zero-mean. Hence, the pdf of the output current from the integrator in the off-state is given by

$$p_0(x) = \frac{1}{\sqrt{2\pi\sigma_g^2}} \exp\left(-\frac{x^2}{2\sigma_g^2}\right) \tag{3.23}$$

It should be noted that it is extremely difficult to solve (3.3) for I_{th} when $p_1(x)$ and $p_0(x)$ are given by (3.17) and (3.23), respectively. However, for very small probability of bit error, a suboptimal threshold which is close to the optimum is the point at which both integrals in (3.4) are equal. By using this condition, the suboptimal point is found to be equal to $6 \cdot \sigma_g$ for $P_e = 10^{-9}$. Substituting this suboptimal point, (3.17), and (3.23) into (3.3), the receiver sensitivity can be solved numerically as a function of m by using the following equation:

$$1=\frac{\left(m\alpha/\sqrt{a}\right)^{2m}}{2(2m-1)!}\left[\Gamma(m)Hyg\left(m,1/2,b^2/4a\right)-\left(b/\sqrt{a}\right)\Gamma(m+1/2)Hyg\left(m+1/2,3/2,b^2/4a\right)\right] \tag{3.24}$$

For $\eta = 0.7$ and C_T =0.1 pF, above relation can be simplified to

$$1=\frac{\left(644m/\overline{N}_p\right)^{2m}}{2(2m-1)!}\left[\Gamma(m)Hyg\left(m,1/2,k\right)-\left(644m/\overline{N}_p-8.5\right)\Gamma(m+1/2)Hyg\left(m+1/2,3/2,k\right)\right] \tag{3.25}$$

where

$$k=\frac{103684.58m^2}{\overline{N}_p^2}-\frac{2732.26m}{\overline{N}_p}+18 \tag{3.26}$$

The resultant receiver sensitivity as a function of m is shown in Fig.3.5. As seen from this figure, the chi-square analysis indicates that smaller values of m can be used than indicated from the Gaussian approximation. This is because the Gaussian assumption is accurate only in the central region of the detected-current distribution whereas the tail of the distribution is the factor that determines the BER performance [67]. Since at small value of m, the excess beat noise is not negligible, the results obtained from the Gaussian approximation deviate from those obtained from the analysis using (3.17).

At large values of m, the receiver sensitivity predicted by both analyses converges to that of the deterministic signal. This can be simply explained by the fact that when m is large, the excess beat noise is small compared to the thermal noise at the receiver. Therefore, the distribution of the on-state current is well approximated to be Gaussian. However, both Gaussian approximation and modified chi-square analysis show that the excess beat noise increases as m decreases. Therefore, operating at high bit rate and narrow optical bandwidth per channel to increase system capacity will result in a power penalty from the dominant excess beat noise.

As seen from (3.11), the variance of the current in the on-state at the decision circuit is larger than that in the off-state due to additional excess beat noise. In other words, the noise is signal dependent. Therefore, the decision threshold in SS-WDM systems is different from that in laser-based systems where noise does not exhibit signal dependence. The optimum decision threshold should be below the midpoint of the vertical eye opening at the receiver [68]. Additionally, the received SNR also varies considerably with time, and it depends on optical pulse shape, lowpass filter at the receiver, and the extinction ratio of the signal [69]. This implies that the decision time has to be precisely selected, and the signal format should be non-return-to-zero (NRZ) since long duration in the on-state is required to stabilize the SNR [69].

Although the results in this section are for the ASE noise, they are also applicable to the case of LEDs and SLDs. This is because the noise at the output from EDFAs, LEDs, and SLDs is due to spontaneous emission, which can be modeled as Gaussian noise. The difference between the noise from EDFAs, and that form LEDs and SLDs is the achievable power. EDFAs can produce noise having much higher power than LEDs and SLDs can produce.

3.4 PROGRESS AND EXPERIMENTS IN EDFA-BASED SS-WDM SYSTEMS

With an EDFA as a light source, SS-WDM performance has been improved dramatically in term of operating bit rate and transmission distance. One factor is due to the high output ASE noise obtained from an EDFA. A broadband ASE source providing an output power above 100 mW (20 dBm) over a bandwidth of 15 nm has been reported in [70]. The flattened ASE spectral profile is achieved by employing two types of fiber amplifiers having different spectral profiles.

Furthermore, it has been experimentally shown that greater than 22 dBm of ASE power can be launched into a 94-km long dispersion-shifted fiber without stimulated Brillouin scattering (SBS) effect [71]. In the case of laser-based systems, the maximum power that can be launched into the same fiber without SBS effect is only about 15 dBm. This is because the optical bandwidth of the ASE signal is considerably larger than that of laser-generated signal, and the nonlinear SBS gain decreases as the signal bandwidth

increases [55]. This suggests that larger power budget can be achieved in SS-WDM systems, which would result in longer transmission distance and higher bit rate operation.

It is clearly seen from the previous sections that the receiver sensitivity of SS-WDM is poorer than that of laser-based WDM systems due to excess beat noise resulting from ASE signal fluctuation. The receiver sensitivity can be improved if signal fluctuation is reduced. Keating *et al.* have proposed a technique to reduce signal fluctuation, called feedforward noise reduction (FFNR) technique [72]. This technique utilizes power addition and subtraction implemented by a multiplying element, e. g. modulator, to stabilize the ASE signal power. In their experiment, BER can be improved up to three orders of magnitude by using this technique. One drawback of this technique is that dispersion causes imperfect cancellation. Dispersion causes the signal to spread in time while the compensation is done at the transmitter where there is no dispersion. Therefore, feedforward noise reduction technique is appropriate only when dispersion is negligible.

Several transmission experiments have demonstrated [73]-[76] the potential of using an EDFA as a source. All of them were intended to demonstrate the possibility of deploying SS-WDM systems in long-span, high-bit-rate systems. With the help of EDFAs as a power amplifier, and an in-line amplifier, a single channel at 2.5 Gb/s was transmitted over 200 km of a dispersion-shifted fiber with only 1.8 dB of power penalty [76]. The values of m in these experiments are more than 50; therefore, severe power penalty was not observed. In addition, the modulators used in these experiments exhibit polarization dependence. Thus, the output ASE from the modulators has only one polarization.

Lee *et al.* has demonstrated that receiver sensitivity can be improved if polarization-insensitive modulators are used [77] as shown in Fig. 3.6. This can be explained by the fact that the excess beat noise in the two orthogonal polarizations does not correlate with each other. On the other hand, the ASE signals, represented by received dc current, in two orthogonal polarizations are added constructively. By employing the polarization-insensitive modulator with an unpolarized ASE source, a 1.5-dB improvement was achieved over a polarized source having the same optical bandwidth in a 1.7 Gb/s transmission experiment. Their results also suggest that the

optical bandwidth can be reduced by 3 dB with small power penalty when an unpolarized source is employed. Since power penalty can be compensated by increasing transmitted power, 3-dB decrease in optical bandwidth per channel implies that the system capacity can be doubled.

Another method that can improve receiver sensitivity in SS-WDM systems is to use a preamplifier to suppress the thermal noise at a receiver. This technique was theoretically proposed by Arya and Jacobs [23], [65]. In their analysis, improvement of more than 10 dB in receiver sensitivity can be achieved, and the deployment of a preamplifier results in an optimum value of m as shown in Fig. 3.7. This is due to two competing effects: the ASE noise from the preamplifier and the excess beat noise caused from signal fluctuation. The ASE noise from the preamplifier increases with the optical bandwidth B_0, which is related to m by $m = B_0 T$, whereas the excess beat noise is stronger as m is decreased. Therefore, for a given bit rate R_b, there is an optimum optical bandwidth per channel $B_{0,opt}$, which can be found from $B_{0,opt} = m_{opt} \cdot R_b$ where m_{opt} is the optimum value of m when a preamplifier is employed.

3.5 SUMMARY

In this chapter, the development of SS-WDM systems has been discussed. The fundamental limitation in SS-WDM systems was also stressed. Also shown were the mathematical formulations and models, used to explain the characteristic of SS-WDM systems. These are the underpinning of the next chapter, which is the theoretical analysis of the effect of dispersion on SS-WDM systems.

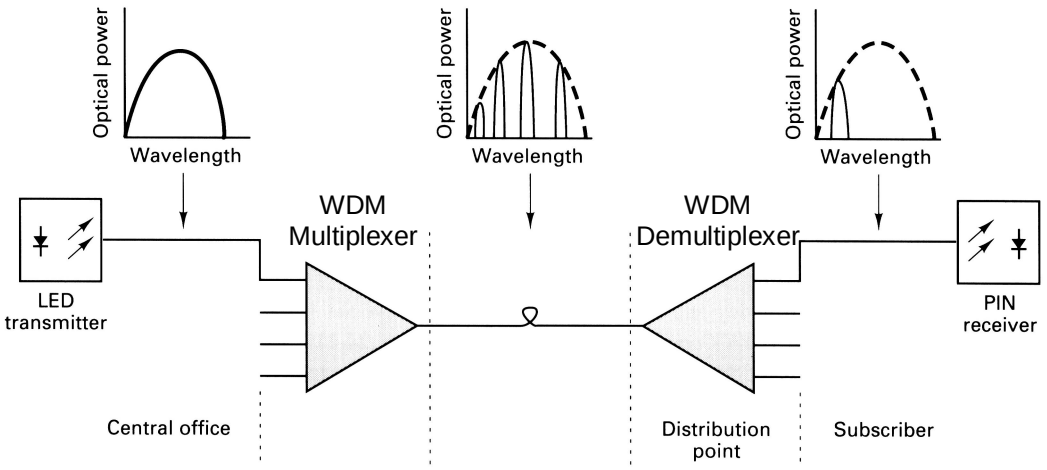

Fig. 3.1: Schematic diagram of the spectral slicing system.

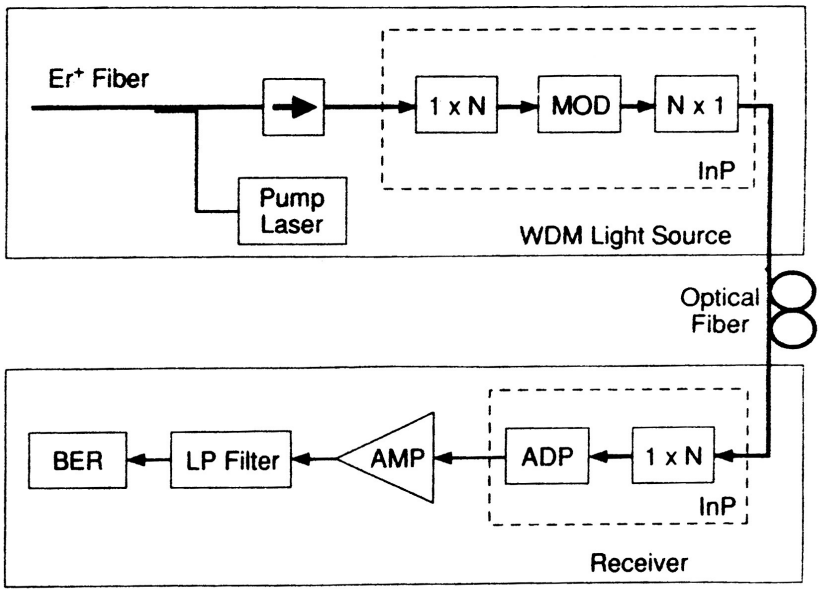

Fig. 3.2: A schematic diagram of the proposed multichannel WDM light source. MOD is an array of N modulators. An identical $1\times N$ demultiplexer can be used at the receiver end [64].

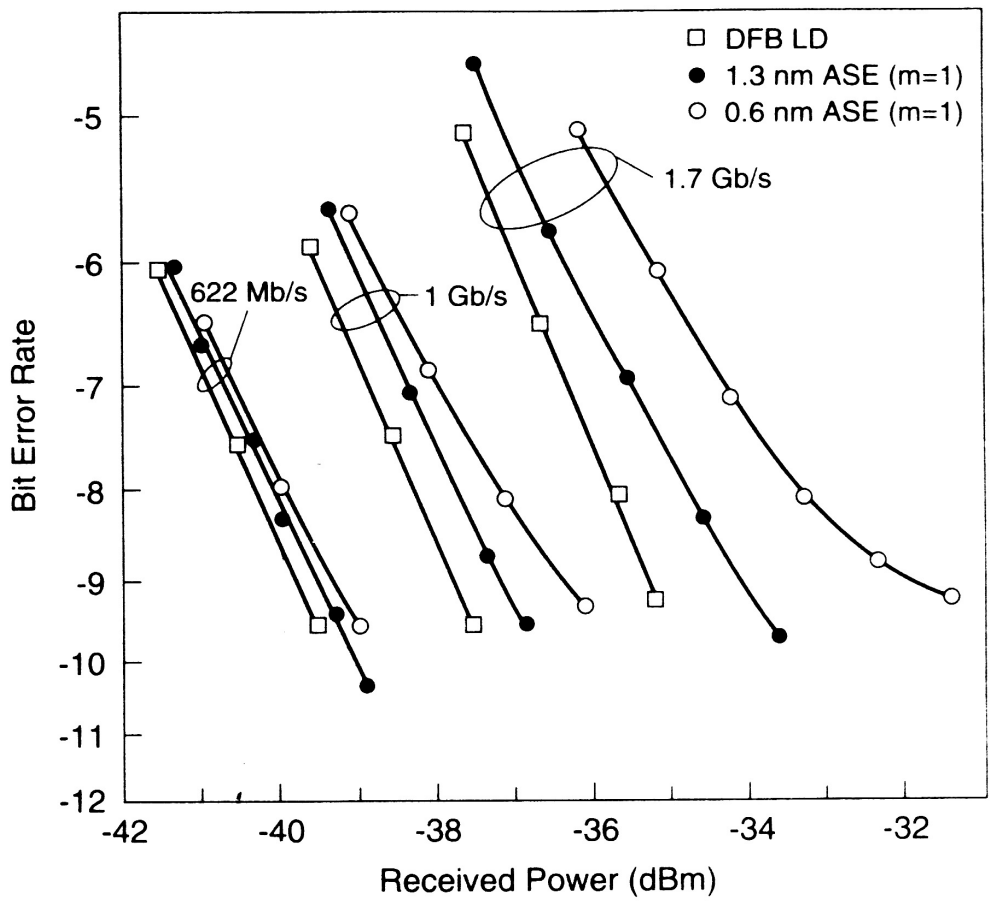

Fig.3.3: The measured bit error curves at 622 Mb/s, 1 Gb/s, and 1.7 Gb/s: ( ) A 1.5-μm DFB laser, (•) the spectrum-sliced ASE light source (bandwidth: 1.3 nm), and (O) the spectrum-sliced ASE light source (bandwidth: 0.6 nm) [64]. Note that m in this figure refers to the degree of polarization ($m = 1$ for a polarized light source and $m = 2$ for an unpolarized light source).

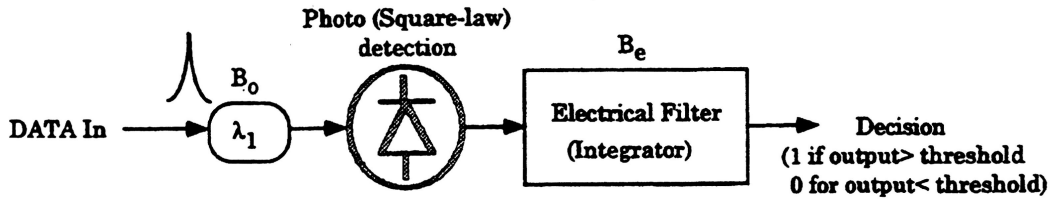

Fig. 3.4: OOK Receiver Model [65].

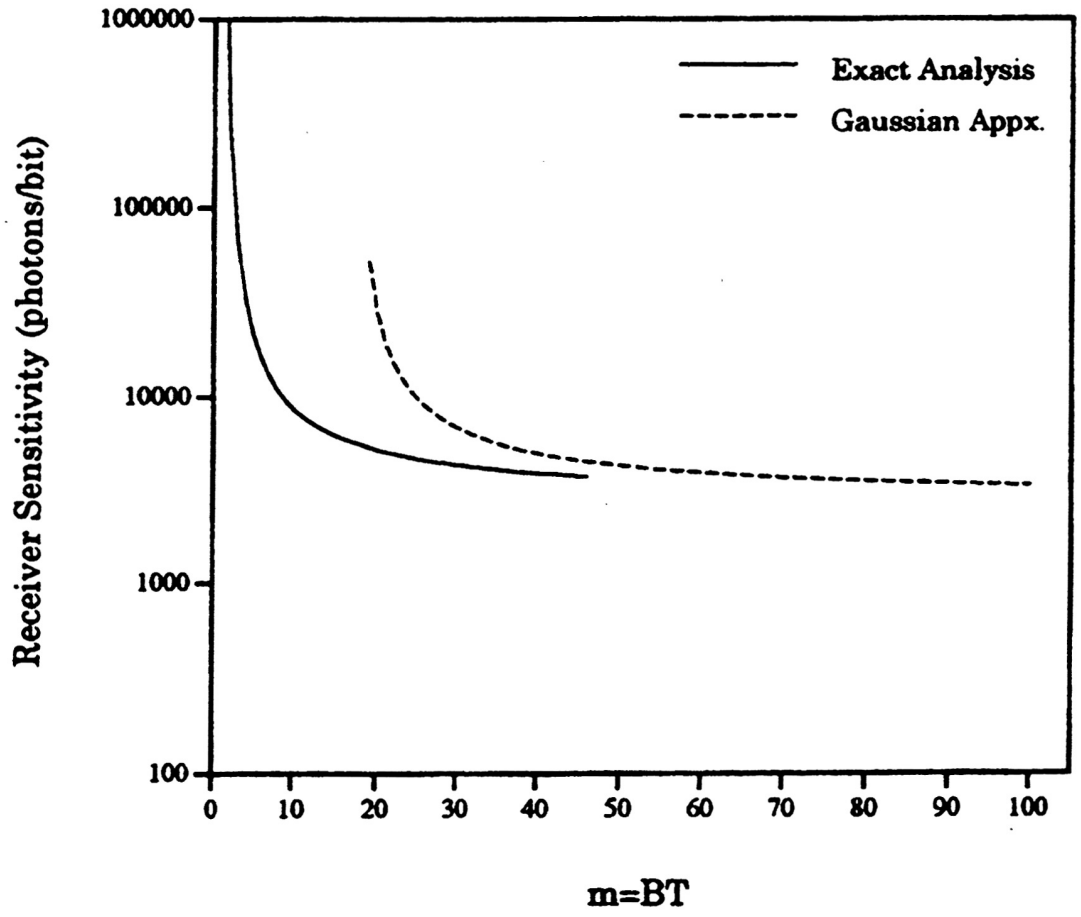

Fig. 3.5: Receiver sensitivity at $P_e = 10^{-9}$ for p-i-n ($C_T = 0.1\,\text{pF}$, η =0.7), as calculated with the exact and Gaussian distributions [65].

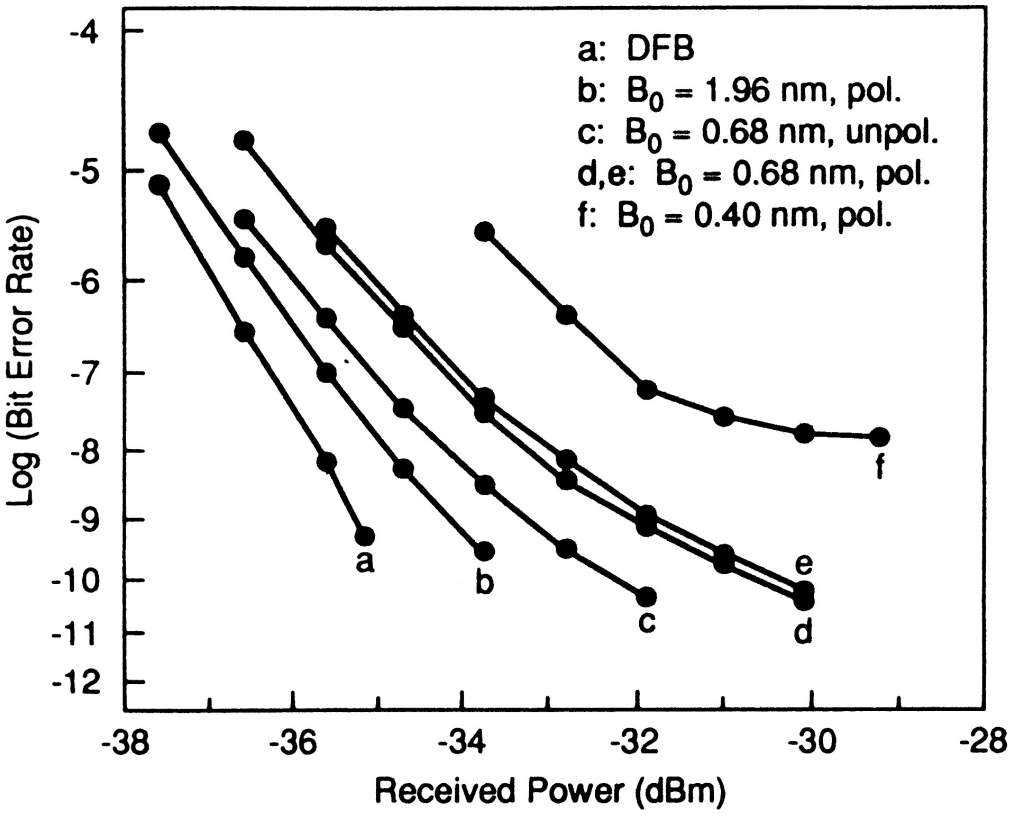

Fig. 3.6: The measured BER curves: (a) 1.55-μm DFB laser with a $LiNbO_3$ modulator; (b) polarized ASE source (equivalent optical bandwidth; 1.96 nm) with a $LiNbO_3$ modulator; (c) unpolarized ASE source (bandwidth; 0.68 nm) with a polarization-insensitive EA modulator; (d) polarized ASE source (bandwidth 0.68 nm) with a $LiNbO_3$ modulator; (e) polarized ASE source (bandwidth 0.68 nm) with a polarization-insensitive EA modulator, and (f) polarized ASE source (bandwidth 0.40 nm) with a $LiNbO_3$ modulator [79].

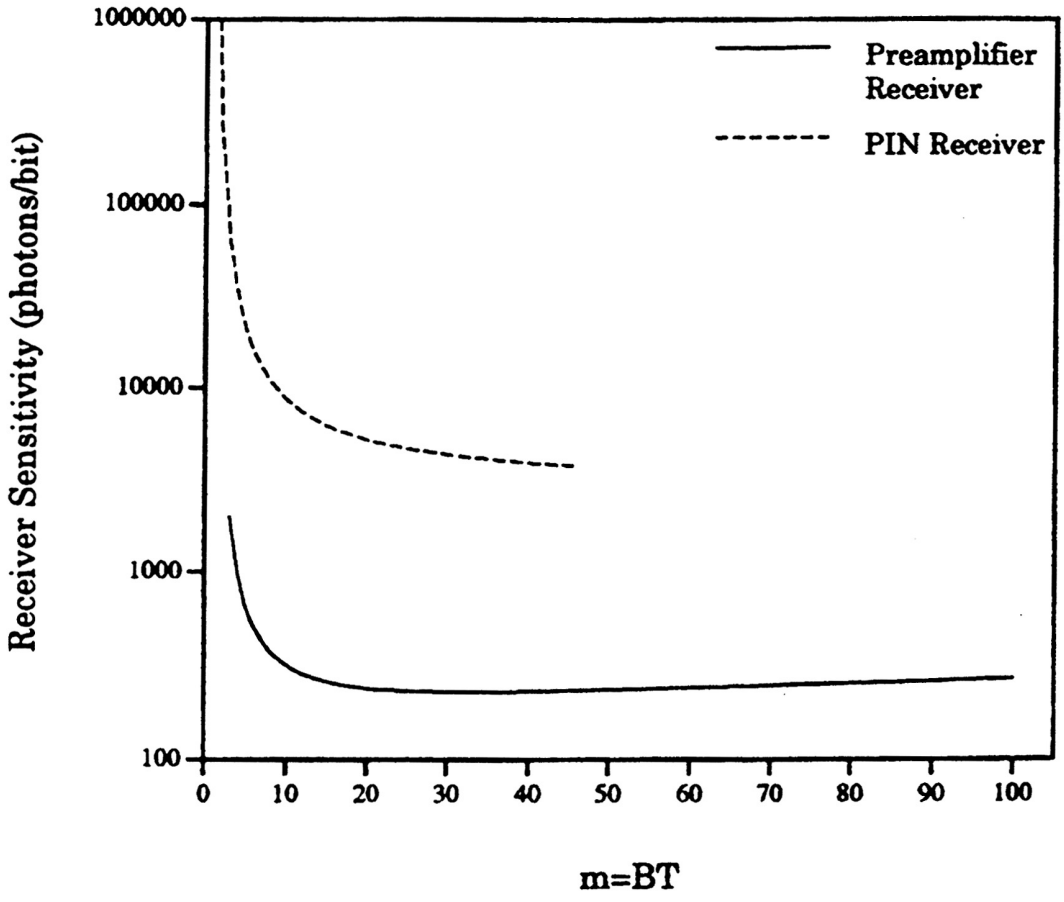

Fig. 3.7: Receiver sensitivity comparison for a p-i-n ($C_T = 0.1\,\text{pF}$, η =0.7) and a preamplifier receiver (n_{sp} =2) for an SS-WDM system [65].

Chapter 4

DISPERSION EFFECT ON SS-WDM SYSTEMS

This chapter is the main contribution of this thesis. In this chapter, the receiver sensitivity of a spectrum-sliced wavelength-division multiplexing (SS-WDM) system employing a single-mode optical fiber is analyzed and evaluated. Unlike a dispersion-shifted fiber, a single-mode fiber exhibits severe dispersion at the 1.55-μm window, which is the same as the usable wavelength band provided by erbium-doped fiber amplifiers (EDFAs). The optical bandwidth per channel of a SS-WDM system is usually large compared to the bit rate. Therefore, dispersion will degrade the performance of a SS-WDM system more severely than that of a conventional laser-based system. The degree of severity caused by dispersion needs to be studied in order to understand the characteristic of a SS-WDM system employing a single-mode fiber. This is the main objective of this thesis and it is presented in this chapter.

This chapter is organized as follows. Section 4.1 provides background information of a SS-WDM system employing a single-mode fiber. The mathematical model used to represent the effect of dispersion is discussed in Section 4.2. Also explained in this section are the system model and formulation used to evaluate the receiver sensitivity. The parameters and conditions used in the evaluation of the receiver sensitivity are discussed in Section 4.3. The receiver sensitivity is provided in Section 4.4, including the approaches that are used in the numerical evaluation. The last section, Section 4.5, is a summary of this chapter.

4.1 INTRODUCTION

The analysis of receiver sensitivity when the effect of dispersion is neglected was discussed in the previous chapter. The receiver sensitivity is usually defined as the average number of photons per bit N_p required for a given bit error probability P_e which

is usually set to 10^{-9}. Unlike laser-based systems, SS-WDM systems commonly operate at a large optical bandwidth per channel compared to the bit rate. Therefore, the receiver sensitivity is generally expressed in terms of the normalized parameter $m = B_0 T = B_0 / R_b$, where B_0 is 3-dB optical bandwidth of the signal, and T is the reciprocal of the bit rate R_b. Two important conclusions that can be drawn from the analysis [23], [65] summarized in the previous chapter are: receiver sensitivity improves as m increases and the Gaussian approximation underestimates system performance when m is small. The former is due to the fact that the excess beat noise is inversely proportional to m. The latter is because when m is small, the distribution of the signal at the input to the decision circuit has tails that are more confined than that implied by a Gaussian distribution.

Although increasing m results in better receiver sensitivity N_p, fewer channels can be employed for a given usable bandwidth of the transmission link. In addition, the usable bandwidth is decreased as the transmission distance increases due to the self-filtering effect of cascaded EDFAs along the link [27]. Moreover, large value of m implies that a signal experiences severe dispersion caused from the frequency dependence of the effective refractive index of an optical fiber. This is usually the case in systems employing single-mode optical fibers with moderate transmission distances, and in systems employing dispersion-shifted fibers with large transmission distance and where the operating wavelength is slightly displaced from the zero-dispersion wavelength.

Dispersion causes a signal to spread beyond its bit period. Therefore, it results in intersymbol interference (ISI), and the reduction of signal power for bit "1", both of which degrade the receiver sensitivity N_p. Consequently, there are now two factors that affect N_p: the excess beat noise and the dispersion. A large optical bandwidth B_0 results in severe dispersion experienced by the signal. On the other hand, the excess beat noise is reduced when the optical bandwidth B_0 is large. Therefore, there should be an optimum value of m (an optimum value of B_0 for a given R_b), which is the result of these two competing effects. The optimum value of m in the presence of dispersion has been

reported in [24]. Unfortunately, the results in [24] are expressed in terms of physical units (e.g. distance is expressed in km) with a limited range of parameters. However, we believe that it is more useful to express the receiver sensitivity in terms of normalized parameters since they intuitively represent the factors that affect the system performance. In addition, normalized parameters can be applied over a broad range of conditions, and be easily converted back to physical parameters.

The main objective of this thesis is to evaluate the receiver sensitivity of a SS-WDM system employing a single-mode fiber. The results are expressed in terms of two normalized parameters: $m = B_0 T$, and z/L_D where z is the transmission distance and L_D is the dispersion length defined as the distance at which the root-mean-square (rms) pulse width of a Gaussian pulse increases by a factor of $\sqrt{2}$ from its initial width [1]. The value of m represents the effect of the excess beat noise, and the normalized distance z/L_D depicts the degree of dispersion. In conventional laser-based systems, the effect of dispersion becomes significant when the transmission distance approaches L_D. The bit rate R_b, optical bandwidth B_0, and transmission distance z for a specific system, can be related back to the corresponding receiver sensitivity via the values of m and z/L_D.

4.2 METHODOLOGY AND MATHEMATICAL MODELS

In this section the mathematical models used to represent components in a SS-WDM system are described in detail. The mathematical formulations derived from these models are then used to find decision parameters, which lead to evaluation of the receiver sensitivity. The initial schematic diagram is identical to that shown in Fig. 1.7. However, we assume that the WDM (de)multiplexers used in a system have rectangular passbands and are lossless. When only a single channel is considered, these WDM (de)multiplexers can be replaced by ideal rectangular bandpass filters having bandwidth of B_0 Hz centered at the operating frequency of the signal f_c. The output signal from a modulator will occupy a bandwidth larger than B_0 Hz due to the effect of modulation. However, the spectral content of the output signal from the modulator located outside the bandwidth

B_0 is small compared to that located inside. Therefore, it is justifiable to neglect the effect of the two ideal rectangular bandpass filters used to represent the WDM multiplexer at the transmitter and the WDM demultiplexer at the receiver.

By using these assumptions, the schematic diagram used in this analysis is as shown in Fig. 4.1. It consists of a broadband unpolarized noise source followed by an optical bandpass filter which does the spectral slicing. A polarization-insensitive modulator is used to embed the transmitted data ("0" and "1") into the noise-like signal. The signal is then transmitted through an optical fiber having a phase (propagation) constant $\beta(f)$ where f is a frequency of interest. Note that optical bandpass filters, which represent the WDM multiplexer at the transmitter and the WDM demultiplexer at the receiver, are omitted since it is assumed that they do not affect the signal.

The receiver contains a p-i-n photodetector, followed an electrical amplifier and an integrate-and-dump filter (integration time equal to T). The p-i-n photodetector is modeled by a square-law detector. The electrical amplifier and integrate-and-dump filter are represented by a receiver thermal noise source and a reset integrator as shown in Fig. 4.1. The receiver output (the output from the reset integrator) is fed to a decision circuit, which compares the received signal with a threshold current denoted by I_{th}.

4.2.1 Methodology

Dispersion causes a signal to spread in time, which results in intersymbol interference (ISI) and reduction of signal power for bit "1". Since the data embedded into the signal is random in nature, the number of possible bit patterns is infinite. Fortunately, there are only two events (bit patterns) that need to be considered in order to construct decision statistics necessary for evaluating receiver sensitivity. These two events correspond to extreme ISI for bit "0" and highest power reduction for bit "1". In order to avoid confusion, both events are denoted by three binary digits 101 and 010, respectively. The second (middle) digit is used to present the current bit. The first digit denotes the transmitted data of all preceding bits when the current bit is considered. Similarly, the last digit denotes transmitted data of all following bits. Note that all preceding bits and following bits are identical in the extreme case.

The decision threshold must be computed from the events that minimize the vertical eye opening at the decision time. These events correspond to 010, and 101. The former results in the lowest average value of the receiver output when the current bit is "1". The latter corresponds to the highest average value of receiver output when the current bit is "0". It is reasonable to choose the threshold to be the point at which the probability density functions (pdf's) of both receiver outputs are equal. This threshold can be numerically found from the following equation.

$$p_{010}(I_{th}) = p_{101}(I_{th}) \tag{4.1}$$

where $p_{010}(x)$ is the pdf of a receiver output when the current bit is "1" and all neighboring bits are "0", and $p_{101}(x)$ corresponds to the current bit being "0" and all neighboring bits being "1". Two events have to be considered in the evaluation of the probability of bit error. The first corresponds to all neighboring bits being "0" whereas the second corresponds to all neighboring bits being "1" when the current bit is considered. In our case, it is found that the worst case corresponds to neighboring bits all being "1". Therefore, it is justified to approximate the bit error probability from

$$P_e = \frac{1}{2}\int_{I_{th}}^{\infty} p_{101}(x)dx + \frac{1}{2}\int_{-\infty}^{I_{th}} p_{111}(x)dx \tag{4.2}$$

where I_{th} is given by (4.1), $p_{111}(x)$ is the pdf of a receiver output when all bits are "1". This is an upper bound to the error probability, because the threshold given by (4.1) may not be strictly optimum, and because we determined that (4.2) represents worst case sequence. It is clearly seen form (4.1) and (4.2) that only three distinct pdf's, $p_{010}(x)$, $p_{101}(x)$, and $p_{111}(x)$, are necessary to evaluate the receiver sensitivity in the presence of dispersion caused by an optical fiber.

In the absence of the dispersion that causes ISI, $p_{010}(x)$ and $p_{111}(x)$ are identical, and can be expressed as $p_1(x)$ given by (3.17) [23], [65]. Similarly, $p_{101}(x)$ is identical

to $p_0(x)$ given by (3.23) [23], [65]. However, when the dispersion is taken into account, these pdf's are extremely difficult to obtain. The dispersion causes the pdf of the receiver output due to a received signal when "1" is transmitted to deviate from the chi-square distribution with $4m$ degrees of freedom presented in [23], and [65]. Likewise, the pdf of the receiver output when "0" is transmitted departs from the Gaussian distribution.

In the case of $p_{010}(x)$ and $p_{111}(x)$, when m is small the excess beat noise dominates the receiver thermal noise. On the other hand, the excess beat noise is negligible compared to the receiver thermal noise when m is large. Therefore, it is reasonable to approximate $p_{010}(x)$ and $p_{111}(x)$ with chi-square distributions whose degrees of freedom and variance are approximated from the evaluated means and variances of the actual receiver outputs. By using a similar approach, $p_{101}(x)$ can be approximated to be a Gaussian distribution since the receiver thermal noise is the dominant effect.

In order to use these approximations, it is necessary to obtain the actual mean and variance of the receiver output in each case. It should be noted that the non-dominant effects are not neglected, but it is assumed that they affect only the distribution parameters, such as mean and variance, but not the form of the distribution. Another approach that is usually used is to approximate all pdf's with Gaussian distributions having the calculated means and variances. However, we believe that the latter approach is inaccurate due to the considerable difference between the approximated Gaussian distributions and the actual distributions of the receiver outputs. Our approach and the Gaussian approach will both be used in evaluating the receiver sensitivity. The results from both approaches are then compared in order to see the difference between both approaches. We will begin with the case when the current bit is "1" and its neighboring bits all are "0" ($p_{010}(x)$).

4.2.2 ASE-Noise Signal

Although the ASE noise can be modeled as that presented in (3.2), such a model is difficult to deal with when the dispersion is taken into account. Fortunately, Marcuse [78], [79] has shown that when m is sufficiently greater than unity the ASE noise

occupying a bandwidth of B_0 Hz can be expressed as a Fourier series of m terms. The coefficients in this series are independent identically distributed (i.i.d.) Gaussian random variables having zero mean and variance equal to the source power in the bandwidth of $1/T$ Hz that corresponds to the increment step in the Fourier series. Consequently, when "1" is transmitted, the electric field (in one polarization) at the input to the optical fiber can be expressed as

$$s_{010,in}(t) = \sum_{i=-(m-1)/2}^{(m-1)/2} \frac{1}{\sqrt{m}} g(t)(x_i + jy_i)\exp\left[j2\pi(f_c + i/T)t\right] \tag{4.3}$$

where $g(t)$ is a rectangular pulse of duration T, x_i and y_i are i.i.d. Gaussian random variables having zero mean and variance $\sigma^2 = N_p h f_c R_b$, and h is Planck's constant which is equal to 1.38054×10^{-23} J/K. Note that the ASE noise used in our analysis is unpolarized; therefore, the electric field contains two orthogonal polarizations. The orthogonal electric field has identical expression as that given by (4.3); however, x_i and y_i are to be replaced by $\tilde{x}_i$ and $\tilde{y}_i$, respectively. $\tilde{x}_i$ and $\tilde{y}_i$ are also i.i.d. Gaussian random variables with mean and variance identical to that of x_i and y_i, and all of them are independent of one another. For mathematical convenience and ease of notation, only the single polarization of the electric field is indicated in (4.3).

4.2.3 Dispersion

The dispersion in an optical fiber is caused by the frequency dependence of the mode index $\bar{n}(f)$ of the fiber. Therefore, signal components at different frequency propagate along the fiber with different velocities, which then results in pulse broadening. This phenomenon can be modeled as different time delays for distinct signal frequencies. In our analysis, the optical fiber of length z is assumed to be an all-pass lossless filter with a transfer function given by

$$H(f) = \exp\left(-j\beta(f)z\right) \tag{4.4}$$

where $\beta(f)$ is the phase (propagation) constant of the optical fiber. It is related to the mode index by $\beta(f) = \bar{n}(f) \cdot 2\pi f / c$ where c is the velocity of light in free space. $\beta(f)$ in (4.4) can be expanded into a Taylor series around the operating frequency f_c [1]; thus, (4.4) becomes

$$H(f) = \exp\left\{-jz\left[\beta_0 + 2\pi\beta_1(f - f_c) + 2\pi^2\beta_2(f - f_c)^2 + \frac{4}{3}\pi^3\beta_3(f - f_c)^3\right]\right\} \quad (4.5)$$

where $\beta_n = \left(\frac{1}{2\pi}\right)^n \left(\frac{d^n\beta}{df^n}\right)_{f=f_c}$. The first two terms in (4.5) do not contribute to pulse broadening; hence, they can be neglected. If the operating frequency is far from the zero dispersion frequency, then the third term dominates the second term. This condition is usually satisfied in 1.55-μm systems employing single-mode fibers. As a result, the transfer function of an optical fiber is reduced to

$$H(f) = \exp\left(-j2\pi^2\beta_2 z(f - f_c)^2\right) \quad (4.6)$$

Since $g(t)$ in (4.3) is a rectangular pulse of duration T, the spectral content of each term in the summation is concentrated around its corresponding frequency $f_c + i/T$. Thus, $H(f)$ given by (4.6) can be linearized around each frequency denoted by $f_c + i/T$. As a result, the transfer function of the optical fiber for each term indexed by i in the Fourier series can be expressed as

$$H_i(f) = \exp\left(-j2\pi^2\beta_2 z(f - f_c)(i/T)\right) \quad (4.7)$$

where β_2 is in the units of ps^2/km, and can be related to the dispersion parameter of an optical fiber by

$$\beta_2 = -D\frac{\lambda_c^{\,2}}{2\pi c} \tag{4.8}$$

where D is the dispersion parameter in the more common units of ps/km-nm, and $\lambda_c = c / f_c$ is the operating wavelength. (4.7) indicates that the dispersion is simplified to a multipath effect where individual signal components at different center frequencies experience distinct time delays. By applying (4.7) to the input signal given by (4.3), the signal (in one polarization) at the output from the optical fiber can be expressed by

$$s_{010,out}(t) = \sum_{i=-(m-1)/2}^{(m-1)/2} \frac{1}{\sqrt{m}} g\big(t - \pi\beta_2 z(i/T)\big)(x_i + jy_i)\exp\big[j2\pi(f_c + i/T)t\big] \tag{4.9}$$

where only the real part of the above expression represents the physical signal. This expression implies that as the distance z increases, the signal becomes broader due to increase in time delays for individual components. The farther they are away from the center frequency f_c, the larger their time delays.

4.3 DECISION PARAMETERS

Mathematical expressions for the receiver outputs are discussed in this section. The receiver outputs are necessary for constructing decision statistics used in evaluation of receiver sensitivity. The mathematical expression for the signal at the output from a single-mode optical fiber described in the previous section is used to find the required receiver output. The main functions of a receiver are to convert an optical signal to an electrical signal, and to process it as necessary. The device in the receiver providing the optical-to-electrical conversion function is a photodetector.

The photodetector used in our analysis is a p-i-n photodetector. The output photocurrent from a p-i-n photodetector is proportional to the power of the incident electromagnetic field; therefore, a p-i-n photodetector is represented by a square-law detector whose output is proportional to the square of the input. The photocurrent from a p-i-n receiver can be expressed by

$$i(t) = \frac{\Re}{2}\left(|e(t)|^2 + |\tilde{e}(t)|^2\right) \tag{4.10}$$

where $e(t)$, and $\tilde{e}(t)$ are the input electric fields to the photodetector in the two orthogonal polarizations, $\Re$ is the responsivity of the photodetector, which is given by

$$\Re = \frac{q\eta}{hf_c} \tag{4.11}$$

where q is the elementary charge constant, which is equal to 1.60218×10^{-19} Coulomb, and η is the photodetector quantum efficiency. The output current from the photodetector can be found by substituting $s_{010,out}(t)$ (as given by (4.9)) for $e(t)$ in (4.10), and similarly replacing x_i and y_i by $\tilde{x}_i$ and $\tilde{y}_i$ to obtain $\tilde{e}(t)$. (Note that the tilt sign denotes the signal components in the orthogonal polarization.) Then, the receiver output (the output current from a reset integrator) when the current bit is "1" and all neighboring bits are "0" can be expressed as

$$I_{010} = \frac{\Re}{2mT}\left\{\sum_{i=-i_{\max}}^{i_{\max}}\left[A_i\left(x_i^2 + y_i^2 + \tilde{x}_i^2 + \tilde{y}_i^2\right)\right] + \sum_{i=-i_{\max}}^{i_{\max}}\sum_{\substack{k=-i_{\max}\\k\neq i}}^{i_{\max}}\left[B_{ik}\left(x_i x_k + y_i y_k + \tilde{x}_i\tilde{x}_k + \tilde{y}_i\tilde{y}_k\right)\right] + \sum_{i=-i_{\max}}^{i_{\max}}\sum_{\substack{k=-i_{\max}\\k\neq i}}^{i_{\max}}\left[C_{ik}\left(x_i y_k - y_i x_k + \tilde{x}_i\tilde{y}_k - \tilde{y}_i\tilde{x}_k\right)\right]\right\} + I_n \tag{4.12}$$

where I_n is the thermal noise current generated at the receiver, and

$$A_i = \int_{-T/2}^{T/2} g^2\left(t - \pi\beta_2 z(i/T)\right)dt \tag{4.13}$$

$$B_{ik} = \int_{-T/2}^{T/2} g\left(t - \pi\beta_2 z(i/T)\right) g\left(t - \pi\beta_2 z(k/T)\right) \cos\left(2\pi(i-k)t/T\right) dt \tag{4.14}$$

$$C_{ik} = \int_{-T/2}^{T/2} g\left(t - \pi\beta_2 z(i/T)\right) g\left(t - \pi\beta_2 z(k/T)\right) \sin\left(2\pi(k-i)t/T\right) dt \tag{4.15}$$

$$i_{\max} = \min\left\{\frac{m-1}{2}, \left\lfloor \frac{T^2}{\pi|\beta_2|z} \right\rfloor\right\} \tag{4.16}$$

where $\min\{a,b\}$ is the minimum between a and b, and $\lfloor d \rfloor$ is the floor function which rounds d to the nearest integer less than or equal to d. The $i_{\max}$ is accounted for the fact that when the distance z is larger, the rectangular pulse $g\left(t - \pi\beta_2 z(i/T)\right)$ is further away from the origin. When the distance z is less than $2T^2/\left(\pi(m-1)|\beta_2|\right)$, all $(m-1)$ rectangular pulses having distinct time delays are still within the current bit slot $[-T/2, T/2]$. However, when z is larger than $2T^2/\left(\pi(m-1)|\beta_2|\right)$, fewer rectangular pulses are within the current bit slot; consequently, the number of terms in the summations depends on the distance z.

It should be noted that the second and the third terms in (4.12) are the additional beat noise terms results from the dispersion. These additional beat noise terms give rise to increasing the fluctuation of the receiver output. When only the receiver output due to a received signal is considered, only the first term of (4.12) is present in the absence of the dispersion ($z = 0$). This first term is identical to (3.7) which has been shown to be chi-square distributed with $4m$ degrees of freedom [23], [65]. However, when z is greater than zero, all three terms in (4.12) are present. Therefore, the pdf of the receiver output due to a received signal is no longer chi-square distributed with $4m$ degrees of freedom, and is extremely difficult to find. Moreover, it is considerably more difficult to find the pdf of the receiver output when the effect of the thermal noise generated at the receiver is also included.

Nevertheless, $p_{010}(x)$ can be reasonably approximated with the chi-square distribution since the excess beat noise is the dominant effect in this case. Two required parameters in this approximation are the actual mean and variance of the receiver output. The last three terms in (4.12) have zero-mean; thus, only the first term contributes to the average value of the receiver output, and it is found to be

$$\bar{I}_{010} = \begin{cases} \dfrac{\Re\sigma^2}{2m}\left[4m - \dfrac{\pi|\beta_2|z(m^2-1)}{4T^2}\right], 0 \le z \le \dfrac{2T^2}{\pi(m-1)|\beta_2|} \\ \dfrac{\Re\sigma^2}{2m}\left\{4 - 4\left\lfloor \dfrac{T^2}{\pi|\beta_2|z}\right\rfloor\left[\dfrac{\pi|\beta_2|z}{T^2}\left(\left\lfloor \dfrac{T^2}{\pi|\beta_2|z}\right\rfloor + 1\right) - 2\right]\right\}, z \ge \dfrac{2T^2}{\pi(m-1)|\beta_2|} \end{cases} \tag{4.17}$$

where σ^2 is the variance of individual i.i.d. Gaussian random variables x_i, y_i, $\tilde{x}_i$, and $\tilde{y}_i$. By using the fact that x_i, y_i, $\tilde{x}_i$, $\tilde{y}_i$, and I_n in (4.12) are independent and have zero mean, the variance of I_{010} is expressed by

$$\begin{aligned} \sigma_{010}^2 = \left(\frac{\Re}{2mT}\right)^2 \Bigg\{ & \sum_{i=-i_{\max}}^{i_{\max}} \left[A_i^2 \operatorname{var}\left(x_i^2 + y_i^2 + \tilde{x}_i^2 + \tilde{y}_i^2\right)\right] \\ & + \sum_{i=-i_{\max}}^{i_{\max}} \sum_{\substack{k=-i_{\max} \\ k\neq i}}^{i_{\max}} \left[2B_{ik}^2 \operatorname{var}\left(x_i x_k + y_i y_k + \tilde{x}_i \tilde{x}_k + \tilde{y}_i \tilde{y}_k\right)\right] \\ & + \sum_{i=-i_{\max}}^{i_{\max}} \sum_{\substack{k=-i_{\max} \\ k\neq i}}^{i_{\max}} \left[2C_{ik}^2 \operatorname{var}\left(x_i y_k - y_i x_k + \tilde{x}_i \tilde{y}_k - \tilde{y}_i \tilde{x}_k\right)\right] \Bigg\} + \operatorname{var}(I_n) \end{aligned} \tag{4.18}$$

where $\operatorname{var}(a) = E(a^2) - E^2(a)$ is the variance of a random variable a, and $E(...)$ is the expected-value operation. The last term in (4.18) represents the thermal-noise power, which is denoted by σ_n^2. Since the variances of x_i, y_i, $\tilde{x}_i$, and $\tilde{y}_i$ in (4.18) are all equal to σ^2, (4.18) can be further simplified to

$$\sigma_{010}^2 = 2\left(\frac{\Re\sigma^2}{m}\right)^2\left[A_{010} + \left(B_{010} + C_{010}\right)\right] + \sigma_n^2 \tag{4.19}$$

where

$$A_{010} = \sum_{i=-i_{\max}}^{i_{\max}} A_i^2 \tag{4.20}$$

$$= \begin{cases} m - \dfrac{\pi|\beta_2|z(m^2-1)}{2T^2}\left(1 - \dfrac{\pi|\beta_2|zm}{6T^2}\right), 0 \le z \le \dfrac{2T^2}{\pi(m-1)|\beta_2|} \\ 1 + 2\left\lfloor \dfrac{T^2}{\pi|\beta_2|z} \right\rfloor \left\{ 1 - \dfrac{\pi|\beta_2|z}{T^2}\left(\left\lfloor \dfrac{T^2}{\pi|\beta_2|z} \right\rfloor + 1 \right)\left[1 - \dfrac{\pi|\beta_2|z}{6T^2}\left(2\left\lfloor \dfrac{T^2}{\pi|\beta_2|z} \right\rfloor + 1 \right)\right]\right\}, z \ge \dfrac{2T^2}{\pi(m-1)|\beta_2|} \end{cases}$$

$$B_{010} + C_{010} = \sum_{i=-i_{\max}}^{i_{\max}} \sum_{\substack{k=-i_{\max} \\ k \ne i}}^{i_{\max}} \left(B_{ik}^2 + C_{ik}^2\right) \tag{4.21}$$

$$= \sum_{i=1}^{i_{\max}} \frac{2}{(\pi i)^2}\left[1 - \cos\left(\frac{2\pi^2|\beta_2|zi^2}{T^2}\right)\right]$$

$$+ \sum_{i=1}^{i_{\max}-1} \sum_{k=i+1}^{i_{\max}} \frac{2}{(\pi(k-i))^2}\left[1 - \cos\left(\frac{2\pi^2|\beta_2|z(k-i)k}{T^2}\right)\right]$$

$$+ \sum_{i=1}^{i'_{\max}} \frac{1}{(2\pi i)^2}\left[1 - \cos\left(\frac{8\pi^2|\beta_2|zi^2}{T^2}\right)\right]$$

$$+ \sum_{i=1}^{i'_{\max}-1} \sum_{k=i+1}^{k'_{\max}} \frac{2}{(\pi(i+k))^2}\left[1 - \cos\left(\frac{2\pi^2|\beta_2|z(i+k)^2}{T^2}\right)\right]$$

where

$$i'_{\max} = \min\left\{\frac{m-1}{2}, \left\lfloor \frac{T^2}{2\pi|\beta_2|z} \right\rfloor\right\} \tag{4.22}$$

$$k'_{\max} = \min\left\{\frac{m-1}{2}, \left\lfloor \frac{T^2}{\pi|\beta_2|z} - i \right\rfloor\right\} \tag{4.23}$$

By using the definition of the dispersion length L_D given earlier in this chapter, the parameters β_2, and T can be related to the dispersion length L_D by the following equation.

$$L_D = \frac{T^2}{12 \cdot |\beta_2|} \tag{4.24}$$

where $T^2/12$ is the mean-square pulse width of a rectangular pulse of duration T. By using (4.24), the average value of the receiver output in (4.17) can be expressed as

$$\bar{I}_{010} = \begin{cases} \dfrac{\Re\sigma^2}{2m}\left[4m - \dfrac{\pi(z/L_D)(m^2-1)}{12}\right], 0 \le z/L_D \le \dfrac{24}{\pi(m-1)} \\ \dfrac{\Re\sigma^2}{2m}\left\{4 - 4\left\lfloor \dfrac{12}{\pi(z/L_D)} \right\rfloor \left[\dfrac{\pi(z/L_D)}{12}\left(\left\lfloor \dfrac{12}{\pi(z/L_D)} \right\rfloor + 1\right) - 2\right]\right\}, z/L_D \ge \dfrac{24}{\pi(m-1)} \end{cases} \tag{4.25}$$

Similarly, (4.20) and (4.21) can be expressed as

$$A_{010} = \begin{cases} m - \dfrac{\pi(z/L_D)(m^2-1)}{24}\left(1 - \dfrac{\pi(z/L_D)m}{72}\right), 0 \le z/L_D \le \dfrac{24}{\pi(m-1)} \\ 1 + 2\left\lfloor \dfrac{12}{\pi(z/L_D)} \right\rfloor \left\{1 - \dfrac{\pi(z/L_D)}{12}\left(\left\lfloor \dfrac{12}{\pi(z/L_D)} \right\rfloor + 1\right)\left[1 - \dfrac{\pi(z/L_D)}{72}\left(2\left\lfloor \dfrac{12}{\pi(z/L_D)} \right\rfloor + 1\right)\right]\right\}, z \ge \dfrac{24}{\pi(m-1)} \end{cases} \tag{4.26}$$

$$B_{010} + C_{010} = \sum_{i=1}^{i_{\max}} \frac{2}{(\pi i)^2}\left[1 - \cos\left(\frac{\pi^2 (z/L_D) i^2}{6}\right)\right] + \sum_{i=1}^{i_{\max}-1} \sum_{k=i+1}^{i_{\max}} \frac{2}{(\pi(k-i))^2}\left[1 - \cos\left(\frac{\pi^2 (z/L_D)(k-i)k}{6}\right)\right] \tag{4.27}$$

$$+\sum_{i=1}^{i'_{\max}}\frac{1}{(2\pi i)^2}\left[1-\cos\left(\frac{2\pi^2(z/L_D)i^2}{3}\right)\right]$$

$$+\sum_{i=1}^{i'_{\max}-1}\sum_{k=i+1}^{k'_{\max}}\frac{2}{(\pi(i+k))^2}\left[1-\cos\left(\frac{\pi^2(z/L_D)(i+k)^2}{6}\right)\right]$$

where

$$i_{\max}=\min\left\{\frac{m-1}{2},\left\lfloor\frac{12}{\pi(z/L_D)}\right\rfloor\right\} \tag{4.28}$$

$$i'_{\max}=\min\left\{\frac{m-1}{2},\left\lfloor\frac{6}{\pi(z/L_D)}\right\rfloor\right\} \tag{4.29}$$

$$k'_{\max}=\min\left\{\frac{m-1}{2},\left\lfloor\frac{12}{\pi(z/L_D)}-i\right\rfloor\right\} \tag{4.30}$$

where (4.28) to (4.30) come from (4.16), (4.23), and (4.24), respectively.

The next parameters that need to be found are the mean and variance of the receiver output when the current bit is "0" and all neighboring bits are "1". In this case, the pdf of the receiver output is denoted by $p_{101}(x)$, which is approximated with a Gaussian distribution because the thermal noise instead of the excess beat noise is the dominant effect. The output electric field (in one polarization) from an optical fiber when the current bit is "0" and the nearest neighboring bits is "1" can be expressed as

$$s_{101,out}(t)=\sum_{i=-(m-1)/2}^{(m-1)/2}\frac{1}{\sqrt{m}}g\left(t+T-\pi\beta_2 z(i/T)\right)(x_{p,i}+jy_{p,i})\exp\left[j2\pi(f_c+i/T)(t+T)\right]$$
$$+\sum_{i=-(m-1)/2}^{(m-1)/2}\frac{1}{\sqrt{m}}g\left(t-T-\pi\beta_2 z(i/T)\right)(x_{f,i}+jy_{f,i})\exp\left[j2\pi(f_c+i/T)(t-T)\right] \tag{4.31}$$

where $x_{p/f,i}$, and $y_{p/f,i}$, are i.i.d. Gaussian random variables having zero mean and variance $\sigma^2 = N_p h f_c R_b$, and subscripts p and f correspond to the previous bit and the future bit, respectively. Note that only nearest neighboring bits are present in (4.31). However, (4.31) can be extended to cover the case when all neighboring bits are "1" and the current bit is "0", and all following expressions are derived from the extension of (4.31).

By substituting $e(t)$ and $\tilde{e}(t)$ in (4.10) by $s_{010,out}(t)$ given by (4.31) with $x_{p/f,i}$ and $y_{p/f,i}$ being replaced by $\tilde{x}_{p/f,i}$ and $\tilde{y}_{p/f,i}$ for $\tilde{e}(t)$, the output current from the photodetector due to the signal in both orthogonal polarizations can be found. Similar to the previous case, $\tilde{x}_{p/f,i}$ and $\tilde{y}_{p/f,i}$ are again i.i.d. Gaussian random variables having the same property as $x_{p/f,i}$ and $y_{p/f,i}$, and all of them are independent of one another. When the effect of the reset integrator and the fact that the signal is unpolarized are taken into account, the average value of the receiver output (the output current from a reset integrator) in this case is given by

$$\bar{I}_{101} = \begin{cases} \dfrac{\Re\sigma^2}{2m}\left[\dfrac{\pi(z/L_D)(m^2-1)}{12}\right], 0 \le z/L_D \le \dfrac{24}{\pi(m-1)} \\ \dfrac{\Re\sigma^2}{2m}\left\{4(m-1)+4\left\lfloor\dfrac{12}{\pi(z/L_D)}\right\rfloor\left[\dfrac{\pi(z/L_D)}{12}\left(\left\lfloor\dfrac{12}{\pi(z/L_D)}\right\rfloor+1\right)-2\right]\right\}, z/L_D \ge \dfrac{24}{\pi(m-1)} \end{cases} \tag{4.32}$$

By using a similar approach, the variance of the receiver output, as functions of the normalized distance z/L_D and m, can be expressed as

$$\sigma_{101}^2 = 2\left(\frac{\Re\sigma^2}{m}\right)^2 \left(A_{101} + B_{101} + C_{101}\right) + \sigma_n^2 \tag{4.33}$$

where

$$A_{101}=\begin{cases}\dfrac{\pi^2(z/L_D)^2(m^2-1)m}{24\cdot 72}, 0\le z/L_D\le\dfrac{24}{\pi(m-1)}\\ (m-1)-2\left\lfloor\dfrac{12}{\pi(z/L_D)}\right\rfloor\left[1-\dfrac{\pi^2(z/L_D)^2}{12\cdot 72}\left(\left\lfloor\dfrac{12}{\pi(z/L_D)}\right\rfloor+1\right)\left(2\left\lfloor\dfrac{12}{\pi(z/L_D)}\right\rfloor+1\right)\right], z\ge\dfrac{24}{\pi(m-1)}\end{cases}$$

(4.34)

$$B_{101}=\sum_{i=1}^{i_{\max}-1}\sum_{k=i+1}^{(m-1)/2}\frac{2}{(\pi(k-i))^2}\left[1-\cos\left(\frac{\pi^2(z/L_D)(k-i)i}{6}\right)\right] \tag{4.35}$$

$$C_{101}=\begin{cases}\left\{\begin{aligned}&\sum_{i=i_{\min}}^{i_{\max}}\frac{1}{(2\sqrt{2}\pi i)^2}\left[1-\cos\left(\frac{2\pi^2(z/L_D)i^2}{3}\right)\right]\\ &+\sum_{i=i_{\min}}^{i_{\max}-1}\sum_{k=k'_{\min}}^{i_{\max}}\frac{1}{(\pi(i+k))^2}\left[1-\cos\left(\frac{2\pi^2(z/L_D)(i+k)^2}{3}\right)\right]\end{aligned}\right\}, \frac{12}{\pi(m-1)}\le z/L_D\le\frac{24}{\pi(m-1)}\\ \left\{\begin{aligned}&\sum_{i=i_{\min}}^{i_{\max}}\frac{1}{(2\sqrt{2}\pi i)^2}\left[1-\cos\left(\frac{2\pi^2(z/L_D)i^2}{3}\right)\right]\\ &+\sum_{i=i'_{\min}}^{i_{\max}-1}\sum_{k=k'_{\min}}^{i_{\max}}\frac{1}{(\pi(i+k))^2}\left[1-\cos\left(\frac{2\pi^2(z/L_D)(i+k)^2}{3}\right)\right]\\ &+\sum_{i=1}^{i_{\max}-1}\sum_{k=i_{\max}+1}^{(m-1)/2}\frac{1}{(\pi(i+k))^2}\left[1-\cos\left(\frac{\pi^2(z/L_D)(i+k)i}{6}\right)\right]\end{aligned}\right\}, z/L_D\ge\frac{24}{\pi(m-1)}\end{cases}$$

(4.36)

where C_{101} is equal to zero when $z/L_D\le\dfrac{12}{\pi(m-1)}$, $i_{\max}$ is given by (4.28), and

$$i_{\min}=\left\lfloor\frac{12}{\pi(z/L_D)}\right\rfloor+1 \tag{4.37}$$

$$i'_{\min}=\left\lfloor\frac{12}{\pi(z/L_D)}-\frac{(m-1)}{2}\right\rfloor+1 \tag{4.38}$$

$$k'_{\min} = \left\lfloor \frac{12}{\pi(z/L_D)} - i \right\rfloor + 1 \tag{4.39}$$

The last parameters required in evaluating receiver sensitivity are the mean and variance of the receiver output when both the current bit and its neighboring bits are "1". In this case, the pdf of the receiver output is $p_{111}(x)$. When all bits are "1", the optical signal at the input to an optical fiber is continuous in the time domain. Consequently, the corresponding electric field (in one polarization) at the input to the optical fiber can be written as

$$s_{111,in}(t) = \sum_{i=-(m-1)/2}^{(m-1)/2} \frac{1}{\sqrt{m}} (x_i + jy_i) \exp\left[j2\pi(f_c + i/T)t\right] \tag{4.40}$$

By using the transfer function of an optical fiber given by (4.7) in conjunction with basic Fourier transform properties, it is easy to show that the output electric field (in one polarization) from an optical fiber is given by

$$s_{111,out}(t) = \sum_{i=-(m-1)/2}^{(m-1)/2} \frac{1}{\sqrt{m}} (x_i + jy_i) \exp\left[j2\pi(f_c + i/T)t\right] \tag{4.41}$$

It should be noted that when both orthogonal polarizations of the electric field are taken into account, the receiver output is identical to that in [23] and [65], which corresponds to the case where dispersion is neglected. The average value and variance of the receiver output in this case are expressed as

$$\bar{I}_{111} = 2\Re\sigma^2 \tag{4.42}$$

$$\sigma^2_{111} = \frac{2}{m}\left(\Re\sigma^2\right)^2 + \sigma_n^2 \tag{4.43}$$

The first term in (4.43) is due to the received-signal fluctuation whereas the second term is due to the thermal noise at the receiver. It has been shown in [23], and [65] that the pdf of the receiver output due to the received optical signal is chi-square distributed with $4m$ degrees of freedom. However, the thermal noise is Gaussian with zero mean. Thus, the pdf of the receiver output when both received-signal fluctuation and the thermal noise are included ($p_{111}(x)$) is extremely complex and difficult to manipulate numerically. Fortunately, it is reasonable to approximate $p_{111}(x)$ with a chi-square distribution whose degrees of freedom are obtained from (4.42), and (4.43). This is because the signal fluctuation dominates the receiver thermal noise when m is small.

Finally, all parameters required to approximate $p_{010}(x)$, $p_{101}(x)$, and $p_{111}(x)$ are obtained. These three pdf's are then characterized by the mean and variance of the corresponding receiver outputs. The receiver sensitivity of a SS-WDM system employing single-mode fibers is analyzed in the following sections based on these parameters.

4.4 RECEIVER SENSITIVITY

In this section, the receiver sensitivity of a SS-WDM system with a single-mode fiber is numerically evaluated. As stated earlier in this chapter, two approaches can be employed to evaluate the receiver sensitivity. The first approach is termed the Gaussian approximation. All pdf's involved in the evaluation of a receiver sensitivity are approximated to be Gaussian distributions with corresponding means and variances. This results in simplification of the analysis. However, some pdf's in the analysis differ significantly from the Gaussian distributions; therefore, the Gaussian approximation may not be appropriate in some applications.

The second approach is the modification of the first approach. In our case, some pdf's are neither truly Gaussian nor Chi-square. Therefore, the pdf's are approximated based on the distribution of the dominant parameters, which may be either Gaussian or chi-square. We believe that this approach yields results that are more accurate. The results obtained from both approaches are compared, and it is shown that the latter approach is more appropriate.

4.4.1 Gaussian Approximation

We begin with the average values and the variances of the pdf's that appear in (4.1). They are used to find the threshold current. From (4.25), (4.32), and (4.42) with the help of (4.11), the average value of the receiver output can be rewritten as

$$\bar{I}_{010/101/111} = 2q\eta N_p R_b \cdot M_{010/101/111} \tag{4.44}$$

where M_{010}, M_{101}, and M_{111} are the average values of the receiver output normalized by the average value in the absence of the dispersion. They are given by

$$M_{010} = \begin{cases} \dfrac{1}{4m}\left[4m - \dfrac{\pi(z/L_D)(m^2-1)}{12}\right], 0 \le z/L_D \le \dfrac{24}{\pi(m-1)} \\ \dfrac{1}{4m}\left\{4 - 4\left\lfloor \dfrac{12}{\pi(z/L_D)} \right\rfloor \left[\dfrac{\pi(z/L_D)}{12}\left(\left\lfloor \dfrac{12}{\pi(z/L_D)} \right\rfloor + 1\right) - 2\right]\right\}, z/L_D \ge \dfrac{24}{\pi(m-1)} \end{cases} \tag{4.45}$$

$$M_{101} = \begin{cases} \dfrac{1}{4m}\left[\dfrac{\pi(z/L_D)(m^2-1)}{12}\right], 0 \le z/L_D \le \dfrac{24}{\pi(m-1)} \\ \dfrac{1}{4m}\left\{4(m-1) + 4\left\lfloor \dfrac{12}{\pi(z/L_D)} \right\rfloor \left[\dfrac{\pi(z/L_D)}{12}\left(\left\lfloor \dfrac{12}{\pi(z/L_D)} \right\rfloor + 1\right) - 2\right]\right\}, z/L_D \ge \dfrac{24}{\pi(m-1)} \end{cases} \tag{4.46}$$

$$M_{111} = 1 \tag{4.47}$$

Similarly, the variances of the receiver output given by (4.19), (4.33), and (4.43) can be expressed as

$$\sigma^2_{010/101/111} = (2/m)\left(q\eta N_p R_b\right)^2 \cdot K_{010/101/111} + \sigma_n^2 \tag{4.48}$$

where

$$K_{010} = (1/m)\left[A_{010} + \left(B_{010} + C_{010}\right)\right] \tag{4.49}$$

$$K_{101} = (1/m)\left(A_{101} + B_{101} + C_{101}\right) \tag{4.50}$$

$$K_{111} = 1 \tag{4.51}$$

and [23], [65]
$$\sigma_n^2 = 8\pi V_T C_T q B_e^2 \tag{4.52}$$

where V_T is the product of Boltzmann's constant and the room temperature (300 K) divided by the elementary charge constant, C_T is the effective noise capacitance of the receiver (0.1 pF is assumed in our calculations), B_e is the receiver electrical bandwidth which is equal to $R_b / 2$ in the case of a reset integrator. The values of K_{010} and K_{101} correspond to the variances of the receiver output normalized by that in the absence of dispersion. It is difficult to find a closed form expression for the decision threshold from (4.1). However, the suboptimum threshold can be easily found from [1]

$$\int_{-\infty}^{I_{th}} p_{010}(x)dx = \int_{I_{th}}^{\infty} p_{101}(x)dx \tag{4.53}$$

which results in

$$I_{th} = \frac{\sigma_{101}\bar{I}_{010} + \sigma_{010}\bar{I}_{101}}{\sigma_{101} + \sigma_{010}} \tag{4.54}$$

By substituting (4.44), (4.48) in (4.54) and using (4.52), the closed form expression of I_{th} is given by

$$I_{th} = 2q\eta N_p R_b \cdot K_{th} \tag{4.55}$$

where

$$K_{th} = \frac{M_{010}\sqrt{(K_{101}/m)(q\eta N_p)^2 + \pi V_T C_T q} + M_{101}\sqrt{(K_{010}/m)(q\eta N_p)^2 + \pi V_T C_T q}}{\sqrt{(K_{101}/m)(q\eta N_p)^2 + \pi V_T C_T q} + \sqrt{(K_{010}/m)(q\eta N_p)^2 + \pi V_T C_T q}} \quad (4.56)$$

Since all distributions involved in the evaluation of the receiver sensitivity are assumed to be Gaussian, the probability of bit error expressed in (4.2) is simplified to [80]

$$P_e = \frac{1}{2}\left[Q\left(\frac{2q\eta N_p (K_{th} - M_{101})}{\sqrt{(2/m)(q\eta N_p)^2 K_{101} + 2\pi V_T C_T q}} \right) + Q\left(\frac{2q\eta N_p (M_{111} - K_{th})}{\sqrt{(2/m)(q\eta N_p)^2 K_{111} + 2\pi V_T C_T q}} \right) \right] \quad (4.57)$$

where [80]

$$Q(x) = \frac{1}{\sqrt{2\pi}} \int_x^\infty e^{-\lambda^2/2} d\lambda \quad (4.58)$$

The first term in (4.57) corresponds to bit "0" whereas the second term corresponds to bit "1" when all neighboring bits are "1". The receiver sensitivity N_p as functions of m and the normalized distance z/L_D can be numerically evaluated from (4.57). It is shown in Fig. 4.2 for the probability of bit error equal to 10^{-9}, $\eta = 0.7$, and $C_T = 0.1$ pF. When z/L_D is equal to zero, the receiver sensitivity improves as m becomes larger. That is, for a given bit rate $R_b = 1/T$, the receiver sensitivity is better (lower) as the optical bandwidth per channel B_0 is larger. This is due to the fact that the excess beat noise caused from signal fluctuation is inversely proportional to B_0.

When the normalized distance z/L_D is not equal to zero, there are now two competing effects: the signal fluctuation and dispersion. The dispersion causes ISI and decrease in signal to excess beat noise ratio. As the optical bandwidth B_0 increases (increase in $m = B_0 T$ for a given bit rate), the effect of dispersion becomes more severe (as shown in (4.3), the optical pulse spreading is proportional to m). Both the excess beat

noise and the dispersion results in an optimum m (m_{opt}) for a given z/L_D as shown in Fig. 4.2. The value of m_{opt} and the corresponding receiver sensitivity $N_{p,opt}$ are shown in Fig. 4.3. Note that m_{opt} is smaller when the normalized distance z/L_D is larger. This implies that increase in the excess beat noise is traded for reduction in the effect of dispersion (the dispersion has stronger effect than the excess beat noise). The increase in $N_{p,opt}$ is the result of an increase in both the dispersion and the excess beat noise with the normalized distance z/L_D. The Gaussian approximation predicts that the maximum normalized distance z/L_D is about 0.0375 and the corresponding m_{opt} is about 60.

4.4.2 Chi-Square Approximation

In this approach, the distribution of the receiver output is approximated to be chi-square distributed when the signal fluctuation dominates the thermal noise. Arya, and Jacobs [23], [65] have shown that the receiver output due to a received signal is chi-square distributed, which results from

$$X = \frac{1}{2m}\sum_{i=1}^{n} X_i^2 \tag{4.59}$$

where X_i is an i.i.d. Gaussian random variable having zero mean and variance equal to σ_c^2, and n is the degrees of freedom. The expected value and the variance of the receiver output are given by

$$\mu_X = \frac{n}{2m}\cdot\sigma_c^2 \tag{4.60}$$

$$\sigma_X^2 = \frac{n}{2m^2}\cdot\sigma_c^4 \tag{4.61}$$

and its pdf can be expressed as

$$p_X(x) = \frac{\left(m/\sigma_c^2\right)^{n/2}}{\Gamma(n/2)} x^{(n/2-1)} \exp\left(-mx/\sigma_c^2\right) \tag{4.62}$$

whose corresponding cdf is given by

$$F_X(x) = \Phi\left(mx/\sigma_c^2, n/2\right) \tag{4.63}$$

where $\Gamma(a)$ is the gamma function , and $\Phi(x,a)$ is the incomplete gamma function defined as [81]

$$\Gamma(a) = \int_0^\infty e^{-t} t^{a-1} dt \tag{4.64}$$

and

$$\Phi(x,a) = \frac{1}{\Gamma(a)} \int_0^x e^{-t} t^{a-1} dt \tag{4.65}$$

In the prior studies where the effect of dispersion is neglected [23], [65], the number of degrees of freedom n is equal to $4m$, and σ_c^2 is equal to σ^2, the optical-signal power in each polarization, which results in $\mu_X = 2\sigma^2$, and $\sigma_X^2 = (2/m)\sigma^2$.

In our approach, the number of degrees of freedom n and the variance of each Gaussian random variable σ_c^2 are to be approximated from the actual mean and variance of the receiver output given by (4.44) and (4.48). Two pdf's, $p_{010}(x)$ and $p_{111}(x)$, are to be approximated with chi-square distributions, whose pdf is given by (4.62), since the signal fluctuation is the dominant effect in these cases. On the other hand, $p_{101}(x)$ is assumed to be Gaussian with mean and variance as given in the previous section. The variance σ_c^2 can be approximated from the following relationship.

$$\frac{\sigma_X^2}{\mu_X} = \frac{\sigma_{010/111}^2}{\bar{I}_{010/111}} \tag{4.66}$$

where the subscript used depends on the sequence considered. Consequently,

$$\sigma_c^2 = m \cdot \frac{\sigma_{010/111}^2}{\bar{I}_{010/111}} \tag{4.67}$$

where $\sigma_{010/111}^2$ and $\bar{I}_{010/111}$ are given by (4.48), and (4.44), respectively. By substituting all related parameters in (4.67), and arranging the result, we obtain

$$\sigma_c^2 = R_b\left[\left(q\eta N_p\right)\cdot\left(\frac{K_{010/111}}{M_{010/111}}\right)+\frac{m\pi V_T C_T q}{M_{010/111}\left(q\eta N_p\right)}\right] \tag{4.68}$$

The degrees of freedom n can be approximated by making μ_X in (4.60) equal to $\bar{I}_{010/111}$ given by (4.44), and solving for n with the value of σ_c^2 given by (4.68). By doing so, the degrees of freedom is given by

$$n = \left(4m\right)\cdot\left[\frac{M_{010/111}^2\left(q\eta N_p\right)^2}{K_{010/111}\left(q\eta N_p\right)^2 + m\pi V_T C_T q}\right] \tag{4.69}$$

By substituting σ_c^2 and n in (4.62), $p_{010}(x)$ and $p_{111}(x)$ can be expressed by $p_X(x)$ with the corresponding parameters.

The first step in evaluation of the receiver sensitivity is to find the threshold current I_{th} as a function of N_p from (4.1). Then the receiver sensitivity N_p can be numerically evaluated from (4.2) for a given probability of bit error P_e. By assuming that $p_{010}(x)$ is chi-square with pdf given by (4.62) and that $p_{101}(x)$ is Gaussian as that in the previous approach, (4.1) can be written as

$$\frac{1}{\sqrt{2\pi\sigma_{101}^2}}\exp\left[\frac{\left(I_{th}-\bar{I}_{101}\right)^2}{2\sigma_{101}^2}\right]=\frac{\left(m/\sigma_c^2\right)^{n/2}}{\Gamma(n/2)}I_{th}^{\,(n/2-1)}\exp\left(-mI_{th}/\sigma_c^2\right) \tag{4.70}$$

where $\bar{I}_{101}$ and σ_{101}^2 are given by (4.44) and (4.48), respectively, and σ_c^2 and n in (4.70) are given by

$$\sigma_c^2=R_b\left[\left(q\eta N_p\right)\cdot\left(\frac{K_{010}}{M_{010}}\right)+\frac{m\pi V_T C_T q}{M_{010}\left(q\eta N_p\right)}\right] \tag{4.71}$$

$$n=\left(4m\right)\cdot\left[\frac{M_{010}^2\left(q\eta N_p\right)^2}{K_{010}\left(q\eta N_p\right)^2+m\pi V_T C_T q}\right] \tag{4.72}$$

By substituting all parameters in (4.2) in conjunction with (4.58) and (4.63), the expression for the probability of bit error P_e simplifies to

$$P_e=\frac{1}{2}\left[Q\left(\frac{I_{th}-\bar{I}_{101}}{\sigma_{101}}\right)+\Phi\left(mI_{th}/\sigma_c^2,n/2\right)\right] \tag{4.73}$$

where σ_c^2 and n in (4.73) are

$$\sigma_c^2=R_b\left[\left(q\eta N_p\right)\left(\frac{K_{111}}{M_{111}}\right)+\frac{m\pi V_T C_T q}{M_{111}\left(q\eta N_p\right)}\right] \tag{4.74}$$

$$n=\left(4m\right)\cdot\left[\frac{M_{111}^2\left(q\eta N_p\right)^2}{K_{111}\left(q\eta N_p\right)^2+m\pi V_T C_T q}\right] \tag{4.75}$$

Finally, we have two equations, (4.70) and (4.73), and two unknown variables, I_{th} and N_p. Thus, the receiver sensitivity N_p can be numerically solved from both equations as functions of m and the normalized distance z/L_D, and it is plotted in Fig. 4.4 for the

probability of bit error equal to 10^{-9}, $\eta = 0.7$, and $C_T = 0.1$ pF. The figure shows that there is an optimum m for a given z/L_D, similar to the result obtained from the Gaussian approximation. In order to test the validity of our approximation, we compare our result at z/L_D equal to zero with that given by Arya and Jacobs [23], [65]. Their analysis uses the exact distribution of the receiver output. The difference in the receiver sensitivity is less than 1 dB, and our analysis predicts better receiver sensitivity, which implies that our model is slightly optimistic.

4.4.3 Discussion

As seen from the plot, the results have the same trend as those calculated by using the Gaussian approximation. However, the chi-square approximation predicts that a system can operate at longer normalized distance z/L_D and at smaller m with better receiver sensitivity. The value of m_{opt} and the corresponding receiver sensitivity $N_{p,opt}$ evaluated from the Gaussian approximation and the chi-square approximation are shown in Fig. 4.5 for comparison. The predicted maximum normalized distance is approximately around 0.07 with m_{opt} about 13 in the case of the chi-square approximation. On the other hand, the Gaussian approximation predicts that the maximum z/L_D and the corresponding m_{opt} are about 0.0375 and 57, respectively with the receiver sensitivity being 7.7 dB poorer than that of a laser-based system without the dispersion effect. On the other hand, $m_{opt} = 29$ with a 3-dB penalty in the receiver sensitivity is obtained from the chi-square approximation at z/L_D equal to 0.0375. This suggests that the Gaussian approximation underestimates the system performance in all system aspects.

Note from Fig. 4.5 that a SS-WDM system can operate at only a small fraction of the dispersion length L_D. The definition of the dispersion length L_D given earlier in this chapter is based on the case where the source is coherent; i. e., the source spectral width is small compared to the modulation bandwidth ($B_0 << R_b$ or $m << 1$). In that case, the signal bandwidth is mainly determined by the operating bit rate R_b. However, a SS-WDM system usually operates at m larger than unity. In order to intuitively interpret and

compare the result more fairly, it is more useful to normalize the dispersion length L_D by m (or m_{opt} if we are interested in the optimum system performance). The new parameter $m \cdot z / L_D$ can be viewed as the effective normalized distance in a SS-WDM system. The plot of the optimum receiver sensitivity $N_{p,opt}$ and its corresponding m_{opt} as a function of the effective normalized distance $m_{opt} \cdot z / L_D$ is shown in Fig. 4.6. At a small effective normalized distance, the penalty in the receiver sensitivity is small. This is because the reduction of m_{opt} decreases the effect of dispersion with only a small increase in the excess beat noise. (Note that m_{opt} decreases steadily as the effective normalized distance increases.) However, the penalty in the receiver sensitivity increases sharply and m_{opt} decreases abruptly as the effective normalized distance approaches unity. This implies that the decrease in m_{opt} cannot efficiently compensate for the effect of dispersion when the effective normalized distance approaches unity, and it results in high degradation in the receiver sensitivity. Such high degradation can be considered as an error floor in practice, and it is due to the balanced effect of both the excess beat noise and the dispersion. One might expect smoother curves for the optimum receiver sensitivity $N_{p,opt}$ and m_{opt} when a practical filter shape is used instead of an ideal rectangular filter used in our analysis. The optimum receiver sensitivity $N_{p,opt}$ and m_{opt} should approach infinity and zero, respectively in that case. Nevertheless, our results indicate that the maximum effective normalized distance of a SS-WDM system is about unity, which corresponds to a small fraction of the dispersion length L_D used in a laser-based system. In a practical system, the effective normalized distance may be required to be somewhat below unity to avoid degradation of the system performance due to the effect of dispersion.

For practical system consideration, the normalized parameters m and z / L_D can be converted back to the actual parameters. In practice, the system parameters that are usually used to specify a system are the operating bit rate R_b, the optical bandwidth $\Delta\lambda$ in wavelength units, and the transmission distance z. For a given bit rate in Mb/s, the optical bandwidth in nm can be found from m by the following equation.

$$\Delta\lambda(nm) = m \cdot \left(\frac{\lambda_c^2(\mu m) \cdot R_b(Mb/s) \cdot 10^3}{c(m/s)} \right) \tag{4.76}$$

where λ_c is the operating wavelength in μm, and c is the velocity of light which is equal to 3×10^8 m/s. The transmission distance z in km can be found from

$$z(km) = (z/L_D) \cdot \left(\frac{c(m/s) \cdot \pi \cdot 10^3}{6 \cdot R_b^2(Mb/s) \cdot D(ps/km \cdot nm) \cdot \lambda_c^2(\mu m)} \right) \tag{4.77}$$

where D is the dispersion parameter of an optical fiber, which is equal to 16 ps/km-nm for a single-mode optical fiber at the operating wavelength λ_c of 1.55 μm. For example, for a system to operate with less than 3 dB of receiver sensitivity degradation, the maximum normalized distance is equal to 0.0375, and the corresponding m_{opt} is 29. By using these two equations, the maximum transmission distance is equal to 24 km and the optical bandwidth is 0.58 nm. This result is better than the simulations in [24] which give a shorter transmission distance (10 km) and a larger optimum bandwidth (1 nm), which is due to differences in the models. In [24], a polarized source, Gaussian spectral shapes and larger receiver bandwidth ($B_e = 0.75 \cdot R_b$) are used. An unpolarized source provides higher signal-to-excess-noise ratio since the excess beat noises from two orthogonal polarizations are not correlated while the received optical power from both polarizations are added constructively. Additionally, a rectangular filter used in our analysis limit the dispersion effect.

4.5 SUMMARY

In conclusion, we have shown that there is an optimum value of m for a given normalized distance z/L_D in a SS-WDM system employing a single-mode optical fiber. This is the result of two competing effects: the dispersion and the excess beat noise. The dispersion due to nonlinear phase response of an optical fiber is represented by the multipath effect. Two approaches were used in this analysis: the Gaussian approximation

and the chi-square approximation. The Gaussian approximation provides overly conservative results, compared to those obtained from the chi-square approximation. The calculated receiver sensitivity is poorer (higher) as the normalized distance increases. It has been shown that there is a maximum transmission distance for a given operating bit rate, and it is only a small fraction of the dispersion length. This indicates that a SS-WDM system is more susceptible to dispersion than is a laser-based system. When our results are compared with those presented in [24], two conclusions can be drawn. An unpolarized source and sharper cut-off optical filter used to spectrally slice a broadband noise source is recommended. Our analysis indicates that a SS-WDM system can be deployed with a single-mode fiber. However, the system parameters need to be carefully selected in order to avoid degradation in the system performance. Nonetheless, our results imply that SS-WDM systems with single-mode optical fibers can be implemented in high-speed local-loop applications with tolerable penalty in the receiver sensitivity if the transmission distance is not large.

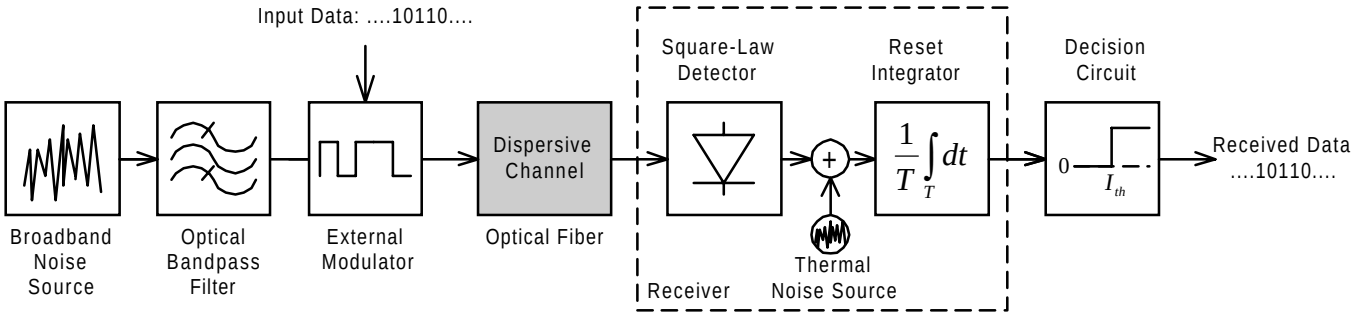

Fig. 4.1: Schematic diagram of system model used to analyze the effect of dispersion on a SS-WDM system.

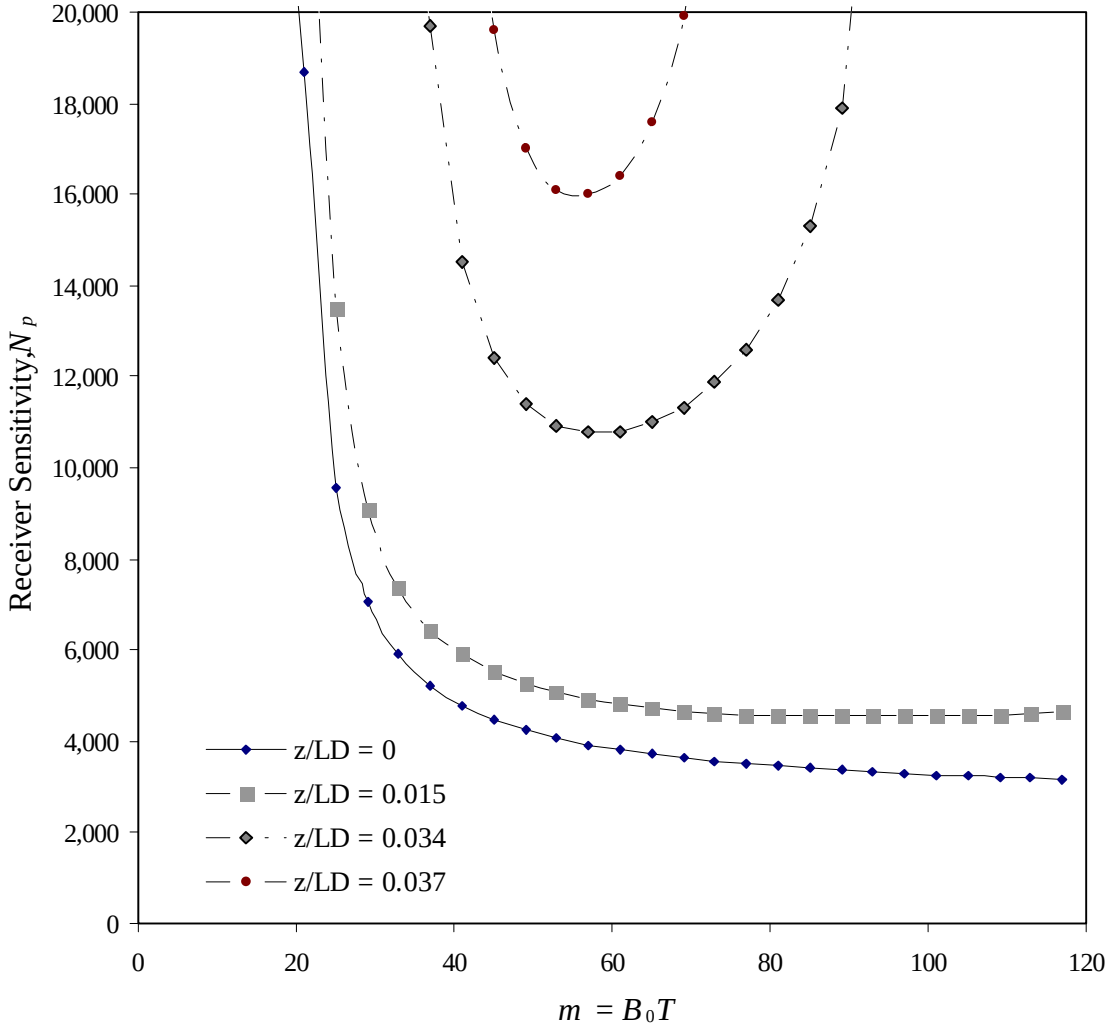

Fig. 4.2: Receiver sensitivity N_p at $P_e = 10^{-9}$ as a function of m at several values of the normalized distance z / L_D (receiver parameters: $C_T = 10$ pF, and $\eta = 0.7$). N_p is evaluated by using Gaussian approximation.

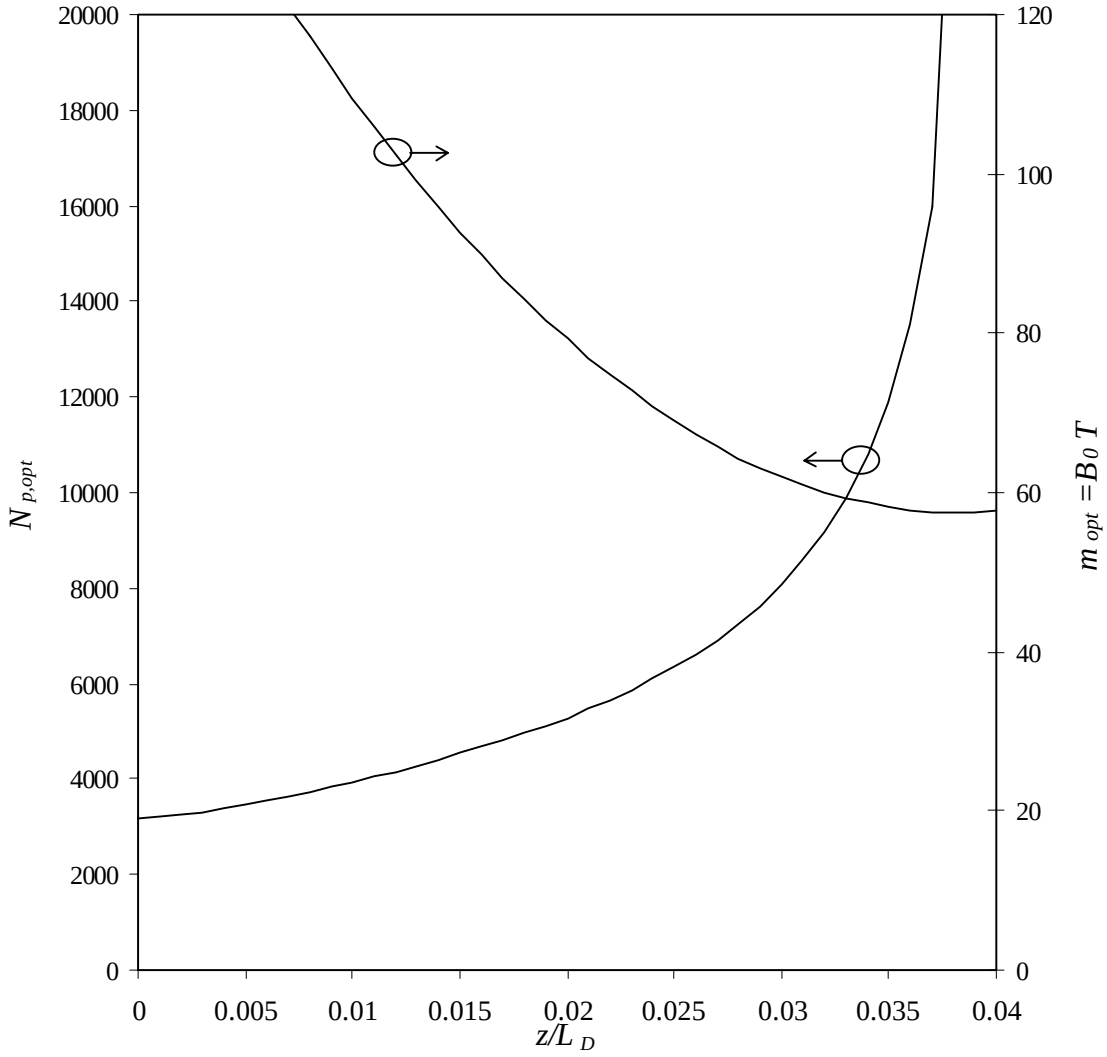

Fig. 4.3: Optimum receiver sensitivity $N_{p,opt}$, and the corresponding m_{opt} versus z/L_D at the probability of bit error $P_e = 10^{-9}$.

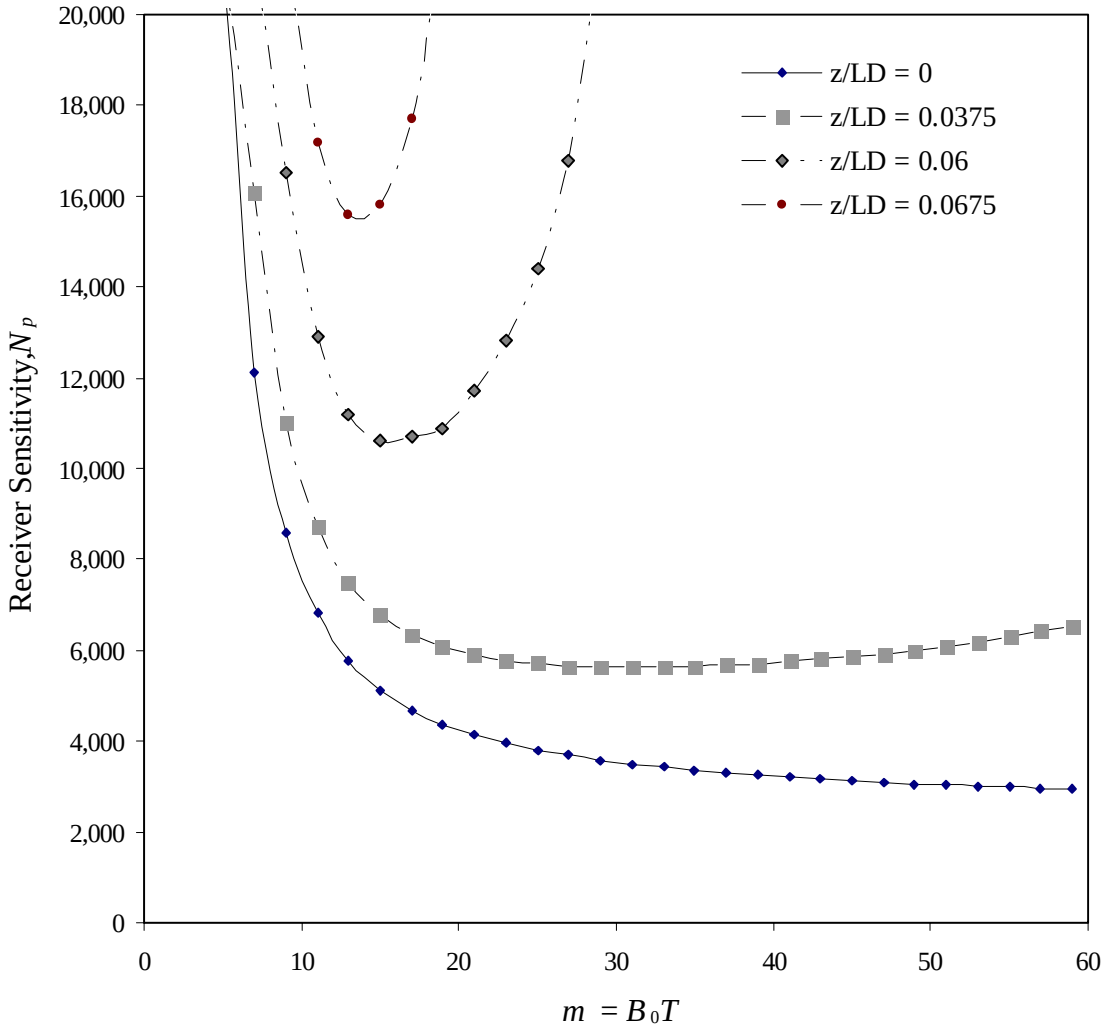

Fig. 4.4: Receiver sensitivity N_p at $P_e = 10^{-9}$ as a function of m at several values of the normalized distance z / L_D (receiver parameters: $C_T = 10$ pF, and $\eta = 0.7$). N_p is evaluated by using chi-square approximation, which is the modification of Gaussian approximation.

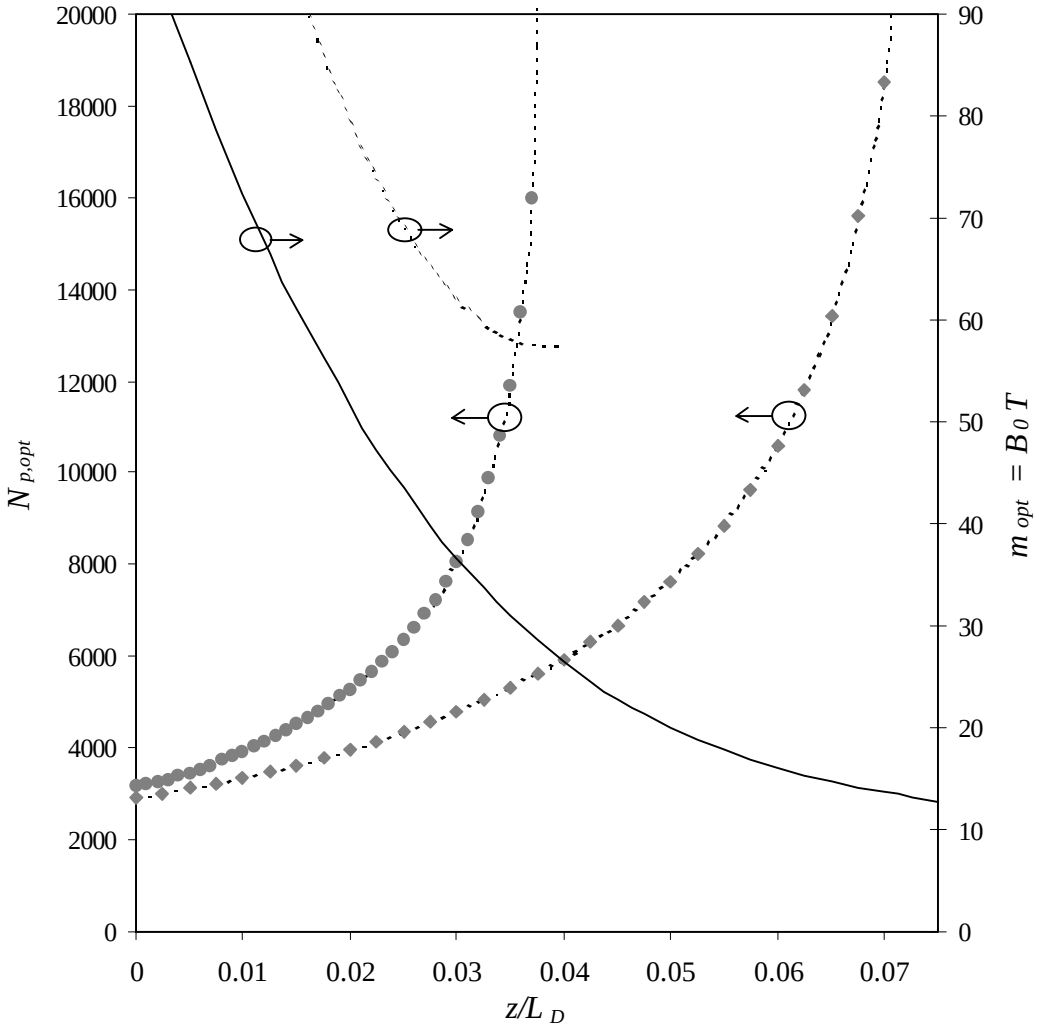

Fig. 4.5: Optimum receiver sensitivity $N_{p,opt}$, and the corresponding m_{opt} versus z/L_D, at the probability of bit error $P_e = 10^{-9}$: (-) and (♦) Chi-square approximation, and (--) and (●) Gaussian approximation.

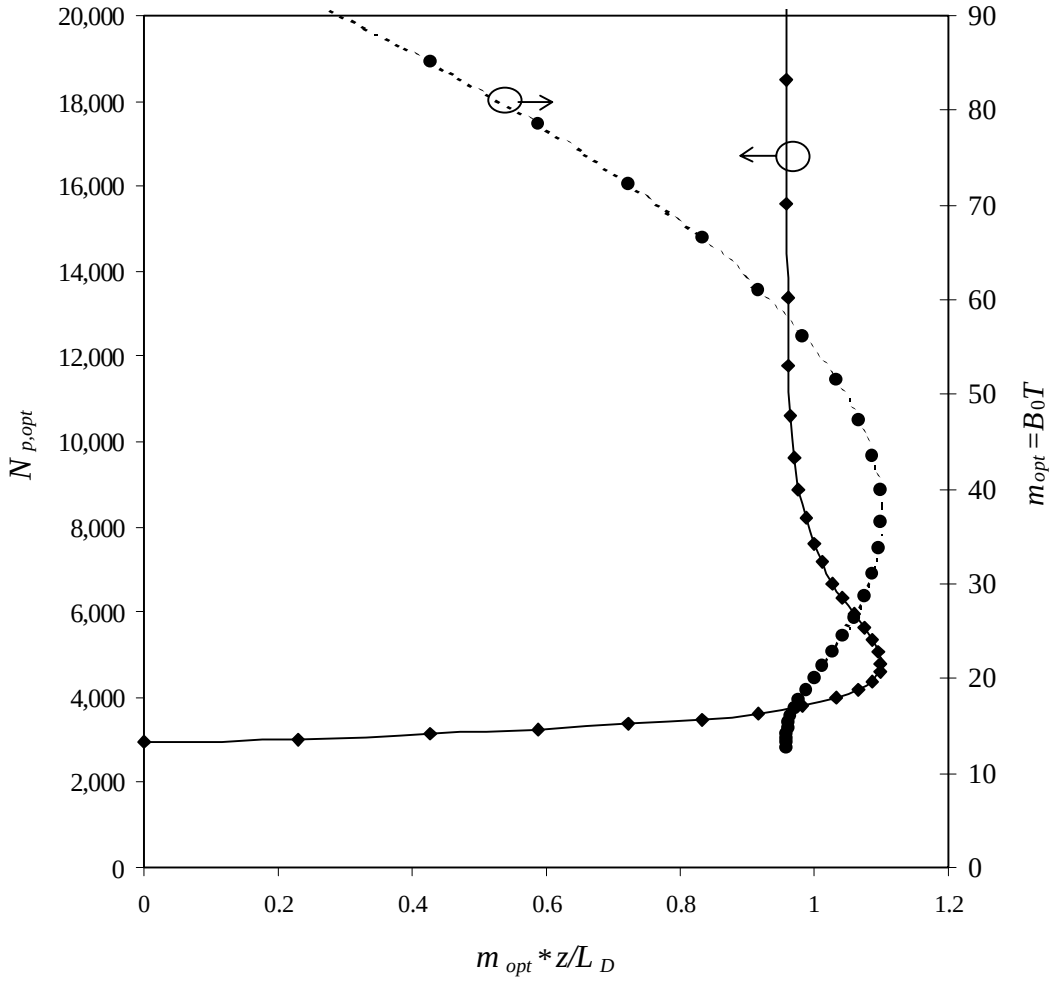

Fig. 4.6: Optimum receiver sensitivity $N_{p,opt}$ and corresponding m_{opt} as a function of the effective normalized distance (the product of m_{opt} and the normalized distance z / L_D).

Chapter 5

CONCLUSIONS

This chapter summarizes the significant results obtained from the analysis of spectrum-sliced wavelength division multiplexing (SS-WDM) systems employing single-mode fibers. The main objective is to analyze the effect of dispersion on the receiver sensitivity of a SS-WDM system under the effect of dispersion. The receiver sensitivity is defined as the average number of photon per bit required for a given probability of bit error (10^{-9} is usually quoted). This final chapter ends with the suggestion for the future research in the area of SS-WDM systems.

5.1 SUMMARY

SS-WDM systems were proposed as an alternative for laser-based WDM systems. The transmitters in SS-WDM systems are broadband noise sources; therefore, a signal fluctuates with time. Such fluctuation results in an additional noise at the receiver. This noise is known as the excess beat noise, and it degrades the system performance, commonly measured in term of the receiver sensitivity. The excess beat noise is inversely proportional to the signal bandwidth. Thus, the performance degradation caused by the signal fluctuation can be reduced by increasing the signal bandwidth. However, wide signal bandwidth implies that the signal experiences large amount of dispersion when single-mode fibers are employed. Consequently, there should be an optimum bandwidth resulting from the excess beat noise and the dispersion.

This thesis is mainly concerned with the theoretical analysis of the effect of dispersion on the performance of a SS-WDM system employing a single-mode optical fiber. The result is expressed as functions of two normalized parameters: the transmission distance normalized by a dispersion distance (z / L_D), and the ratio of the optical

bandwidth per channel and the bit rate ($m = B_0 / R_b = B_0 T$). The first step is to construct a model describing the effect of dispersion. Since the dispersion causes an optical pulse to spread in time, it can be modeled as a multipath effect.

At the receiver, there are two noise sources that affect the decision statistics used to evaluate the receiver sensitivity. The first is the thermal noise generated from electronic components at the receiver. The second source of noise is the result of signal fluctuation from the current bit and neighboring bits. The former is well characterized to be a Gaussian random process with zero mean. However, the latter is very difficult to characterize in the presence of the intersymbol interference (ISI) caused from the dispersion. In the absence of ISI (dispersion), the signal fluctuation is found to be chi-square distributed [23], [65]. The decision statistics required to evaluate the receiver sensitivity are the receiver outputs when "1" and "0" are transmitted. The most commonly-used approach is to assume that the corresponding probability density functions (pdf's) are Gaussian with the calculated means and variances. However, the Gaussian assumption is questionable when the signal fluctuation is the dominant noise source.

Proposed in this thesis is the modification of the Gaussian approximation. Although the decision statistic when the signal fluctuation dominates is very difficult to find, we believe that it is better to describe the decision statistics with chi-square distributions (as in [23], and [65]) whose parameters are approximated from the calculated means and variances of the corresponding receiver outputs. On the other hand, the decision statistic is approximated to be Gaussian distributed when the thermal noise dominates. Note that the non-dominant noise source is not neglected, but it affects only the parameters of the corresponding pdf's. The receiver sensitivity is expressed in term of the average number of received photons per bit N_p required for a probability of bit error equal to 10^{-9}. We investigate the case of a broadband unpolarized noise source spectrally sliced by an ideal rectangular filter. The signal is then gated on or off by a modulator having perfect extinction ratio – no signal in the off state.

The result has shown that there is an optimum m (an optimum B_o) resulting from two effects: the excess beat noise and the dispersion causing ISI. In addition, m_{opt}

decreases as the dispersion increases (increase in the normalized distance z / L_D). This suggests that the dispersion strongly affects the performance of a SS-WDM system. The increase in the excess beat noise is traded for the decrease in the dispersion effect. The dependence of the optimum bandwidth on the degree of dispersion implies that a SS-WDM system is bandwidth constrained, i.e., the optimum bandwidth depends on the normalized distance. In a practical system, the optical bandwidth per channel needs to be carefully chosen to optimize the system performance. The chosen bandwidth depends on the transmission distance and the operating bit rate, which varies among systems.

Unlike a laser-based system, the optical bandwidth B_0 of a SS-WDM system is usually much larger than the operating bit rate R_b. However, the dispersion length L_D is defined from the case where the source spectral width is negligibly small, compared to the bit rate. Therefore, it should be more beneficial to normalize the dispersion length L_D by m, which results in an effective normalized distance $m \cdot z / L_D$. The results as a function of the effective normalized distance $m \cdot z / L_D$ indicate that the optimum receiver sensitivity $N_{p,opt}$ and the corresponding m_{opt} approach infinity and zero, respectively, as the effective normalized distance $m \cdot z / L_D$ approaches unity.

In practical consideration, our analysis also shows that the penalty in the receiver sensitivity increases (becomes poorer) with the transmission distance for a given bit rate. In addition, for a given penalty, the transmission distance is shorter as the bit rate is higher. This limits the applications of SS-WDM systems employing single-mode optical fibers. For a bit rate of the order of 1 Gb/s with 3-dB penalty in the receiver sensitivity, the maximum transmission distance is only of the order of a hundred km. Therefore, it can be concluded that SS-WDM systems with single-mode fibers are not suitable for high-speed long-haul lightwave systems. However, they can be an alternative for expensive laser-based WDM systems in high-speed short-haul lightwave systems, such as local access networks.

5.2 FUTURE WORK

In our model, ideal components are used, such as a perfect-extinction-ratio modulator and a rectangular bandpass filter. However, the components in a practical

system differ from those used in our model. Imperfect extinction ratio causes the signal to exist when the modulator is in the off state – the modulator is not completely turned-off in the off state. The transmission passband of an actual WDM multiplexer does not have sharp cut-off characteristic. Therefore, there is an additional interference from neighboring channels, which is called interchannel interference (ICI), and the dispersion might affect the system performance differently from that presented in this analysis. It would be interesting to model practical components and to analyze the effects of imperfections inherent in these components. The results should be more accurate than our result and they would provide us deeper understanding of SS-WDM systems. When a single channel is considered, the results can be used to verify the relation between the optimum receiver sensitivity $N_{p,opt}$ and the corresponding m_{opt}, and the effective normalized distance $m \cdot z / L_D$. In addition, this thesis does not include any simulations. It should be useful to simulate a system employing actual components. The results obtained from the simulation could then be used to confirm the assumptions used in the theoretical analysis.

References

[1] G. P. Agrawal, *Fiber-Optic Communication Systems*, New York: John Wiley & Sons, 1992.

[2] K.C. Kao and G.A. Hockham, "Dielectric fiber surface waveguides for optical frequencies," *Proceedings of the IEE, vol.* 133, pp 1151-1158, Jul. 1966.

[3] J. Bellamy, *Digital-Telephony*, New York: Wiley Interscience, 1991.

[4] W. B. Jones, Jr., *Introduction to Optical Fiber Communication Systems*, Texas: Saunders College Publishing, 1988.

[5] J. R. Ryan, and R. H. Kent, "WDM: North American deployment trends," *IEEE Communications Magazine*, vol. 36, no. 2, pp. 40-44, Feb. 1998.

[6] F. W. Kerfoot, and P. K. Runge, "Future for undersea communications," *AT&T Technical Journal*, pp. 93-102, Jan./Feb. 1995.

[7] C. Lorattanasane, and K. Kikuchi, "Design theory of long-distance optical transmission systems using midway optical phase conjugation," *Proc. Conf. Lasers Electro-Opt. (CLEO'95)*, Baltimore, MD, May 21-26, 1995, paper CTuN3
Also: C. Lorattanasane, and K. Kikuchi, "Design theory of long-distance optical transmission systems using midway optical phase conjugation," *Journal of Lightwave Technology*, vol. 15, no. 6, pp. 948-955, Jun. 1997.

[8] S. Wen, "Optical phase conjugation of multiwavelength signals in a dispersion-shifted fiber," *Journal of Lightwave Technology*, vol. 15, no. 7, pp. 1061-1070, Jul. 1997.

[9] N. S. Bergano, C. R. Davidson, "Wavelength division multiplexing in long-haul transmission systems," *Journal of Lightwave Technology*, vol. 14, no. 6, pp. 1299-1308, Jun. 1996.

[10] P. Trischitta, M. Colas, M. Green, G. Wuzniak, and J. Arena, "The TAT-12/13 cable network," *IEEE Communications Magazine*, vol. 34, no. 2, pp. 24-28, Feb. 1996.

[11] W. C. Barnett, H. Takahira, G. C. Baroni, and Y. Ogi, "The TPC-5 cable network," *IEEE Communications Magazine*, vol. 34, no. 2, pp. 36-40, Feb. 1996.

[12] T. Welsh, R. Smith, H. Azami, and R. Chrisner, "The FLAG cable system," *IEEE Communications Magazine*, vol. 34, no. 2, pp. 30-35, Feb. 1996.

[13] D. R. Gunderson, A. Lecroart, and K. Tatekura, "The Asia Pacific cable network," *IEEE Communications Magazine*, vol. 34, no. 2, pp. 42-48, Feb. 1996.

[14] B. W. Hakki, "Polarization mode dispersion in a single mode fiber," *Journal of Lightwave Technology*, vol. 14, no. 10, pp. 2202-2207, Oct. 1996.

[15] C. D. Poole, R. W. Tkach, A. R. Chraplyvy, and D. A. Fishman, "Fading in lightwave systems due to polarization-mode dispersion," *IEEE Photonics Technology Letters*, vol. 3, no. 1, pp. 68-70, Jan. 1991.

[16] Y. Sun, J. B. Judkins, A. K. Srivastava, L. Garrett, J. L. Zyskind, J. W. Sulhoff, C. Wolf, R. M. Derosier, A. H. Gnauck, R. W. Tkach, J. Zhou, R. P. Espindola, A. M. Vengsarkar, and A. R. Chraplyvy, "Transmission of 32-WDM 10-Gb/s channels over 640 km using broad-band, gain-flattened erbium-doped silica fiber amplifiers," *IEEE Photonics Technology Letters,* vol. 9, no. 12, pp. 1652-1654, Dec. 1997.

[17] W. C. Marra, and J. Schesser, "Africa ONE: the Africa optical network," *IEEE Communications Magazine*, vol. 34, no. 2, pp. 50-57, Feb. 1996.

[18] A. M. Hill, D. B. Payne, K. J. Blyth, D. S. Forrester, A. Silvertown, J. W. Arkwright, D. W. Faulkner, and J. W. Balance, "An experimental broadband and telephony passive optical network," *Proc. IEEE Global Telecommunications Conference and Exhibition (GLOBECOM' 90)*, San Diego, CA, vol. 3, pp. 1856-1860.

[19] M. Zirngibl, C. H. Joyner, L. W. Stulz, C. Dragone, H. M. Presby, and I. P. Kaminow, "LARNet: a local access router network," *IEEE Photonics Technology Letters*, vol. 7, no. 2, pp. 215-217, Feb. 1995.

[20] P. P. Iannone, N. J. Frigo, and K. C. Reichmann, "Enhanced privacy in broadcast passive optical networks through use of spectral slicing in waveguide grating routers," *Proc. Opt. Fiber Commun. (OFC'97)*, Dallas, TX, Feb. 16-21, 1997, paper TuK2.

Also: P. P. Iannone, N. J. Frigo, and K. C. Reichmann, "Enhanced privacy in broadcast passive optical networks through the use of spectral slicing in

waveguide grating routers," *IEEE Photonics Technology Letters*, vol. 9, no. 7, pp. 1044-1046, Jul. 1997.

[21] M. H. Reeve, A. R. Hunwicks, W. Zhao, S. G. Methley, L. Bickers, and S. Hornung, "LED spectral slicing for single-mode local loop applications," *Electronics Letters*, vol.v24, no. 7, pp. 389-390, Mar. 1988.

[22] T. E. Chapuran, S. S. Wagner, R. C. Menendez, H. E. Tohme, and L. A. Wang, "Broadband multichannel WDM transmission with superluminescent diodes and LEDs," *Proc. IEEE Global Telecommunications Conference and Exhibition (GLOBECOM' 91)*, Phoenix, AZ, part 1 (of 3), pp. 612-618.

[23] V. Arya, and I. Jacobs, "Optical preamplifier receiver for spectrum-sliced WDM," *Journal of Lightwave Technology*, vol. 15, no. 4, pp. 576-583, Apr. 1997.

[24] G. J. Pendock, and D. D. Sampson, "Transmission performance of high bit rate spectrum-sliced WDM systems," *Journal of Lightwave Technology*, vol. 14, no. 10, pp. 2141-2148, Oct. 1996.

[25] E. Desurvire, *Erbium-Doped Fiber Amplifiers*, New York: John Wiley & Sons, Inc., 1994.

[26] R. Ramaswami, and K. N. Sivarajan, *Optical Networks: A Practical Perspective*, San Francisco: Morgan Kaufmann Publisher, Inc., 1998.

[27] H. Taga, "Long distance transmission experiments using the WDM technology," *Journal of Lightwave Technology*, vol. 14, no. 6, pp. 1287-1298, Jun. 1996.

[28] B. Clesca, D. Ronarc' h, D. Bayart, Y. Sorel, L. Hamon, M. Guibert, J. L. Beylat, J. F. Kerdiles, and M. Semenkoff, "Gain flatness comparison between Erbium-doped fluoride and silica fiber amplifiers with wavelength-multiplexed signals," *IEEE Photonics Technology Letters*, vol. 6, no. 4, pp. 509-512, Jul. 1994.

[29] M. Chbat, S. Artigaud, D. Bayart, A. Jourdan, M. Sotom, J. L. Beylat, "Systems aspects of fluoride-based EDFAs," *Proc. Opt. Fiber Commun. (OFC'97)*, Dallas, TX, Feb. 16-21, 1997, paper TuP3.

[30] A. R. Chraplyvy, J. A. Nagel, and R. W. Tkach, "Equalization in amplified WDM lightwave transmission systems," *IEEE Photonics Technology Letters*, vol. 4, no. 8, pp. 920-922, Aug. 1996.

[31] K. P. Jones, M. S. Chaudhry, D. Simeonidou, N. H. Taylor, and P. R. Morkel, "Optical wavelength add-drop multiplexer in installed submarine WDM network," *Electronics Letters*, vol. 31, no. 24, pp. 2117-2118, Nov. 1995.

[32] M. Tachibana, R. I. Laming, P. R. Morkel, and D. N. Payne, "Erbium-doped fiber amplifier with flattened gain spectrum," *IEEE Photonics Technology Letters*, vol. 3, no. 2, pp. 118-120, Feb. 1991.

[33] N. Park, P. Wysocki, R. Pedrazzani, S. Grubb, D. DiGiovanni, and K. Walker, "High-power Er-Yb doped fiber amplifier with multichannel gain flatness within 0.2 dB over 14 nm," *IEEE Photonics Technology Letters*, vol. 8, no. 9, pp. 1148-1150, Sep. 1996.

[34] P. F. Wysocki, J. B. Judkins, R. P. Espindola, M. Andrejco, and A. M. Vengsarkar, "Broad-band erbium-doped fiber amplifier flattened beyond 40 nm using long-period grating filter," *IEEE Photonics Technology Letters*, vol. 9, no. 10, pp. 1343-1345, Oct. 1997.

[35] J. Pan, M. A. Ali, A. F. Elrefaie, and R. E. Wagner, "Multiwavelength fiber-amplifier cascades with equalization employing Mach-Zehnder optical filter," *IEEE Photonics Technology Letters*, vol. 7, no. 12, pp. 1501-1503, Dec. 1995.

[36] R. Kashyap, R. Wyatt, and P. F. McKee, "Wavelength flattened saturated erbium amplifier using multiple side-tap Bragg gratings," *Electronics Letters*, vol.29, no. 11, pp. 1025-1026, May. 1993.

[37] S.-M. Hwang, X. Y. Zou, S. H. Huang, W. Shieh, and A. E. Willner, "Passive equalisation of four 2.5 Gbits/s WDM channels over 1000 km using notch filters," *Electronics Letters*, vol.32, no. 7, pp. 676-677, Mar. 1996.

[38] J.-L. Archambault, and S. G. Grubb, "Fiber gratings in lasers and amplifiers," *Journal of Lightwave Technology*, vol.15, no. 8, pp. 1378-1390, Aug. 1997.

[39] K. Inoue, T. Kominato, and H. Toba, "Tunable gain equalization using a Mach-Zehnder optical filter in multistage fiber amplifiers," *IEEE Photonics Technology Letters*, vol. 3, no. 8, pp. 718-720, Aug. 1991.

[40] H. Toba, K. Naganichi, K. Oda, K. Inoue, and T. Kominato, "A 100-channel optical FDM six-stage in-line amplifier system employing tunable gain

equalizers," *IEEE Photonics Technology Letters*, vol. 5, no. 2, pp. 248-251, Feb. 1993.

[41] K. Oda, M. Fukutoku, H. Toba, and T. Kominato, "128 channel, 480 km FSK-DD transmission experiment using 0.98 μm pumped erbium-doped fibre amplifiers and a tunable gain equaliser," *Electronics Letters*, vol. 30, no. 12, pp. 982-984, Jun. 1994.

[42] S.-M. Hwang, and A. E. Willner, "Active equalization of non-uniform EDFA gain by using multiple AOTF passbands for megameter WDM transmission," *Proc. Conf. Lasers Electro-Opt. (CLEO'95)*, Baltimore, MD, May 21-26, 1995, paper CTuS3.

[43] H. S. Kim, S. H. Yun, H. K. Kim, N. Park, and B. Y. Kim, "Actively gain-flattened erbium-doped fiber amplifier over 35 nm by using all-fiber acoustooptic tunable filters," *IEEE Photonics Technology Letters*, vol. 10, no. 6, pp. 790-792, Jun. 1998.

[44] B. Glance, I. P. Kaminow, and R. W. Wilson, "Applications of the integrated waveguide grating router," *Journal of Lightwave Technology*, vol. 12, no. 6, pp. 957-962, Jun. 1994.

[45] C. Dragone, "An $N \times N$ optical multiplexer using a planar arrangement of two star couplers," *IEEE Photonics Technology Letters*, vol. 3, no. 9, pp. 812-815, Sep. 1991.

[46] H. Takahashi, K. Oda, H. Toba, and Y. Inoue, "Transmission characteristics of arrayed waveguide $N \times N$ wavelength multiplexer," *Journal of Lightwave Technology*, vol. 13, no. 3, pp. 447-455, Mar. 1995.

[47] N. Takato, K. Jinguji, M. Yasu, H. Toba, and M. Kawachi, "silica-based single-mode waveguides on silicon and their application to guided-wave optical interferometers," *Journal of Lightwave Technology*, vol. 6, no. 6, pp. 1003-1010, Jun. 1988.

[48] J. C. Chen, and C. Dragone, "Waveguide grating routers with greater channel uniformity," *Electronics Letters*, vol. 30, no. 23, pp. 1951-1952, Nov. 1997.

[49] Y. Inoue, A. Kaneko, F. Hanawa, H. Takahashi, K. Hattori, and S. Sumida, "Athermal silica-based arrayed-waveguide grating multiplexer," *Electronics Letters*, vol. 33, no. 23, pp. 1945-1946, Nov. 1997.

[50] T. Mizuochi, T. Kitayama, K. Shimizu, and K. Ito, "Interferometric Crosstalk-free optical add-drop multiplexer using Mach-Zehnder-based fiber gratings," *Journal of Lightwave Technology*, vol. 16, no. 2, pp. 265-276, Feb. 1998.

[51] J. Hubner, D. Zauner, and M. Kristensen, "Strong sampled Bragg gratings for WDM applications," *IEEE Photonics Technology Letters*, vol. 10, no. 4, pp. 552-554, Apr. 1998.

[52] Y. Tachikawa, Y. Inoue, M. Kawachi, H. Takahashi, and K. Inoue, "Arrayed-waveguide grating add-drop multiplexer with loop-back optical paths," *Electronics Letters*, vol. 29, no. 24, pp. 2133-2134, Nov. 1993.

[53] O. Ishida and H. Takahashi, "Loss-imbalance equalisation of arrayed-waveguide grating add-drop multiplexer," *Electronics Letters*, vol. 30, no. 14, pp. 1160-1162, Jul. 1994.

[54] W. D. Zhong, S. Dods, J. P. R. Lacey, and R. S. Tucker, "Reconfigurable multichannel add-drop multiplexer with improved performance," *Electronics Letters*, vol. 32, no. 16, pp. 1477-1478, Aug. 1996.

[55] A. R. Chraplyvy, "Limitation on lightwave communications imposed by optical-fiber nonlinearities," *Journal of Lightwave Technology*, vol. 8, no. 10, pp. 1548-1557, Oct. 1990.

[56] K. Inoue, "Four-wave mixing in an optical fiber in the zero-dispersion wavelength region," *Journal of Lightwave Technology*, vol. 10, no. 11, pp. 1553-1561, Nov. 1992.

[57] K. Okamoto, M. Ishii, Y. Hibino, Y. Ohmori, and H. Toba, "Fabrication of unequal channel spacing arrayed-waveguide grating multiplexer modules," *Electronics Letters*, vol. 31, no. 17, pp. 1464-1466, Aug. 1995.

[58] M. Fukui, K. Oda, H. Toba, K. Okamoto, and M. Ishii, "10 channel × 10 Gbits/s WDM add-drop multiplexing/transmission experiment over 240 km of dispersion-shifted fibre employing unequally-spaced arrayed-waveguide-grating ADM filter

with fold-back configuration," *Electronics Letters*, vol. 31, no. 20, pp. 1757-1759, Sep. 1995.

[59] X. Y. Zou, M. I. Hayee, S.-M. Hwang, and Alan E. Willner, "Limitations in 10 Gb/s WDM optical-fiber transmission when using a variety of fiber types to manage dispersion and nonlinearities," *Journal of Lightwave Technology*, vol. 14, no. 6, pp. 1144-1152, Jun. 1996.

[60] M. I. Hayee, and A. E. Willner, "Pre- and post-compensation of dispersion and nonlinearities in 10-Gb/s WDM systems," *IEEE Photonics Technology Letters*, vol. 9, no. 9, pp. 1271-1273, Sep. 1997.

[61] S. S. Wagner, and T. E. Chapuran, "Broadband high-density WDM transmission using superluminescent diodes," *Electronics Letters*, vol. 26, no. 11, pp. 696-697, May. 1990.

[62] P. D. D. Kilkelly, P. J. Chidgey, and G. Hill, "Experimental demonstration of a three channel WDM system over 110 km using superluminescent diodes," *Electronics Letters*, vol. 26, no. 20, pp. 1671-1673, Sep. 1990.

[63] K. Liu, "Noise limits of spectral slicing in wavelength-division multiplexing applications," *Proc. Opt. Fiber Commun. (OFC'92)*, San Jose, CA, Feb. 2-7, 1992, paper WM7.

[64] J. S. Lee, Y. C. Chung, and D. J. DiGiovanni, "Spectrum-sliced fiber amplifier light source for multichannel WDM applications," *IEEE Photonics Technology Letters*, vol. 5, no. 12, pp. 1458-1461, Dec. 1993.

[65] V. Arya, "Analysis, Design and Performance Evaluation of Optical Fiber Spectrum-Sliced WDM Systems," Ph. D. Diss., Virginia Polytechnic Institute and State University, 1997.
http://scholar.lib.vt.edu/theses/delayed/etd-52897-17181/etd-title.html

[66] I. Jacobs, "Dependence of optical amplifier noise figure on relative-intensity-noise," *Journal of Lightwave Technology*, vol.13, no. 7, pp. 1461-1465, Jul. 1995.

[67] L. Nguyen, J. F. Young, and B. Aazhang, "Photoelectric current distribution and bit error rate in optical communication systems using a superfluorescent fiber source," *Journal of Lightwave Technology*, vol. 14, no. 6, pp. 1455-1466, Jun. 1996.

[68] A. A. Al-Orainy, and J. J. O' Reilly, "Optimized threshold setting for performance enhancement of spectrum sliced WDM systems," *Proc. Conf. Lasers Electro-Opt. (CLEO'95)*, San Francisco, CA, 1995, vol.2, pp. 63-64.

[69] J.-S. Lee, "Signal-to-noise ratio of spectrum-sliced incoherent light sources including optical modulation effects," *Journal of Lightwave Technology*, vol. 14, no. 10, pp. 2197-2201, Oct. 1996.
Also: J.-S. Lee, "signal-to-noise ratio measurement of 2.5-Gb/s spectrum-sliced incoherent light channel," *IEEE Photonics Technology Letters*, vol. 9, no. 1, pp. 94-96, Jan. 1997.

[70] D. D. Sampson, and W. T. Holloway, "100 mW spectrally-uniform broadband ASE source for spectrum-sliced WDM systems," *Electronics Letters*, vol. 30, no. 19, pp. 1611-1612, Sep. 1994.

[71] Y. C. Chung, R. W. Tkach, and D. J. DiGiovanni, "SBS limitation on a spectrum-sliced fiber-amplifier light source," *Proc. Opt. Fiber Commun. (OFC'97)*, Dallas, TX, Feb. 16-21, 1997, paper TuH6.

[72] A. J. Keating, W. T. Holloway, and D. D. Sampson, "Feedforward noise reduction of incoherent light for spectrum-sliced transmission at 2.5 Gb/s," *IEEE Photonics Technology Letters*, vol. 7, no. 12, pp. 1513-1515, Dec. 1995.
Also: A. J. Keating, and D. D. Sampson, "Reduction of excess intensity noise in spectrum-sliced incoherent light for WDM applications," *Journal of Lightwave Technology*, vol. 15, no. 1, pp. 53-61, Jan. 1997.

[73] Y. C. Chung, J. S. Lee, R. M. Derosier, and D. J. DiGiovanni, "1.7 Gb/s transmission over 165 km of dispersion-shifted fibre using spectrum-sliced fibre-amplifier light source," *Electronics Letters*, vol. 30, no. 17, pp. 1427-1428, Aug. 1994.

[74] D. D. Sampson, and W. T. Holloway, "Transmission of 622 Mbit/s spectrum-sliced WDM channel over 60 km of nondispersion-shifted fibre at 1550 nm," *Electronics Letters*, vol. 30, no. 21, pp. 1767-1768, Oct. 1994.

[75] J. S. Lee, and Y. C. Chung, "Spectrum-sliced channel transmission over 94 km of dispersion-shifted fibre at $1.7Gbs^{-1}$ using a double-stage fibre amplifier light

source," *Optical and Quantum Electronics*, vol. 27, no. 5, pp. 541-546, May 1995.

[76] J.-H. Han, J.-S. Lee, S.-S. Lee, T.-Y. Yun, H.-K. Kim, C.-H. Lee, and S.-Y. Shin, "2.5 Gbit/s transmission of spectrum-sliced fibre amplifier light source channels over 200 km of dispersion-shifted fibre," *Electronics Letters*, vol. 31, no. 12, pp. 989-991, Jun. 1995.

[77] J. S. Lee, Y. C. Chung, T. H. Wood, J. P. Meester, C. H. Joyner, C. A. Burrus, J. Stone, H. M. Presby, and D. J. DiGiovanni, "Spectrum-sliced fiber amplifier light source with a polarization-insensitive electroabsorption modulator," *IEEE Photonics Technology Letters*, vol. 6, no. 8, pp.1035-1038, Aug. 1994.

[78] D. Marcuse, "Derivation of analytical expressions for the bit-error probability in lightwave systems with optical amplifiers," *Journal of Lightwave Technology*, vol. 8, no. 12, pp. 1816-1823, Dec. 1990.

[79] _____, "Calculation of bit-error probability for a lightwave system with optical amplifiers and post-detection Gaussian noise," *Journal of Lightwave Technology*, vol. 9, no. 4, pp. 505-513, Apr. 1991.

[80] L. W. Couch II, *Digital and Analog Communication Systems*, New York: Macmillan Publishing Company, 1993.

[81] *The Student edition of MATLAB: User's Guide*, New Jersey: Prentice Hall, 1995.

Vita

Virach Wongpaibool was born in Bangkok, the capital of Thailand, on January 21, 1972. In 1990, he was admitted to the college of engineering, Chulalongkorn University, Bangkok. After four years of intense study, he graduated with a Bachelor Degree (Second Class Honors) in electrical engineering. His major is telecommunications. In 1994, he joined Advanced Info Service PCL, the company that provides wireless telephone service in Thailand. He worked as an engineer in the GSM base station installation department where he gained valuable experience in wireless communication field. He joined Virginia Polytechnic Institute and State University in August 1996 to pursue his graduate studies. He conducts research under the advisory of Prof. Ira Jacobs who motivated him to be interested in optical fiber communications. His current research of interest is in the area of optical fiber communication systems. After he finishes his graduate study, he plans to continue his study toward Ph. D. degree at the same university, Virginia Tech. Virach is a student member of IEEE.